PURDUE UNIVERSITY

AAE 451

METRO-SCOUT

UAV PROPOSAL

CONCEPTUAL DESIGN REVIEW DOCUMENTATION

TEAM 4

Kevin Kwan

Dan Pothala

Mohammed Abdul Rahim

Nicole Risley

Sara Tassan

John Thornton

Sean Woock

Alvin Yip

Table of Contents

EXECUTIVE SUMMARY:

Throughout the world today, there is an increased demand for Unmanned Aerial System (UAS) in many different industries for many different purposes. A particularly high need has developed for UAVs with continuous area coverage capabilities. There are several industries in which these vehicles would be useful; however, few options are available for the customer at an affordable price. In recent years, there has been a realization among aircraft manufacturers and the public of the huge potential that exists in a civilian UAS market. Law enforcement and news agencies, with their helicopter fleets, have to deal with acquisition costs in the millions, and operating costs in the thousands of dollars every hour. The market is ready for the introduction of an Unmanned Aerial System that can provide most of the advantages of a helicopter, while providing huge cost savings and eliminating the risks of putting a crew in the air.

The Metro-Scout UAS is designed specifically around payload packages such as the Cineflex V14 high resolution aerial TV camera, and the ThermaCam SC3000, both of which are recognized as top of the line equipment in their respective categories of news coverage and surveillance. In addition, customers can pick a camera of choice to use as long as it meets weight, size, and mount adaptability requirements for the Metro-Scout. The Metro-Scout will be capable of carrying two similar, but alternate payload load-outs based on the mission requirements. For instance, a customer using the Metro-Scout for news coverage would be able to carry single high-resolution TV camera weighing 67 lbs, while a customer using the Metro-Scout for news coverage would be able to carry a payload package comprised of a low to moderate resolution surveillance day/night/IR camera, a still-shot camera, and a radar gun weighing 64 lbs in total. The Metro-Scout will be able to take-off from small airports in runway distances as short as 1000 feet. It can travel as far as a 200 miles, and loiter on-station for 7 hours. Current estimates put the take-off gross weight at 381 lbs.

The Metro-Scout features an unconventional and innovative three surface design featuring canards, mid-fuselage mounted main wing and a horizontal stabilizer, that provide a number of advantages in terms of stability, stall safety, drag reduction, and fuel-savings. The high aspect ratio main wing allows the Metro-Scout to loiter on station for nearly 7 hours, and have a range of nearly 200 nm. In addition, the use of winglets to complement directional stability also allows the Metro-Scout to

have a decreased vertical tail area, and reduce induced drag off the main wing. The Metro-Scout will also feature a pusher-prop engine in order to minimize vibrations and electrical interference to the camera payloads it will be carrying. It also incorporates the use of an innovative exhaust system similar to some that are used in automobiles, which diverts exhaust gases away from the propeller in order to significantly reduce the noise footprint of the aircraft.

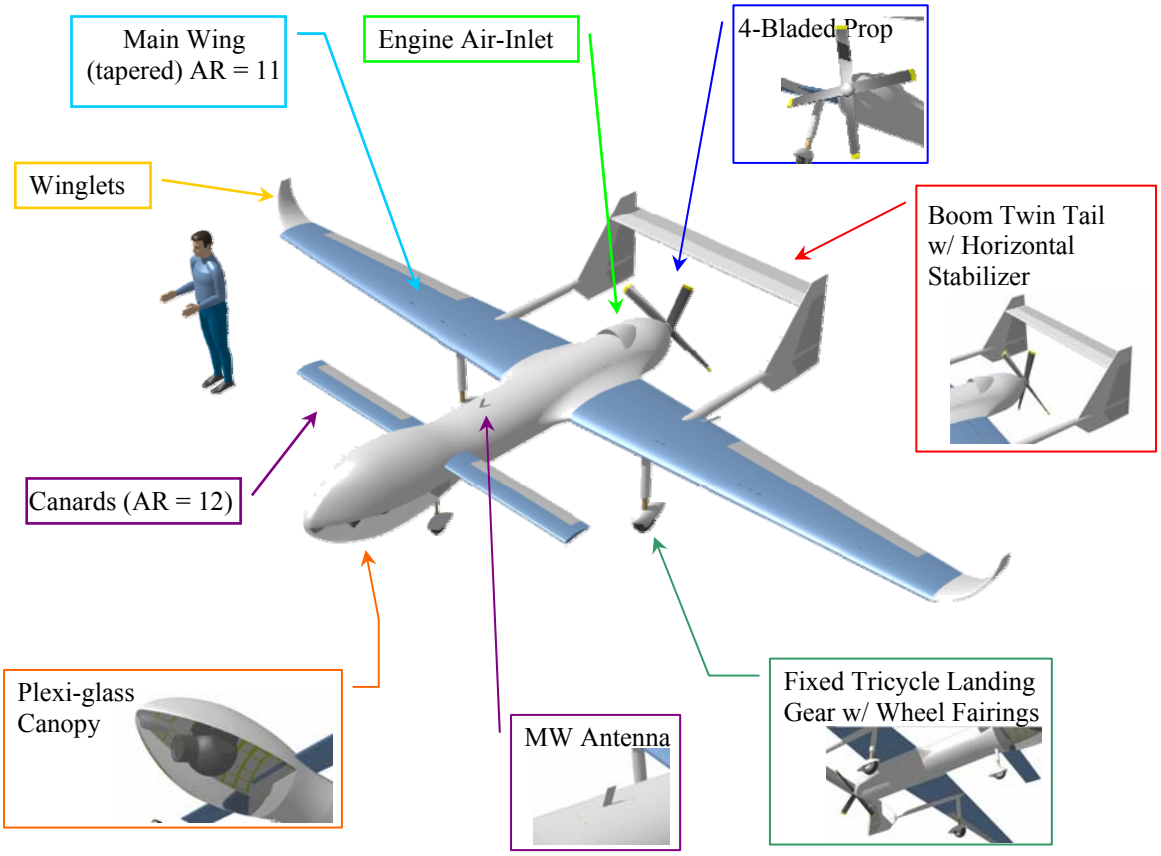

Figure ES.1: Metro-Scout concept layout

In addition, the Metro-Scout UAS will have a competitive acquisition cost of $285,000 and operating costs of just $117/hour including ground crew/operator expenses, far below the current average for news and law enforcement helicopters, and competitively on par with similar UAVs. Team 4's goal with the Metro-Scout UAS is to provide news coverage and law enforcement customers with an intelligently and collaboratively-designed competitive, efficient UAS to achieve mission objectives with less risk, less expenditure, and a greater degree of customer satisfaction.

1.0 Introduction

1.1 Product Definition

The Metro-Scout will be a remotely flown, multi-purpose Unmanned Aerial System designed to operate over highly populated metropolitan environments safely and quietly, in support of the activities of various news agencies and law enforcement departments nationwide. It will be designed to perform continuous area coverage and meet all current FAA regulations for an Unmanned Aerial System operating in airspace over urban areas in the United States. The aerial activities of news and law enforcement agencies have mission requirements that have distinctly different goals, but similar characteristics in terms of endurance, range, and many other aspects. Each type of customer would require different payload load-outs for their type of mission. However, both types of mission load-outs have similar payload weights and set-ups, and therefore, a single airframe can satisfy the mission requirements of both types of customers.

2.0 Business Case Recap

2.1 Customer Attributes

The anticipated primary customers of the Metro-Scout include news agencies and law enforcement departments in urban areas nationwide that currently depend on helicopters and to a much lesser extent, manned fixed-wing aircraft for their aerial operations. The disadvantages of using helicopters are primarily cost-related. Helicopter operations are extremely expensive, with operating costs on the order of several hundred dollars an hour. In addition, putting a crew in the air introduces a risk factor that can result in additional insurance and other miscellaneous expenses.

2.2 Business Strategy

Team 4's business strategy is centered around providing the target customers with a cost-effective alternative to either replacing or supplementing their current helicopter fleets. Team 4 envisions that the introduction of the Metro-Scout will reinvigorate sales in the target market, and open up many new smaller markets for sales that previously could not afford the steep prices associated with helicopter operations. As a result, Team 4 believes that the Metro-Scout will gain marketplace acceptance very rapidly, and outsell the competition within just three years of introduction. The cost-savings and risk-reduction

alone should be enough to convince a number of target customers to use the Metro-Scout for a majority of their operations in order to relieve the pressure on their helicopter fleets.

Table 2.1 below highlights the expected market-share for the Metro-Scout against competing options such as helicopters and other UAVs in three year periods from the start of sales in 2010 through 2021 when product retirement is expected.

According to studies conducted by Helicopter International Association ([3.1], [2.2]), approximately 650 helicopters have been sold to law enforcement agencies, and 250 to news agencies over the past 20 years. The HIA and AOPA reports suggest that the number of helicopters currently in use by the target customers is mostly composed of new sales made in the past 20 years. This allows the team to predict a large number of sales, approximately 75+ a year from 2010 through 2021. As with the introduction of any new technology, Team 4 anticipates that the number of sales will be small right after product introduction. Team 4 predicts 20 sales in the first year of production, 50 in the second year, 75 in the third year and so on. The justification for this expected near-exponential growth in sales is product acceptance in the marketplace as a cost-effective alternative to existing alternatives. Additionally, a number of smaller market customers should see the Metro-Scout as an attractive option for aerial operations, and these smaller market customers should net the Metro-Scout a sizeable proportion of sales.

Period	Market Share (%)	Metro-Scout Sales	Total Sales (Helis + UAVs)
2010 - '12	44.7	145	305
2013 - '15	60.7	345	568
2016 - '18	45.1	295	652
2019 - '21	27.9	160	570
Average / (3 years)	**44.6 %**	**236**	**523**

Table 2. 1: Anticipated Market Share for the Metro-Scout Product

Table 2.1 above, shows that Team 4 expects to have an average market share of 44.7% within the first three years as customers begin to realize the potential that the Metro-Scout offers them in terms of cost-savings, and ease of operations compared to traditional helicopter operations. The market-share should increase quite dramatically to 60% in the

2013-2015 period as the Metro-Scout reaches peak sales due to its increasing attractiveness to the target customers. By 2021, the single year market share should however have dropped to just below 20%. This is because Team 4 anticipates that the market will receive an influx of newer UAV designs aimed at the target customers around 2015-'16 as other manufacturers catch on to the market potential of Team 4's target market. Depending on the actual success of the Metro-Scout, the 2019-'21 period might be the time for the manufacturer of the Metro-Scout to investigate developing and introducing a newer model or a brand new product to compete with the newer UASs that will start to flood the target market.

In summary, Team 4 anticipates that a total market for over 900 sales for the Metro-Scout. This seems like a reasonable figure considering the current size of the helicopter fleet in use by the target customers is nearly 2000. Team 4's business goal is to capture 40% of this existing market size, with sales to newer smaller markets constituting the remaining market-share for the product.

It should finally be noted that Team 4 does anticipate the future use of the Metro-Scout for applications it wasn't specifically designed for, but might be quite reasonably adapted for. For instance, Search and Rescue operations could take advantage of the Metro-Scout's high endurance and range to cover vast stretches of land or ocean. Wildlife film-makers and scientists could find it very economical and efficient to use the Metro-Scout for aerial observation activities – (For example, *Planet Earth* – a mini-series on the Discovery channel made news this year for their ingenious use of helicopter mounted cameras such as the Cineflex V14 to capture stunning aerial wildlife footage). Homeland Security, Traffic observation, forest service use, wildfire observation, climate observation – the possibilities are nearly infinite for the Metro-Scout due to the generic nature of some of its operating capabilities. Predicting the number of sales to these miscellaneous not-designed for users is hard to predict, but a good marketing effort targeted at such potential customers might net a profitable number of sales, beyond those already covered.

3.0 Concept Selection

3.1 Selected Concept

Team 4 has selected a three surface twin tail pusher prop aircraft concept to be the most viable solution for the mission engineering requirements, based on the results from the use of Pugh's method of concept selection. The three surfaces are the main wing, canards up front, and a boom mounted horizontal tail mounted in between two vertical tails.

Shown below is a walk-around view of the selected concept, detailing the layout of the Metro-Scout.

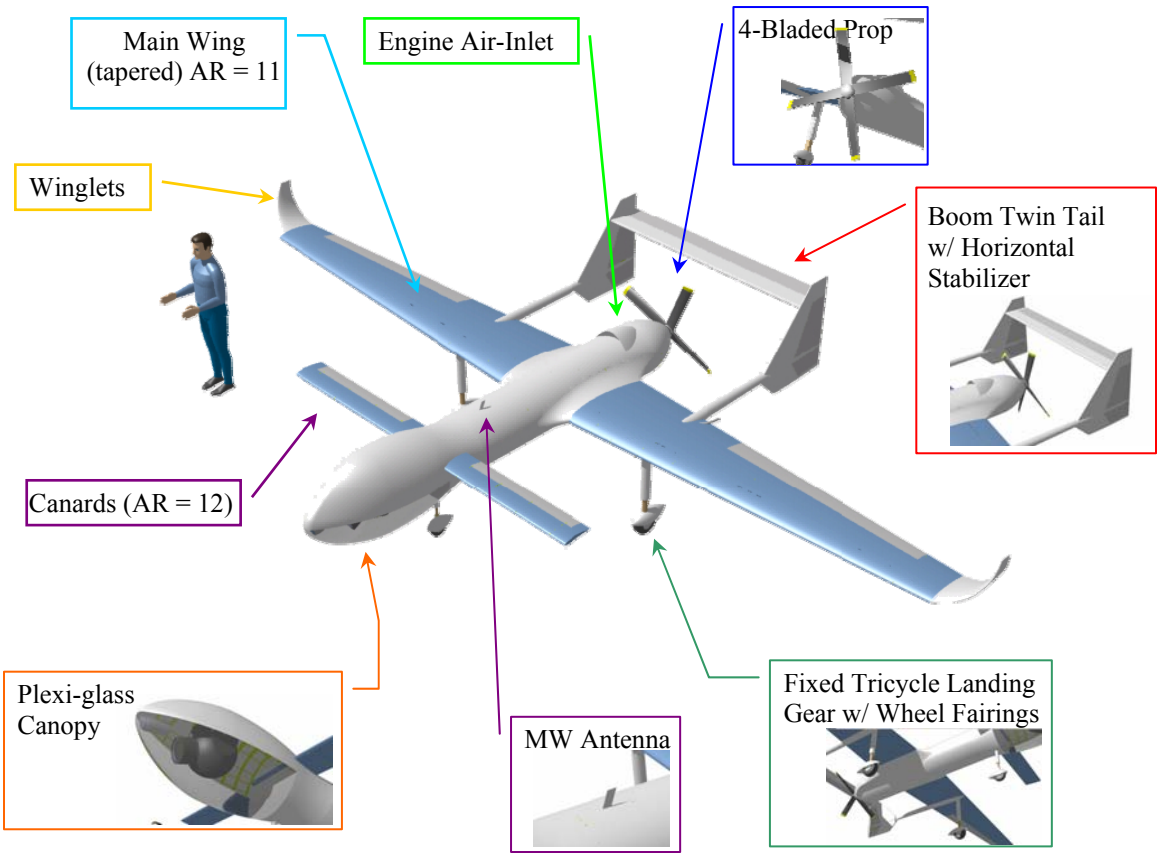

Figure 3.1: CAD walk-around image of the Metro-Scout concept - Note the Canards and Pusher Prop

The external and internal layouts are explained further in sections 3.2 and 3.3 below.

Benefits/Justification of a three surface design:

Since the System Definition review, the Metro-Scout has undergone a major redesign primarily due to tail sizing, and stability concerns. As explained later in the stability and performance section of this report, the need to obtain a reasonable static margin of 10-15% was the primary driving force behind the addition of the aft horizontal tail. One of the lessons learned during this redesign effort was that three surface designs that incorporate canards, main wing and an aft horizontal stabilizer can offer an aerodynamic benefit, because the canard could be designed so that the lift it generated cancels out the negative lift generated from the aft horizontal tail. The benefit is that unlike conventional tailed aircraft, the main wing does not need to be made larger to account for the extra lift needed to counter the negative lift from the aft horizontal tail.

Also, the length of the canard can be reduced, because the aft horizontal tail is also contributing to stability. This reduces the canard's effect on reducing the main wing efficiency. An additional benefit for the Metro-Scout is that the location of the payload, camera, and fuel tank place packaging constraints in terms of the structure. The canards and their associated carry-through structure have to be clear of these other components. Team 4 found that the canard could be located at 4 feet from the nose of the aircraft at the most. To maximize the distance between the main wing and canard for stability, this location of 4 feet was chosen. The benefit of having the three surface design is that the canard and main wing can be close-coupled without the need for a inefficient close-coupled tandem wing configuration. Other aircraft such as the Piaggio Avanti, and the Boeing X-50A dragonfly canard rotor wing demonstrator aircraft have used the three surface design concept to a successful extent.

Another design change since the SDR is that Team 4 has scrapped the single vertical tail concept and gone with a boom-mounted twin vertical tail approximately 6 feet aft of the main wing. Due to sizing concerns, it was found that the vertical tail would need to be over 10 feet high for the aircraft to maintain directional stability due to the close-coupling between the CG and the vertical tail. Pugh's method was used to analyze/conduct a trade-study for five different configurations according to a list of criteria for expected benefits and

negative effects (See appendix A.3 for the Pugh's method excel worksheet) – a single vertical tail, winglets/vertical tails mounted on wingtips, winglets + a single vertical tail, winglets on a swept wing, twin vertical tails mounted on a boom, twin vertical tails mounted on a boom + winglets on the main wing. It was found that the boom mounted twin vertical tails + winglets on the main wing concept provided the most benefits in terms of both parasite and induced drag savings, and height and total surface area required of the vertical tails with minimal weight penalty.

3.2 External Layout

The Metro-Scout is sized based primarily on the following requirements:

(1) To allow all internal equipment such as payload, engine, avionics, and structure to be mounted safely and with ample room to allow easy access for maintenance, and freedom of interference from neighboring equipment.

(2) To allow the positioning of the wings, canards, vertical & horizontal tails and control surfaces to achieve the desired levels of stability, maneuverability, and controllability in all flight conditions.

Figures 3.2 shows the external dimensioning on the Metro-Scout.

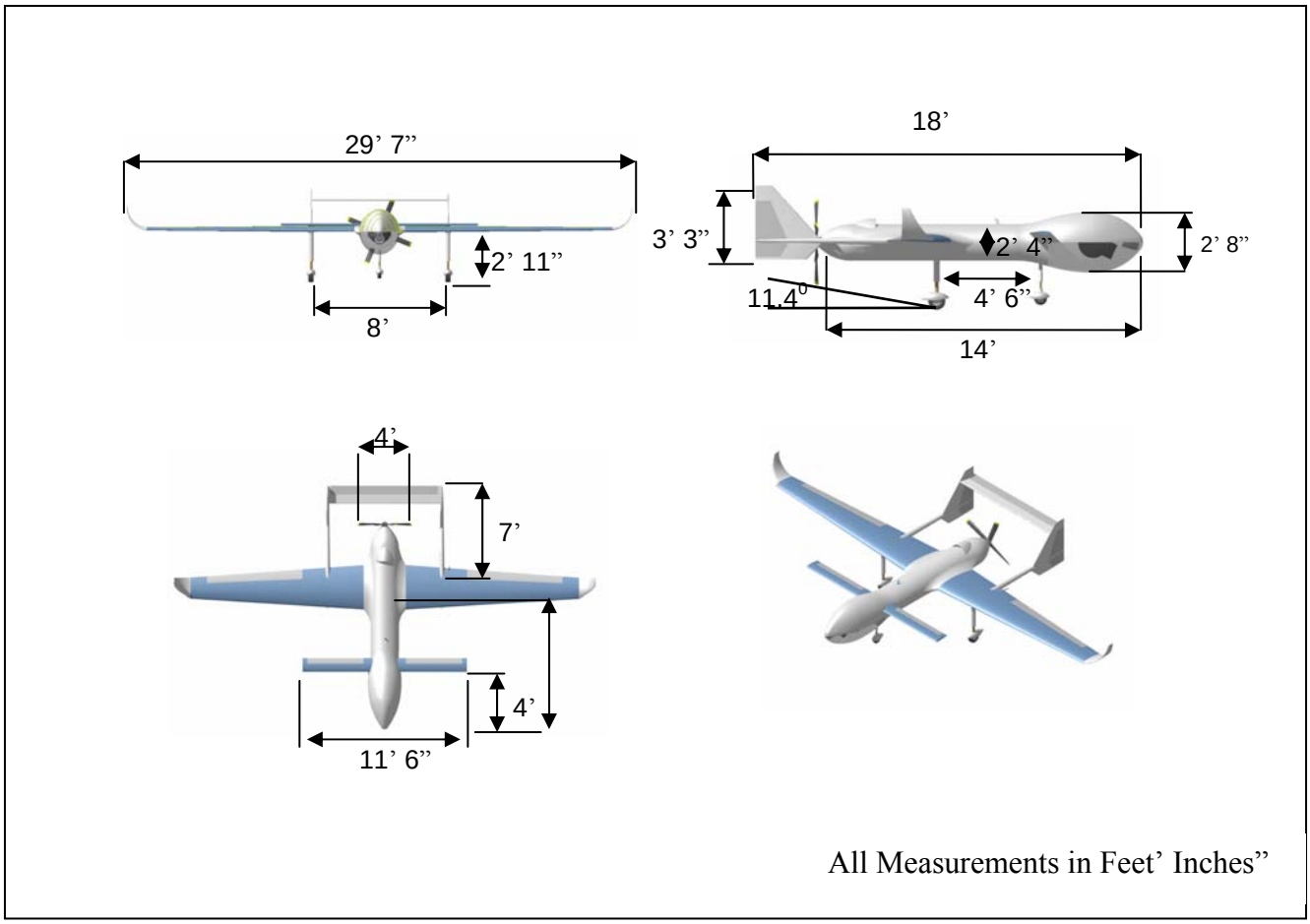

Figure 3.2: Dimensioned 3 view of the Metro-Scout

The main wing, as with most canard aircraft is placed toward the rear of the fuselage in order to position the center of gravity in an optimum location. The engine and propeller are located directly behind the main wing box. An additional benefit of this positioning is that the engine, the vertical tail, and the main wing share a rigid common root support-structure that connects them to the rest of the fuselage.

The main wings are not swept back because the payload weight in the nose provides sufficient ballast to maintain the c.g. within controllable limits so that the engine weight cannot tip the airplane over during rotation for takeoff or landing. This negated the need for wing sweep to move the engine closer to the aircraft center of gravity.

The main wing span is 29.5 feet (including winglets, but 27 feet without) with a root chord of approx. 3.16 feet, and a tip chord of 1.58 feet. Based on the requirements for stability and controllability, the canard was placed at a distance of 4 feet from the nose of the fuselage. The canard span is 115 feet from tip to tip. It is based on a rectangular planform with a chord of approximately 1 foot.

3.3 Internal Layout

The fuselage of the aircraft was designed in three separate parts, each with a different driving force behind the design. The position of the components of the aircraft (payload, canard, transmitter, fuel tank, wing, tail and engine) had already been roughly chosen, so the fuselage was split up according to which components it would need to house. The front section houses the payload and the canard and requires a "bubble" of glass on the belly so that the cameras will not add to drag but still be able to function. The mid section houses the fuel tank and the transmitter and the last section houses the wing box and tail structure.

The front of the fuselage needs to be wide enough to accommodate a 24 inch x 24 inch cube which represents the area in which the largest camera can move. Giving the cube a 2 inch buffer from any point on the fuselage ensures that any vibrations will not cause the camera to hit the glass bubble. The 8 inches of distance between the top of the camera mount and the top of the fuselage allows sufficient space for both mounting structures and wiring. The canards are also placed in this section of the fuselage, located behind the payload. The aerodynamic center of the canard is 3.7 feet behind the nose of the aircraft.

The size of the fuel tank was the driving force behind the design of the next section of the fuselage, between the bubble and the wing. The fuel tank needs to be located outside and in front of the wings because of the wing box, the small thickness of the wing, and in order to move the center of gravity forward. A short and wide tank was chosen so that as the fuel level lowers and the fuel has more freedom of movement, it will not change the c.g. significantly during maneuvering. Also, the fuselage needed to be as skinny as possible in order to reduce surface drag. The final tank size was 13.12 inches x 26 inches x 14inches. This fits into the midsection of the fuselage with a 7 inch clearance on each side and a 5

inch clearance on the top and bottom. This is enough space for structures to mount the fuel tank. The microwave transmitter was also placed in this section, just forward of the fuel tank. This 12 inch x 9inch x 4inch box weighs approximately 11 pounds and will share a mounting platform with the autopilot controller, which is of negligible size and weight.

The last section of the fuselage, which will extend from behind the fuel tank to the trailing edge of the tail will house the wing box and tail structure. Neither of these has been designed yet but they are anticipated to require that the size of the fuselage will be larger than the fuselage surrounding the fuel tank and microwave transmitter. Though it is modeled as an inboard engine in the Catia model, a decision has been made to mount the engine outside of the fuselage in order to use the air to cool it.

Figure 3.3 is a cutaway view of the Metro-Scout that illustrate internal component placement on the Metro-Scout.

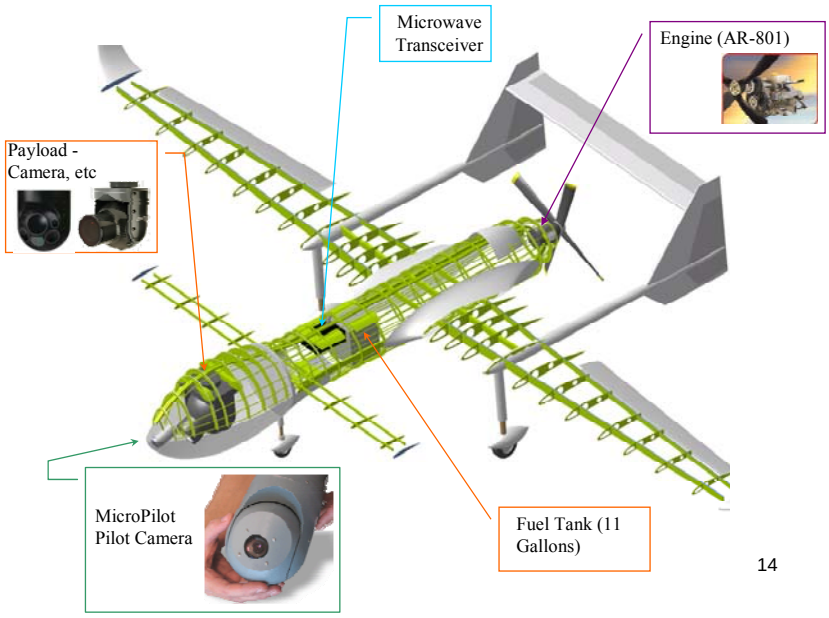

Figure 3.3: Inboard Layout

4.0 Payload

Different payloads are required for the different missions designed for the law enforcement agencies and the news agencies. These payloads were created based on the concept of operations described above and the different customer attributes requested.

Table 4.1 lays out exactly what pieces of equipment are compiled to make up the payload package that will be sold to law enforcement.

Package	Payload	Weight(lb)	Dimensions(ft)
Police package	Radar gun	1	0.5 x 0.19 x 0.45
	Camera gimbal	51	.92 x 1.25
	ThermaCAM SC3000 Sony DSR-PD150 (video cam) Canon powershot S3 IS (still camera)	7 3.1 0.9	mounted on gimbal mounted on gimbal mounted on gimbal
	Canon lens f/4.5-5.6 II USM	0.7	on camera
	Autopilot	0.2	.34 x .17 x .14
	Total weight	64	

Avionics and transmitter Power Requirements

Computer (kW)	75
Mircrowave transmitter (kW)	52
Total power requirement (kW)	419.5

Table 4.1: Payload Package for Law Enforcement[4.2],[4.3],[4.4],[4.5],[4.6],[4.7],[4.8]

During highway patrols for speeding vehicles, the Metro-Scout will fly at the speed limit set for the highway and any car moving faster than the UAV will trigger the radar gun to record the exact speed of the speeding vehicle. This in turns triggers the still camera to snap a picture of the vehicle's license plate. Law enforcement officers can then issue the violators a ticket and mail it to them.

In search and rescue operations, the video camera, infrared and still camera will work in tandem with one another. If the infrared camera detects a possible target, the video and still cameras will be used to positively identify the target. These images are then sent back via live feeds through a transmitter.

The radar gun has an accuracy of 1.25 miles per hour and is able to measure a target speed moving in a co-direction takes place if the speed difference is varied from 2.5 up to 62 miles per hour. It is also not important where the target is located – in front of UAV is or behind the UAV, the UAV catches up with target or the UAV is left behind target - in any case the correct evaluation of a target speed is guaranteed by Semicon. This lightweight radar gun of less than 1 pound will be placed on the UAV and feed back information on traffic violators.

The Camera gimbal has a 4-axis gyro stabilized video system. It is able to rotate 360 degrees and track stationary and moving targets from up to 3000 feet. [4.3] The camera operator can control the gimbals' system which then transmits the video feeds and still images through microwaves back to the ground.

The ThermaCAM is an infrared camera coupled with its software can provide live feeds of an extensive temperature range. It is able to measure extremely small and distant targets with great accuracy (±1%) and high resolution. [4.4] This will assist law enforcement in criminal pursuit during the day and even at night. In the event that the suspect is hidden from the regular view of a regular camera, the infrared can still detect the heat signature of the suspect. This infrared camera is also relatively light at seven pounds, providing an additional capability which aids the capture of criminal suspects.

Most importantly, a video camera is also mounted on the gimbal. The Sony DSR-PD150 has a build in image stabilizer with a 12 X optical and 48X digital zoom. [4.5] This camera will be able to provide close up aerial videos from the air. This camera is also very light weighing only 3.1 pounds.

A high resolution still camera is also essential for law enforcement agencies. The Canon powershot S3 IS will be equipped with a 50-200 millimeter lens that will be able to take high resolution still images of license plate numbers from up to a distance of 3000 feet. [4.7] This camera can also be used by law enforcement to take high quality pictures of evidence against fleeing suspects.

The autopilot's software for the UAV is capable of flying at a Maximum Altitude of 16,000 feet above sea level and a maximum airspeed of 150 miles per hour. It comes with a transmitter to broadcast airspeed, pressure and temperature to the ground in compliance with FAA regulations.

The payloads for the news stations are as follows:

Package	Payload	Weight(lb)	Dimensions(ft)
News Station/filming package	Cineflex V14	67	1.21 X 1.63 X 1.63
	Autopilot	0.1875	0.34 X 0.17 X 0.14
	Total weight	67.1875	

Power Requirements

Computer (kW)	75
Microwave transmitter (kW)	52
Total power requirement (kW)	447

Table 4.2: Payload Package for News Agency [4.8],[4.9]

The camera for the news station allows for high definition live video feeds. This camera weighs more than the entire payload for the law enforcement as it is a high definition filming camera mounted on a gimbal, but the 67lbs includes the weight of the gimbal. The Cineflex camera is also currently mounted on helicopters and also used for filming movies. The built in wide angle view and infrared cameras allow for filming at all times of the day. Lastly, the Cineflex also has a 25X zoom enabling aerial footages to be filmed from up to 3000 feet. [4.9]

This summary of the total aircraft power requirement equates to 0.56 horsepower for the police package and 0.6 horsepower for the news and filming package. However, the entire

payload is not consuming power when the Metro-Scout is in operation. This power required for the payload will be taken from the engine's generator. In an event of an engine failure, batteries would be used instead to control the avionics in order to get the Metro-Scout to safety.

5.0 Constraint Analysis

5.1 Constraints

The performance analysis, in most cases, answers the question of whether a particular aircraft design will meet a customer's needs. The process of constraint analysis is to narrow down the choices of the many interrelated variables to control and make choices to which to design an aircraft such that it will have the desired performance capabilities. Constraint analysis provides ranges of values for an aircraft concept's take-off wing loading and take-off power loading, which allow the design to meet specific performance requirements.

The constraint analysis is based on a modification on equation 5.1 for specific excess power

$$\frac{T}{W} = \frac{D}{W} + \frac{1}{V}\frac{dh}{dt} + \frac{1}{g}\frac{dV}{dt} \qquad 5.1$$

In equation 5.1, T/W is the thrust to weight ratio, D is drag, V is velocity, dh/ht is the altitude derivative and dV/dt is the velocity derivative. By substituting equations 5.2, 5.3, 5.4 and 5.5 into equation 5.1, the new constraint equation is stated in equation 5.6.

$$T = \alpha T_{SL} \qquad 5.2$$

$$W = \beta W_{TO} \qquad 5.3$$

$$C_L = \frac{L}{qS} = \frac{nW}{qS} \qquad 5.4$$

$$D = C_D qS = (C_{D0} + \frac{C_L^2}{\pi A \mathrm{Re}})qS \qquad 5.5$$

$$\frac{T_{SL}}{W_{TO}} = \frac{\beta}{\alpha}\left\{\frac{q}{\beta}\left[\frac{C_{D0}}{(W_{TO}/S)} + \frac{1}{\pi A \mathrm{Re}}\left(\frac{n\beta}{q}\right)^2\left(\frac{W_{TO}}{S}\right)\right] + \frac{1}{V}\frac{dh}{dt} + \frac{1}{g}\frac{dV}{dt}\right\} \qquad 5.6$$

In equation 5.2, α is the thrust lapse ratio which depends on the density ratio ρ/ρ_{SL}. In equation 5.3, β is the weight fraction for a given constraint. This fuel fraction is necessary

because the weight loss from the fuel has to be taken into consideration at every moment throughout the flight. Equation 5.4 is the equation for the lift coefficient. Equation 5.5 is the drag equation based on the lift coefficient found in equation 5.4. Equation 5.6 is the newly defined power equation for take-off weight. [3.1]

5.2 Takeoff Constraint

While equation 5.6 models in-flight performance, the takeoff constraint requires a different equation. Assuming $V_{TO} = 1.2V_{stall}$, equations 5.7, 5.8, and 5.9 are written below.

$$V_{TO} = 1.2\sqrt{\frac{2W_{TO}}{\rho S C_{L\max}}} \qquad 5.7$$

$$t_{TO} = \frac{1.2W}{\{g[T - D - \mu(W_{TO} - L)]\}^2}\sqrt{\frac{2W}{\rho S C_{L\max}}} \qquad 5.8$$

$$s_{TO} = \frac{1}{2}at_{TO}^2 = \frac{1.44W_{TO}^2}{\rho S C_{L\max} g[T - D - \mu(W_{TO} - L)]} \qquad 5.9$$

Rewriting equation 5.6 using equations 5.7, 5.8 and 5.9, equation 5.11 is the new power equation in terms of power loading, equation 5.10, and wing loading.

$$\frac{P}{W_{TO}} = \frac{T_{SL}}{W_{TO}}\left(\frac{V_{TO}}{550\eta_p}\right) \qquad 5.10$$

$$\frac{T_{SL}}{W_{TO}} = \frac{1.44\beta^2}{\alpha\rho C_{L\max} g s_{TO}}\left(\frac{W_{TO}}{S}\right) + \frac{C_{D0}q}{\beta(W_{TO}/S)} + \mu \qquad 5.11$$

The unit of power in the above equation is horsepower. These equations also assume that lift is approximately zero prior to rotation. [3.1]

5.3 Sustained Turn Constraint

Maximizing thrust loading and lift to drag ratio (L/D) maximizes the load factor in a sustained turn. At max L/D, the coefficient of drag is C_{D0}, therefore deriving equation 5.12.

$$\frac{W}{S} = \frac{q}{n}\sqrt{\pi A \mathrm{Re} C_{D0}} \qquad 5.12$$

Equation 5.12 is the wing loading equation for the max range and max propeller loiter for a propeller aircraft. This equation proves that as weight reduces due to fuel burned, the wing loading also decreases during cruise. Optimizing cruise efficiency while wing loading is decreasing requires the reduction of the dynamic pressure by the same percent as seen in equation 5.12. The concept of max L/D and the above wing loading equation yields equation 5.13; the available thrust equation. [3.1]

$$\frac{T}{W} = \frac{qC_{D0}}{W/S} + \frac{W}{S}\left(\frac{n^2}{q\pi Ae}\right) \qquad 5.13$$

5.4 Landing Constraint

The landing constraint determines the maximum value of wing loading of the UAV. The maximum wing loading bounded by the landing constraint is calculated from the landing constraint equation below.

$$\frac{W}{S} = \frac{d_{land}\rho C_{L\max} g\mu}{1.68\beta} \qquad 5.14$$

In equations 5.14 d_{land} is the landing distance, μ_{land} is the friction coefficient when landing, β is the landing weight fraction (W_{land}/W_o).

5.5 Constraint Results

By running MATLAB code developed by team members, the group determined a design point for power loading and wing loading. Figure 5.1 shows this design point in terms of a specified power loading and wing loading value. [3.1]

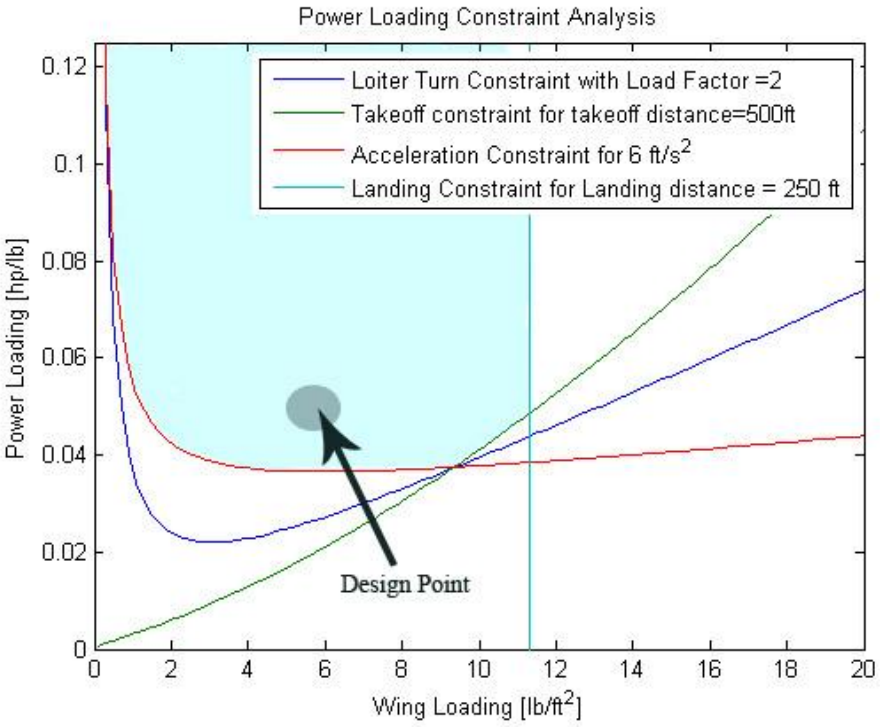

Figure 5.1: Power Loading Constraint Analysis

This point represents a ratio of power loading to wing loading that best blends the loiter turn, max speed turn, and takeoff constraints. It does not necessarily optimize any of these constraints, but rather suggests a point where changing one constraint would adversely affect another. Table 5.1 below, shows the optimum design point.

Power Loading	0.0525 hp/lb
Wing Loading	5.9 lb/ ft^2

Table 5.1: Power Loading and Wing Loading Data

The driving constraints were the acceleration and the max-speed turn load factor constraints. The driving constraints determined the power loading and wing loading of the UAV. The non-driving constraints are also shown in figure 5.1 to demonstrate the capability of the UAV.

	Mission Requirement	Value Achieved
Acceleration for loiter to max speed	6 ft/s^2	6 ft/s^2
Take-off distance	1500 ft	250 ft
Load Factor	2g	2g
Landing Distance	1500 ft	250 ft

Table 5. 1 : Performance Capability

5.6 Sizing

Sizing is the process to determine how large the aircraft must be to carry enough fuel and payload to be able to loiter for up to five hours and to take surveillance for new agencies and law enforcement. A crude estimate of the maximum L/D is obtained. Specific fuel consumption is dependent on the engine chosen for the UAV which is discussed in section 6. SFC ($C_{hpb)}$ was taken to be 0.52 and 0.56 lb/hp/hr for cruise and loiter respectively [6.1]. C_{D0} was obtained from the wetted area calculated for the estimated shape of the UAV. Since empty weight is calculated using a guess of the takeoff weight, it is necessary to iterate towards a solution. The initial empty weight fraction was obtained from regression analysis on historical similar UAVs. The empty weight is an estimation of combination of all component weight uncertainties. Equation 5.15 is the actual equation used to determine the empty weight fraction of the Metro-Scout.

$$\frac{W_e}{W_0} = -0.1 + 0.71 W_0^{-0.13} AR^{0.085} Powerloading^{0.08} Wingloading^{-0.05} V_{MAX}^{0.21} \qquad 5.15$$

The results from the MATLAB program, developed by the team, to calculate the total takeoff weight is shown in table 5.2.

	Value Inputted
Power loading	0.0525 hp/lb
Wing loading	5.9 lb/ft^2
SFC for cruise	0.6 lb/hp.hr
SFC for loiter	0.56 lb/hp.hr
AR	11
L/D	16
C_{D0}	0.0239
η_p	0.75
Oswald's efficiency	0.75

Table5.2 : Inputs of Sizing Program

5.7 Fuel Fraction for Cruise and Loiter

The gross weight equation is based on the fuel fraction and the empty weight fraction. Both of these equations are based on L/D. The L/D equation shown in equation 5.16 is derived on the premise that C_{D0} is .0239, *AR* is 13, and *e* is 0.75. This equation is also under the assumption that V_{loiter} is 73ft/s and V_{cruise} is 176 ft/s.

$$\frac{L}{D} = \frac{1}{\left[\frac{qC_{D0}}{(W/S)} + \frac{W}{S}\frac{1}{q\pi A\mathrm{Re}}\right]} \qquad 5.16$$

The fuel fraction and weight equations derived from the Breguet equation for cruise and loiter, used to find the gross weight, are shown in equations 5.17 and 5.18 respectively.

$$\frac{W_i}{W_{i-1}} = \exp\left[\frac{-RC_{bhp}}{550\eta_p(L/D)}\right] \qquad 5.17$$

$$\frac{W_i}{W_{i-1}} = \exp\left[\frac{EVC_{bhp}}{550\eta_p(L/D)}\right] \qquad 5.18$$

In these equations *R* is range, *E* is endurance, C_{bhp} is the specific fuel consumption for propeller aircraft. η_p is the propeller efficiency. The *i* index in the above equations is the segment number. In any given flight there are multiple segments. For example, in a normal flight, the loiter segment would by i=4 after the take-off (i=1), climb (i=2), and cruise (i=3).

The aircraft weight is calculated throughout the mission. For each segment the aircraft weight is reduce by fuel burned. Total fuel burned is calculated throughout the mission and found by summing the weight fractions from each flight segment in equation 4.19.

$$W_{fuel} = 1.06\left(\sum_{i}^{x} W_{fi}\right) \qquad 5.19$$

In equation 5.19, 6% of extra fuel is added for landing, takeoff, taxi and reserve. Equation 5.20 is the takeoff weight equation.

$$W_0 = W_{pay} + W_{fuel} + \left(\frac{W_e}{W_0}\right)W_0 \qquad 5.20$$

This equation is a summation of the different weights calculated from the various fuel fractions. [3.1]

Using data collected from the above analysis, table 5.4 is a compilation of the initial sizing results.

Total Aircraft Takeoff weight	378 lb
Fuel Weight	67 lb
Payload Weight	67 lbs
Power Required	31 HP
Wing Area	69 ft^2

Table 5.4: Sizing Data

5.8 Carpet Plot

The carpet plot shows a direct relationship between gross take-off weight, and a range of wing loading and power loading. It also provides estimates of the gross take-off weight with variants in wing loading and power loading. The carpet plot is generated by inputting a range of wing loading and power loading values into the sizing MATLAB code developed by the team.

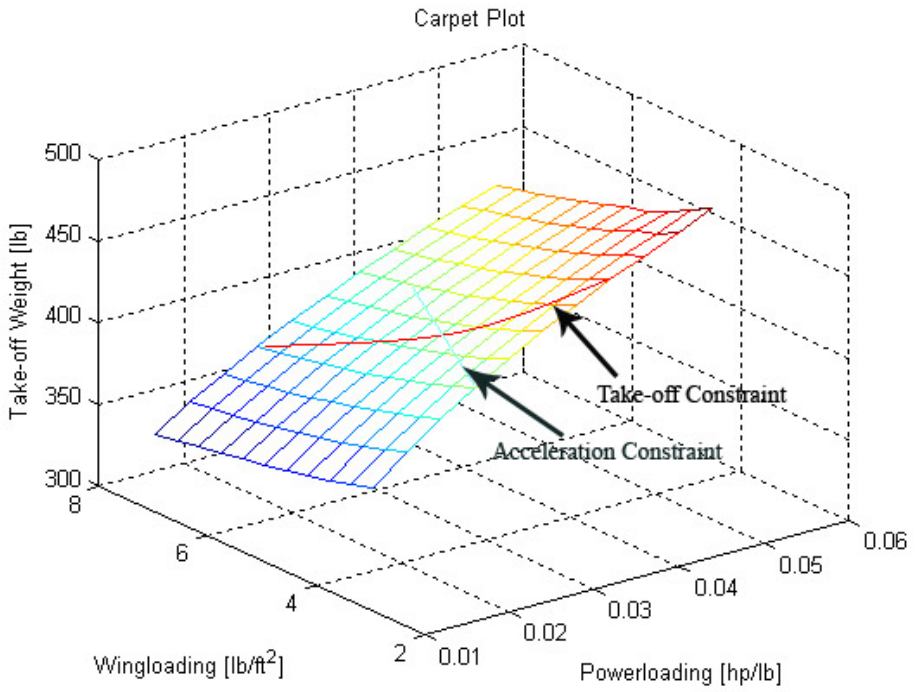

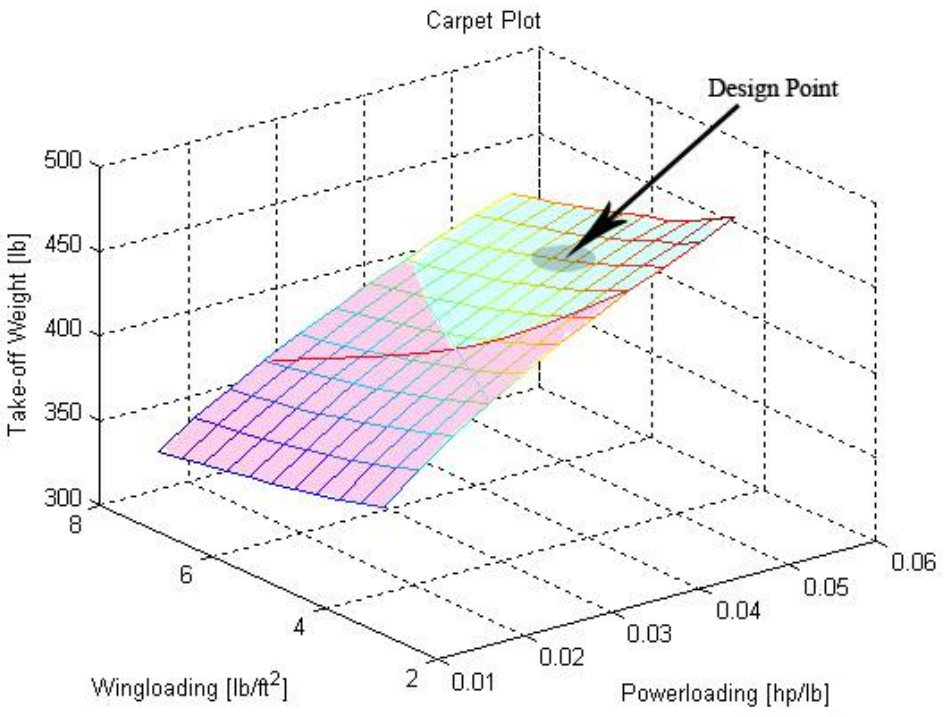

Figure 5.2 Carpet Plot

5.9 Design Trade-offs

Each of the three plots in Figure 5.2 represents different endurance time with constant coverage radius of 200 nm. The plots illustrate that takeoff weight increases as endurance increases. The design endurance, stated in the mission target, was 5 hours. Plots for 3 hour and 7 hour endurance time demonstrate how much the take-off weight will increase or decrease as a function of endurance.

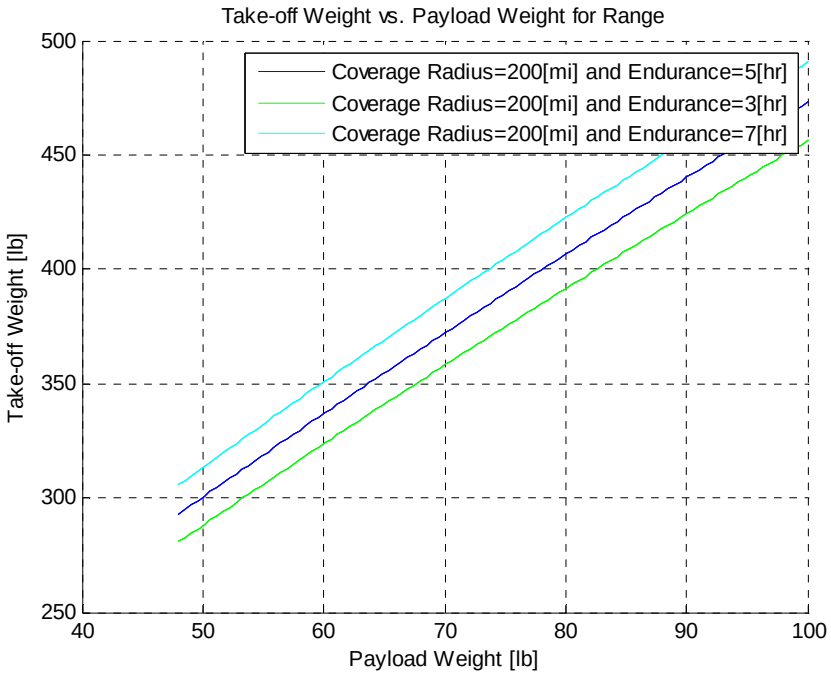

Figure 5.3: Takeoff Weight vs. Payload Weight

Figure 5.4 displays the variance in endurance with takeoff weight. Although current design of the Metro-Scout only carry a payload of 67lb, Figure 5.4 shows two plots with different payload to illustrate variation in takeoff weight with different payload weights. Takeoff weight increases quite linearly with endurance.

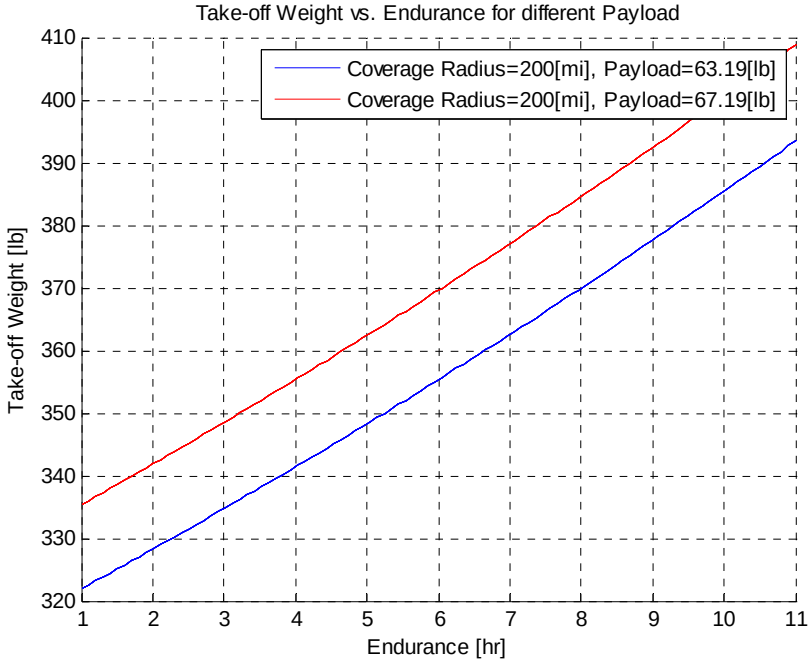

Figure 5.4: Takeoff Weight vs. Endurance

5.10 Aspect Ratio Analysis

By generating carpet plot for a range of aspect ratios, and taking the lowest talk-off gross weight for each aspect ratio, a plot of the take-off gross weight versus aspect ratio is shown below.

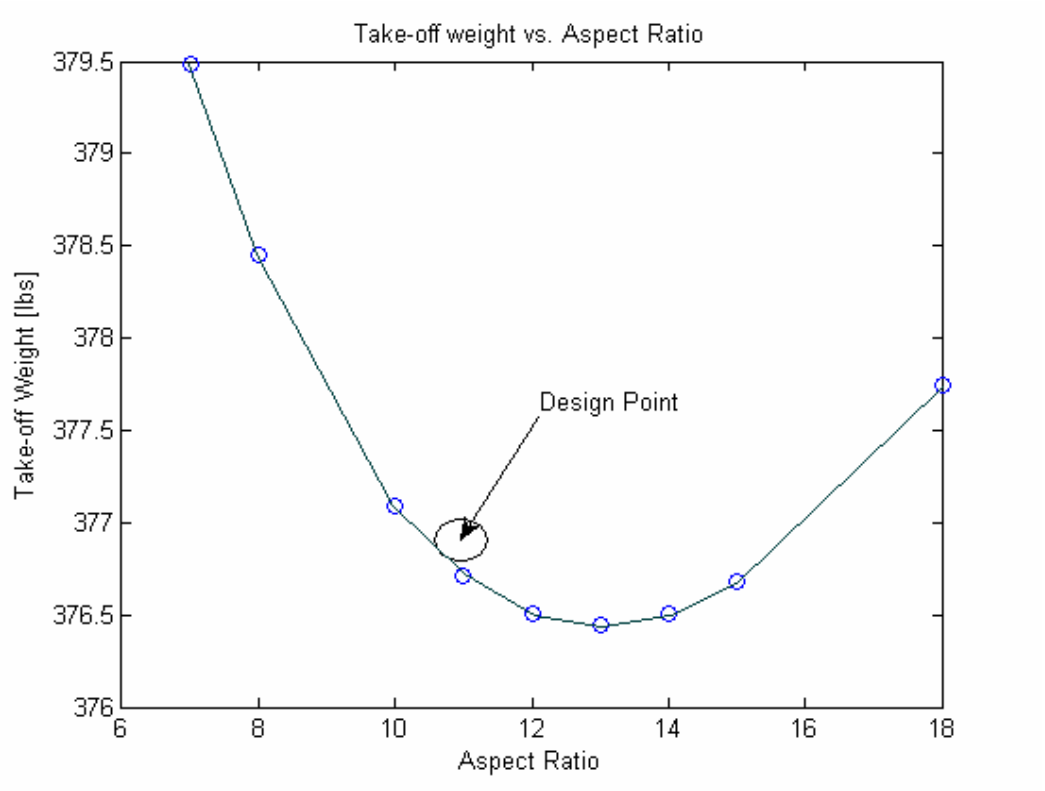

Figure 5.4 Take-off Weight versus Aspect Ratio

The plot shows the optimal aspect ratio at 13. Team 4 has chosen the final aspect ratio for Metro-Scout is 11 because of the advantage in storing and transporting the UAV with a lower wing span with the cost of 0.5lb weight increase was an affordable trade-off.

6.0 Propulsion System

The propulsion system for the Metro-Scout is a pusher piston propeller engine as mentioned in section 3.1. To reiterate, it will be best located at the back of the airplane thus making it a pusher propeller type. This configuration is the best for the Metro-Scout because the camera part of the payload is in the nose. The propeller blades need to be out of the line of site of the camera. Placing the propulsion system in the front of the aircraft would not only obstruct the

view of the camera but it would also create very turbulent flow around the camera creating extra vibrations and noise that will distort the picture.

6.1 Engine Selection

The initial horsepower requirement of the engine, 40 brake horsepower, was determined based on the weight, endurance, range, max speed, and power loading constraints of the UAV. This value was then taken to the UAV database to find off-the-shelf engines that met the power requirement. Table 6.1 shows the list of engines that were initially considered.

Engine	Lightening Aircraft Engines 604D4-F1	AR 801	AR 801R	Rotax 503	Rotax 582
Power (bhp)	50 +	35-60	51	45.6-49.6	53.6-65
RPM	6500	8000	8000	6800	6800
SFC		0.56	0.57		
Weight (lbs)	41	43	56		

Table 6.1: Engine List [6.1][6.3]

The AR-801 is a Wankel-type rotary, single rotor engine with a capacity of 294cc, brake horsepower of 35-60bhp at 8000RPM, and a specific fuel consumption of 0.56 at max power. It was chosen for its size, weight, specific fuel consumption and brake horsepower. The AR-801 engine has dimension of 1foot x 1.06 feet x 0.82 feet. This engine is known to be a highly optimized, light-weight, single rotor, liquid cooled engine. It is designed such that the mounting of alternators between 0.9 and 2.0 KW is feasible. It has been designed and developed specifically for UAVs requiring 35 to 60 bhp, with direct drive to propeller or vehicle gearbox. Other engines built by the same company are currently being used in other UAVs such as the RQ-6 Outsider and RQ-7 Shadow-200. [6.2] Below is a list of the major advantages to the use of this particular engine. Figure 6.1 is a picture of what the AR-801 engine looks like with 4 blades. This is currently the chosen engine for the Metro-Scout.

Figure 6.1: AR-801 engine [6.1]

Use of an AR-801 engine: Advantages:

Team 4 has chosen the AR-801 UAV engine for the Metro-Scout for the following reasons:

(1) *High Power to Weight Ratio*: A larger power to weight ratio allows for better speed control and maneuverability of smaller aircraft. It also helps to decrease the overall weight of the aircraft but still producing enough power to meet the power requirement.

(2) Economic Fuel Consumption: An economic fuel consumption allows for the aircraft to fly farther per gallon of fuel used. This in turn can increase the endurance time and range of the aircraft, thus allowing for more continuous area coverage.

(3) Low Levels of Vibration: Vibration levels are extremely important when dealing with aircraft design. The lower the levels of vibration, the less stress acts on the aircraft. In the instance of the Metro-Scout, this means that although there is more stress on the tail section, overall there is less stress on the aircraft as a whole.

(4) Low Cross Sectional Area: The low cross sectional area of the AR-801 engine helps to decrease the amount of drag that is produced. On the Metro-Scout the engine is not streamlined into the fuselage, it is in fact, a separate entity that it attached to the back of the tail section. In most cases the pusher prop engine creates a large amount of drag, but the lower the cross sectional area of the engine, the less it sticks out around the fuselage, and less additional drag is created.

(5) *Long Life:* Although the lifespan of the engine is not a requirement, it is a definite advantage for the engine to have a longer lifespan so that it doesn't have to be replaced often. Replacing engines is extremely expensive and time consuming.

This engine type supports a variable pitch propeller. The variable pitch makes it possible for the pilot to change the blade angle of the propeller at will in order to obtain the best performance of the aircraft engine. At take-off the propeller is set at the low blade angle so that the engine can attain the max allowable power and rpm. Shortly after take-off the angle is increased slightly to prevent overspeeding of the engine and to obtain the best climb conditions of the engine rpm and aircraft speed. When the aircraft has reached cruise or loiter altitude, the propeller can be adjusted to a comparatively high pitch for low cruising rpm. This would allow for the Metro-Scout to be much more adaptable to flight conditions in the instance of a high speed chase. [6.4]

6.2 Propeller Sizing

Although the engine came with a known size of propeller blades, they were too long for the current design of the Metro-Scout. The blades would have struck the ground on take-off and so in order fix this problem, the propeller blades were sized using the following method.

Using the power required, many other parameters and specifications of the engine were calculated. The advance ratio and the activity factor are two very important parameters when understanding the blade design of the propulsion system. The advance ratio, found in equation 6.1, is just based on velocity, rotational speed and diameter of the blades.

$$J = V/nD \tag{6.1}$$

The advance ratio, much like the wing angle of attack, is the related distance the aircraft moves with one turn of the propeller. The advance ratio for the Metro-Scout is 0.1875. The activity factor is a measure of the effect of blade width and width distribution on the propeller and is a measure of the propeller's ability to absorb power. Equation 6.2 is the equation of the activity factor per blade.

$$AF_{perblade} = \frac{10^5}{D^5} \int_{0.15R}^{R} cr^3 dr \tag{6.2}$$

The average activity factor for small, light aircraft is approximately 100. The activity factor for the blades on the Metro-Scout is 97.

Equation 6.4 below shows how the thrust required was obtained. The coefficient of thrust (c_T) was found using the propeller polar relation, shown in equation 6.3 and figure 6.2, between the power coefficient and thrust coefficient.

$$\frac{c_T}{J^2} = m\frac{c_P}{J^2} + b \tag{6.3}$$

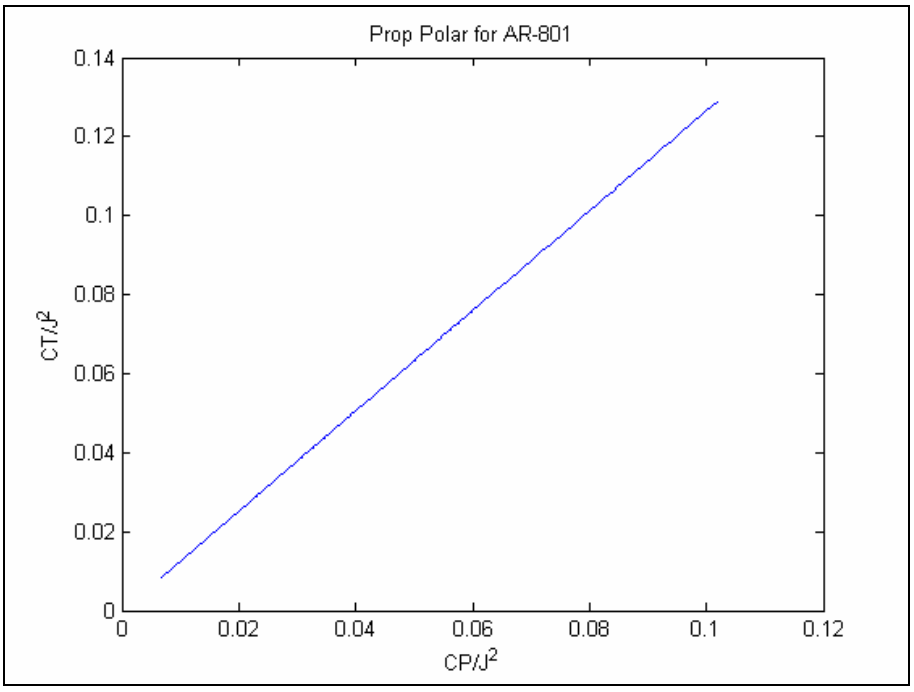

Figure 6.2: Propeller Polar Plot for AR-801 Engine

In equation 6.3, m and b are the slope and y-intercept of the propeller polar plot. The power coefficient (c_P) was found, seen in equation 6.4, since the power required was already known.

$$P = c_P \rho n^3 D^5 \tag{6.4}$$

$$T = c_T \rho n^2 D^4 \tag{6.5}$$

In equations 6.4 and 6.5, ρ is the density of air at sea level, *n* is the rotation speed, and *D* is the propeller diameter. From the thrust equation, equation 6.5, the propeller efficiency was calculated to be 0.76 in equation 6.6. [3.1]

$$\eta_P = \frac{TV}{550 * bhp} \tag{6.6}$$

6.3 Inlet Sizing

The inlet was sized under the assumption of isentropic flow at the front of the engine, and the isentropic flow tables were used to obtain the following data. Cruising at 1500ft on a standard day was another assumption that gave an inlet temperature and pressure of 278.4 K and 84.6 kPa respectively. Using the isentropic relations shown in equations 6.7 and 6.8, the stagnation temperature was found to be 278.7 K and the stagnation pressure was 84.9kPa.

$$P_1^0 = P_1(1 + \frac{\gamma - 1}{2} M^2)^{\frac{\gamma}{\gamma - 1}} \tag{6.7}$$

$$T_1^0 = T_1(1 + \frac{\gamma - 1}{2} M^2) \tag{6.8}$$

These values were calculated at γ = 1.4 and a Mach number of 0.16, which is equivalent to 106kts at cruise. Using area ratios, a known power of 40bhp and an SFC of 0.56, the area needed for the inlet is 25.04 in^2. As seen above in the current concept design, the inlet is a semi circle mounted at the front of the engine at the back of the fuselage. This design was chosen because it will allow for the most amount of air to flow freely into the engine.

6.4 Exhaust System

The next step in the design process of the propulsion system is an exhaust system to reduce the amount of noise created by the pusher-prop engine. In the past, pusher-prop aircraft have had trouble because the exhaust leaving the engine goes straight through the propellers, which creates more noise than if the airplane had a tracker engine. The object of this exhaust system is to keep the air free flowing through a piping system that has smooth bends, i.e. mandrel bent and to keep the air away from the propeller blades to reduce the noise. This system is still under development.

7.0 Aerodynamic Analysis

7.1 Airfoil Selection

In selecting an airfoil, the aircraft design requirements must be found, such as how it should perform and how it should handle. In general, a higher section coefficient of lift (c_l) causes in a higher section coefficient of moment (c_m) during cruise. [7.1] As a result of this pitching moment, the canard must, in turn, provide necessary lift to balance the nose down effect which in turn leads to a higher trim drag.

From the customers and mission requirements, a loiter speed of 50miles per hour and maximum speed of 120 miles per hour were below 130 miles per hour at which NACA airfoils are proven to work. Because of this, the analysis was done using 4-digit NACA airfoils. The 4-digit series was also chosen due to its small center of pressure movement across a large speed range. [7.1]

The main criteria of the airfoil selection were a high c_{l0} and a high c_{lmax} with c_l over coefficient of drag (c_{di}) and c_m as secondary requirements. This was because of the need for a high c_{l0} to cruise efficiently without requiring a larger planform area at the required loiter velocity of 50 miles per hour. A high c_{lmax} would provide a higher wing loading for a shorter takeoff distance and for a better sustained turn rate. [7.2] A low pitching moment close to zero about the aerodynamic center would lower trim drag induced by the canard. This, however, can be adjusted by adding counter weights such as payloads or varying the location of the fuel tank in the fuselage to minimize this effect.

The analysis was done with varying camber, while the location of the camber from the leading edge remained constant at 40% chord length and the thickness remained at 12% chord length.

As the location of the camber from the leading edge increased, c_l increased, thus the location of the camber from the leading edge was picked to be as far back as possible. However, to maintain a small coefficient of moment, we need to keep the location close to the first quarter of the chord.[7.3] Therefore a compromise was reached in picking a camber

at 40% chord length which has a reasonably low pitching moment and provides high c_l values.

When airfoil thickness increases, the c_l values increase. However, c_l values stop changing significantly after 12% thickness to chord for NACA 4-digit airfoils. [4] Since a greater thickness to chord ratio increases drag and the wings of the UAV are not going to store fuel, an airfoil thicker than 12% chord is not practical. Thus a thickness of 12% chord was chosen.

The following four graphs were plotted from the output of XFOIL. Assumptions made include a Reynolds number, Re, of a constant 2.3E5 and a Mach number, M, of constant 0.0663.

Plots of c_l versus alpha for five airfoils with increasing camber are shown in Figure 7.1. This graph allows us to identify the c_{lmax} of the various airfoils which is the maximum point for the five plots.

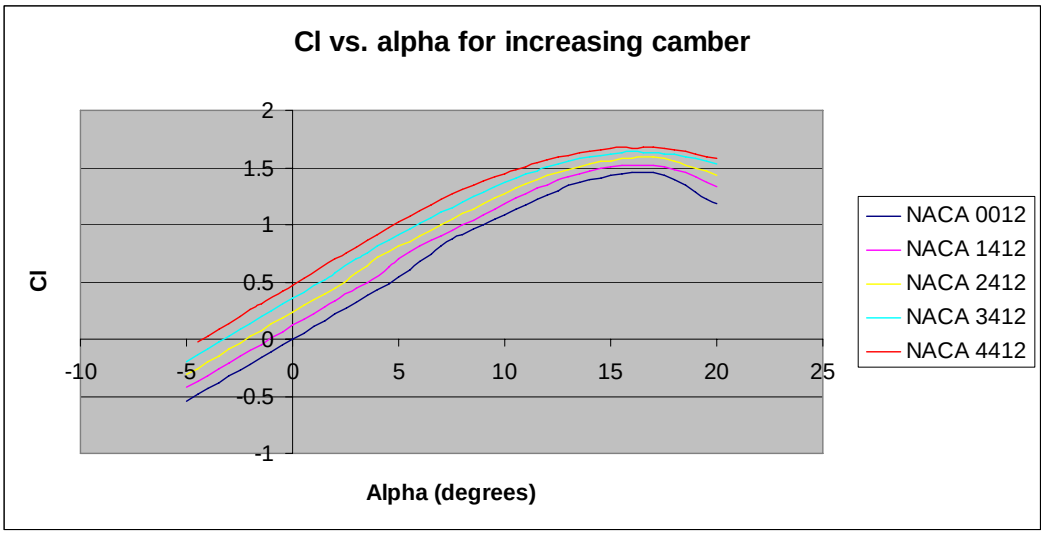

Figure 7.1 C_l versus Alpha for Increasing Camber

Figure 7.1 shows that an increased angle of attack increases the coefficient of lift. The maximum point of each line in the graph represents the c_{lmax}. The NACA 4412 has the highest c_{lmax}, 1.65 and cl0, 0.5.

Plots of c_m vs. alpha for five airfoils with increasing camber can be seen in Figure 7.2. These plots show the fluctuations in c_m as alpha is increased.

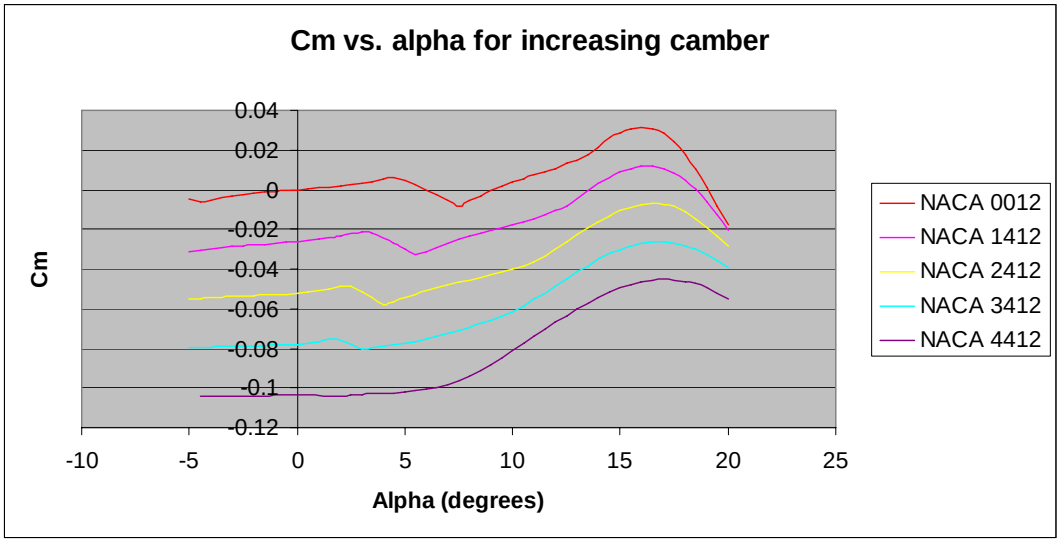

Figure 7.2: C_m versus Alpha for Increasing Camber

As alpha changes, the c_m fluctuates as shown above. NACA 0012 has zero pitching moment when angle of attack, alpha, is zero because it acts as a symmetric airfoil. However, as NACA 4412 produces the most lift, at c_{l0}, it also has the largest moment coefficient.

Plots of c_d vs. alpha for five airfoils with increasing camber follow in Figure 7.3. The plots show how c_d increases with an increased alpha.

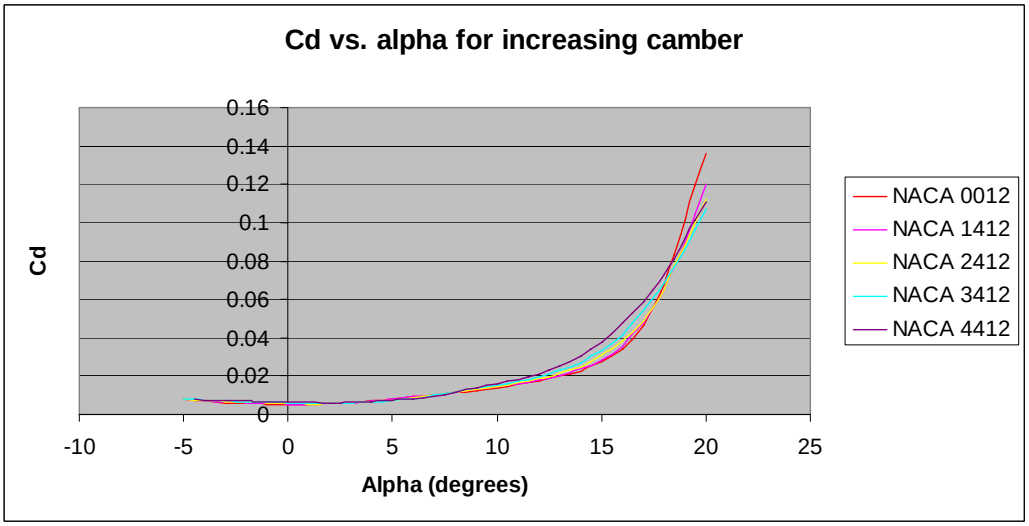

Figure 7.3 C_d versus Alpha for Increasing Camber

The coefficients of drag for the five airfoils are similar. This shows that an increase in camber does not greatly affect the drag produced by each airfoil.

Plots of drag polar c_d vs. c_l for five airfoils follow in Figure 7.4. The optimal point for cruise would be the point with the highest c_l/c_d which is the point furthest to the right for each plot.

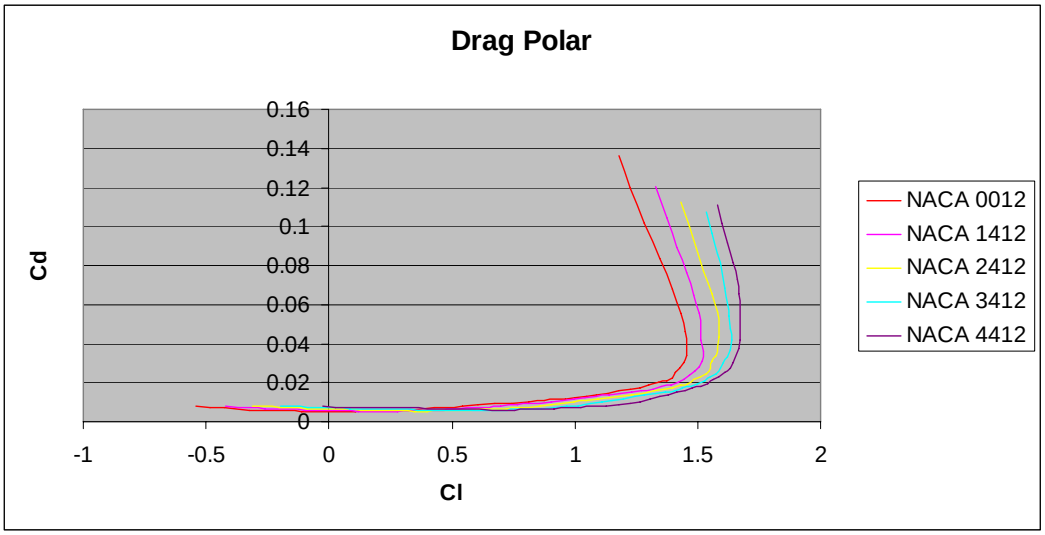

Figure 7.4 Drag Polar

Since the drags for the five airfoils are similar, the airfoil with the highest lift to drag ratio, L/D, would be the NACA 4412 airfoil.

Ultimately, the NACA 4412 airfoil was chosen for its high c_{l0} and c_{lmax}, a low drag, a small center of pressure movement across large speed range, a reasonable pitching moment.
The airfoil selected for the main wing of the Metro-Scout was the NACA 4412. This airfoil has a high C_{lmax} and a low C_d as a function of C_l. The reason the NACA 2412 was chosen for the canards was that the high C_l value of the NACA 4412 would move our aerodynamic center too far forward for our aircraft to be stable. Selecting a lower lift airfoil helped with many of our stability issues. The reason that the NACA 2412 was chosen for the rear horizontal stabilizer was mainly a structural consideration. With the tail booms already under torsion and horizontal bending, the selection of lower lift airfoil would minimize the vertical bending from the tail structure on the booms. Also, it would be balanced with the canards, preventing the plane from nosing down. Lastly, the NACA 0012 airfoil was chosen for the two vertical stabilizers because it is a symmetrical airfoil, which is optimal for vertical stabilizers.

7.2 Wing Sweep

Wing sweep serves the purpose of reducing transonic shock and supersonic flow. However, since the UAVs maximum speed is below Mach 0.2, wing sweep would not be required as it would add to manufacturing cost. [7.4] However, if the aerodynamic center of the aircraft needs to be moved back far enough for balance, swept wings may be an option.

7.3 Taper

Tapered wings are used to simulate an elliptical wing loading. An elliptical wing loading is desirable as it minimizes induced drag for a given span. Thus, a plot was generated on MATLAB from the following equations and assumptions to obtain a taper ratio for a minimum wing area. A taper ratio will save material and allow for a higher wing loading.

From lifting line theory, certain assumptions were made, such as: elliptical wing loading, size of planform does not affect the weight of the aircraft (weight is kept constant at gross takeoff weight), effect of the canard is small, and steady level flight. [7.5]

Variables :

C_l=lift coefficient

$\Gamma(y)$ =vortex distribution

c(y)=chord length along planform

V=velocity

b=span

S=planform area

L=W=603 lb (from constrain analysis)

$$c_l = \frac{L'}{0.5\rho V_\infty^2 c(y)} = \frac{2\Gamma(y)}{V_\infty c(y)} = \frac{2\Gamma}{V_\infty c(y)}\sqrt{1-(2y/b)^2}_s \qquad 7.1$$

$$c(y) = c_s(1-\frac{|y|}{2b}) \rightarrow \alpha - \alpha_{lo} = \frac{\Gamma(y)}{2V_\infty b}\left[1+\frac{2\Gamma b\sqrt{1-(2y/b)^2}}{\pi c_s(1-|y|/b)}\right] \qquad 7.2$$

$$c_l = \frac{2\Gamma}{V_\infty c_s}\frac{\sqrt{1-(2y/b)^2}}{1-|y|/b} = \frac{2\Gamma_s}{V_\infty c_s} f(y) \qquad 7.3$$

For minimum wing area, f'(y)=0,taper ratio =0.5

y =b/4
$f(y=b/4)=(3/4)^{-.5}$

$$c_l = \frac{2\Gamma_s}{V_\infty c_s} f(y) \Rightarrow \frac{\Gamma_s}{c_s} = \frac{c_{l\max} V_\infty}{2 f(y)} \qquad 7.4$$

$$\Gamma_{\max} b = 4/\pi \times \frac{L}{\rho V_\infty^2} \qquad 7.5$$

$$\frac{\Gamma_{\max} b}{\Gamma_s / c_s} = b c_{\max} \qquad 7.6$$

$$S_{\min} = .75 b c_{\max} = 68\, ft^2 \qquad 7.7$$

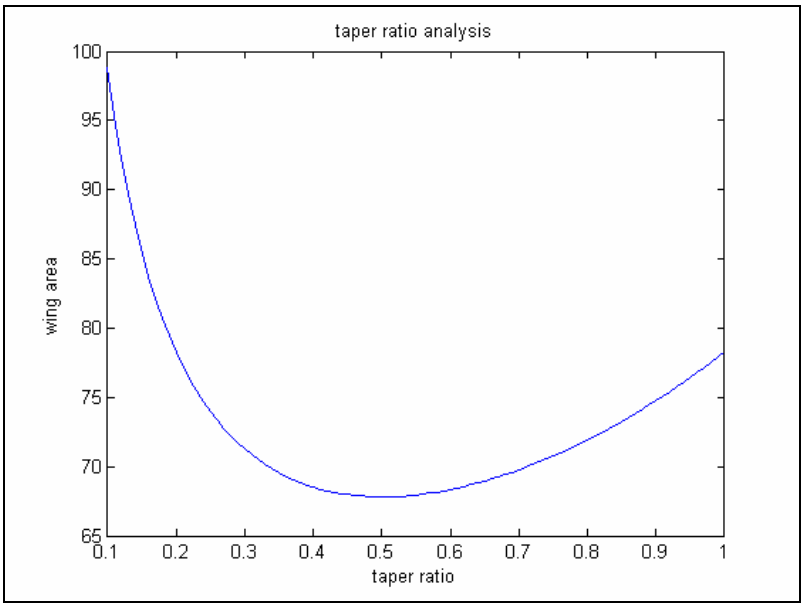

Figure 7.5 Wing Area versus Taper Ratio

When compared to a wing without taper ratio, a savings of over 10% of material results by using a taper ratio of 0.5 (minimum point on graph). Therefore, the wing area is reduced from 78 square feet to 69 square feet. From this wing area and an aspect ratio of 13 which was obtained from the constrain analysis, the resulting span (b) was 30 feet and the maximum chord length (cs) was 3 feet. The maximum lift coefficient (C_{lmax}) for the entire wing was also obtained as 1.45.

7.4 Twist

To obtain an elliptical wing loading, wing twist must be added. [7.5]

$$\delta = k - 1 \qquad 7.8$$

Where δ is twist and k is elliptical efficiency. Since the wing is tapered, the elliptical efficiency would be close to 1, about 1.04. [7.6]

Figure 7.6 shows a wing twist of 0.04 radians or 2.23 degrees is needed. Based on the taper ratio and wing twist, an elliptical wing loading can be obtained which in turn reduces induced drag.

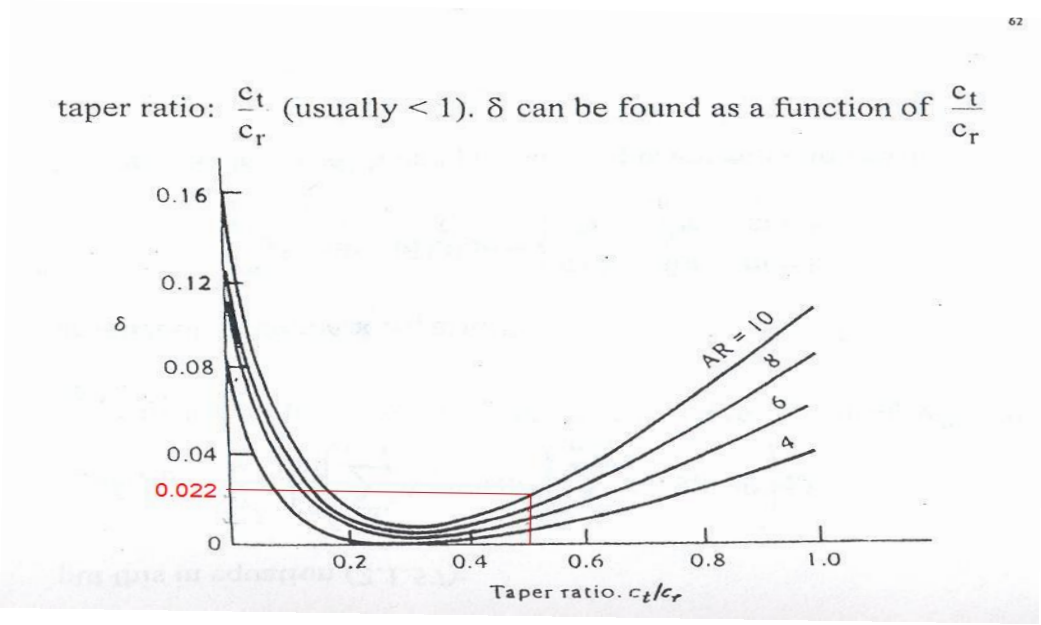

Figure 7.6: Taper Twist versus Taper Ratio

8.0 Performance

8.1 V-n Diagram

A V-n diagram, shown in figure 8.1, shows the limitations on the Metro-Scout's ability to generate lift or structurally sustain the loading capacity to perform a specific turn. At low speed, the maximum load factor is limited by the stall speed seen in equation 8.1.

$$V_{stall} = \sqrt{\frac{2nW}{\rho S C_{L\max}}} \qquad 8.1$$

On the other hand, at high speeds, the maximum load factor is limited by the structural limit. The Metro-Scout's structural limits appear on the V-n diagram as horizontal lines because the structural limits are not a function of velocity. The vertical line on the V-n diagram represents the structure airspeed limit. This is the ability of the Metro-Scout to withstand the dynamic pressure caused by speed. Since the Metro-Scout's operating altitude is low, density of air is assumed to be constant during flight missions.

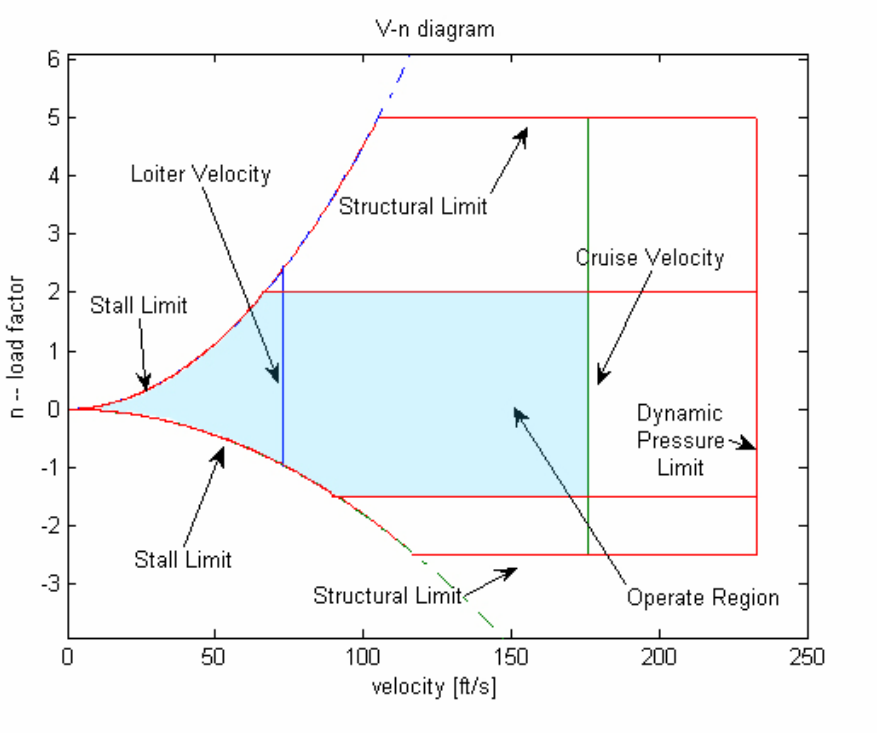

Figure 8.1: V-n Diagram

8.2 Load Distribution

The load distribution across the wing is important when designing the ribs and spars accordingly. The lift distribution across the wing should be elliptical according to the lifting line theory. Due to the vortices generated by the canards, the wing section directly behind the canards will generate less lift. An analysis of this phenomenon on the UAV is pivotal in designing a wing to carry the necessary load required.

The following equations were used to obtain the sectional lift behind the canards. Figure 8.2 depicts a section of the wings and canard.

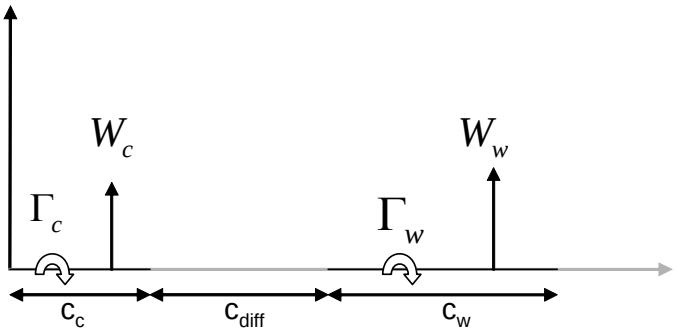

Figure 8.2: Free Body Diagram of Wing

Variables

c_c =chord length of the canard

c_w =sectional chord length of the wing

c_{diff} = sectional distance from the end of the canard to the tip of the wing

c_l =sectional coefficient of lift

Γ_w = vortices' at canard

Γ_c =vortices' at wing

V_∞ = Cruise velocity

$$W_c = \frac{-\Gamma_c}{0.5 c_l c_c} + \frac{\Gamma_w}{c_l (c_{diff} + 0.25 c_c + c_w)} + V_\infty = 0 \qquad 8.1$$

$$W_w = \frac{-\Gamma_c}{c_l (c_{diff} + 0.75 c_c + 0.75 c_w)} + \frac{-\Gamma_w}{0.5 c_w c_l} + V_\infty = 0 \qquad 8.2$$

Solving for Γ_w from the 2 equations above, the sectional lift of the wing can be solved by using the relationship shown in equation 8.3.

$$L' = \rho V_\infty \Gamma_w \qquad 8.3$$

Thus figure 8.3 was derived by a succession of iterations in MATLAB which varied the sectional lift coefficient and sectional distance according to varying chord length. This analysis was done based on 600 pounds of lift generated by the wings at standard sea level conditions but non-steady level flight conditions such that the team could analyze how the Metro-Scout would react in these conditions.

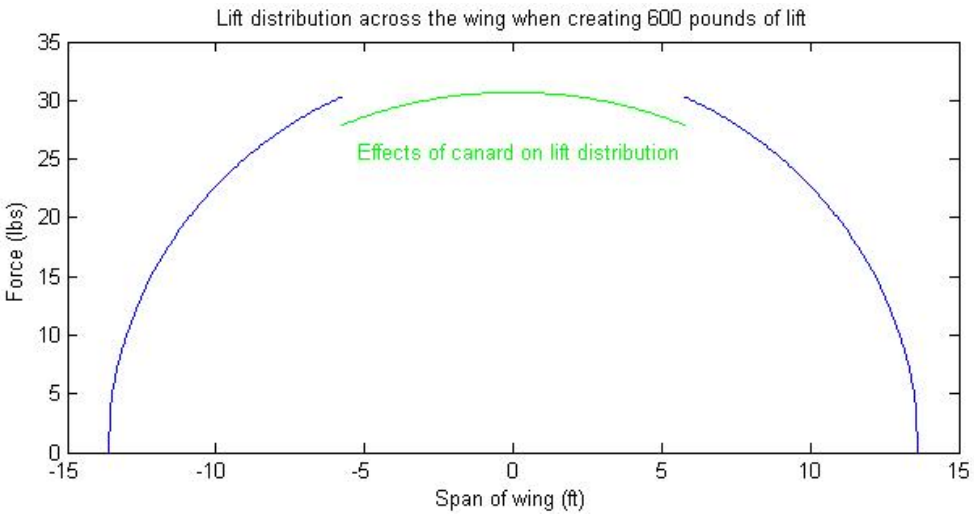

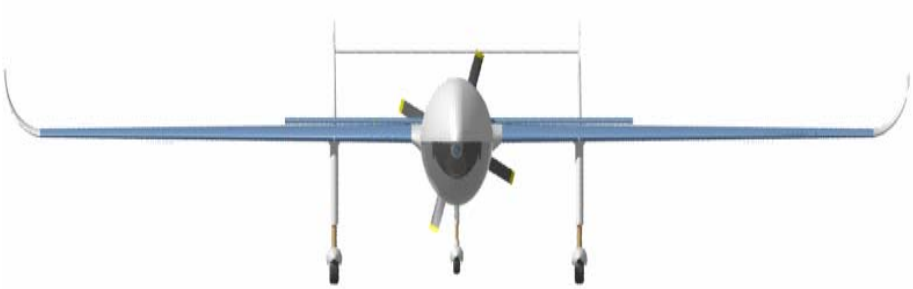

Figure 8.3: Lift Distribution

8.3 Operating Envelope

The operating envelope illustrates the altitude and velocity that the aircraft is designed to withstand. The flight envelopes were obtained by setting the specific excess thrust, derived in equations 8.4 and 8.5.

$$\frac{T}{W} = \frac{550}{380} \times P_{sealevel} \left(\frac{\rho}{\rho_o} - \frac{1 - \frac{\rho}{\rho_o}}{7.55} \right) \varepsilon_p \Big/ \left(M \left(\sqrt{\gamma RT} \right) \right) \qquad 8.4$$

$$P_s = V\left[\frac{T}{W} - \frac{qC_{Do}}{W/S} - n^2\frac{K}{q}\frac{W}{S}\right] \qquad 8.5$$

In equations 8.4 and 8.4 P_s is specific excess power, $P_{sealevel}$ is max power at sea level, n is the load factor and velocity is a function of Mach number and speed of sound.

Since thrust to weight ratio varies with altitude, equation 8.4 was substituted into equation 8.5. Then, P_s was set to 0 to solve for Mach number. Reiterating this process in MATLAB with varying altitudes eventually yields the 2 curves for the flight envelope. The stall limit equation was plotted in MATLAB by solving for the Mach number at $C_{l\max}$ with varying densities at different altitudes seen in equation 8.6.

$$M = \sqrt{2W/(\rho\gamma RTC_{l\max})} \qquad 8.6$$

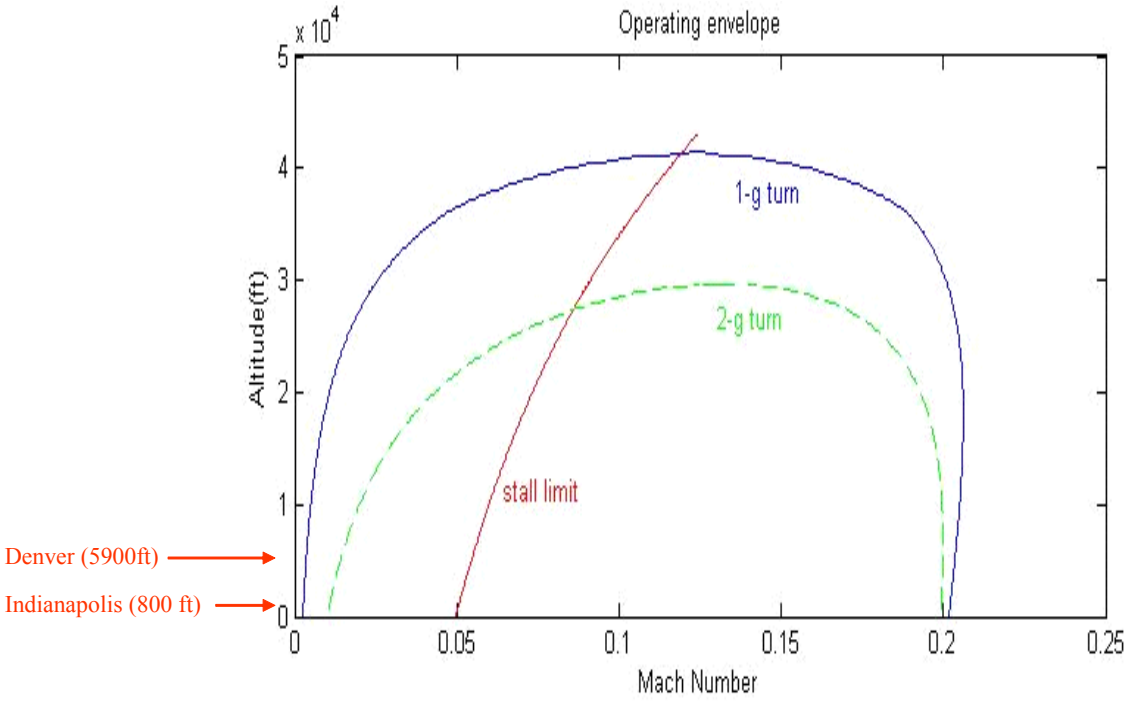

Figure 8.4: Operating Envelope

From the graph above, the flight ceiling would be about 40 000 feet above sea level at steady level flight, while the flight ceiling would be 28 000 feet above sea level if the UAV is to safely make a 2-g turn. This would allow the UAV to operate in Denver and cities located in higher grounds.

9.0 Structures

The Metro-Scout will be constructed using a semi-monocoque internal structure. The wing and canards will be constructed using a double spar configuration (possibly single spar for the canards). This configuration for the wing and canards should be able to withstand the stress the structure would undergo. Of course, at this design phase, there are still many questions (i.e. skin thickness, thickness of internal structures, unexpected loads/vibrations) which need further consideration.

A third spar was created for the wing box that is thicker than, and placed in between, the two spars running the span of the wing. The two spars are thicker in this section of the wing.

The tail configuration also required special structural considerations. Since the two booms extending back will be under bending and torsional stresses, it will be constructed of a hollow tube made for aluminum 2024. AL 2024 resists torsional forces much more efficiently than a solid structure. The horizontal stabilizer spanning the two vertical stabilizers will also assist in transferring any bending moments between the two booms. Lastly, the middle spar created for the wing box will be extended to the boom structure. This will help resist twisting in the wing due to a moment from the horizontal stabilizer.

9.1 Landing Gear

For the Metro-Scout's landing gear, Team 4 elected to go with a fixed tricycle landing gear setup. A tricycle landing gear setup is inherently stable as opposed to a tail-dragger design, and additionally it is a highly conventional proven setup seen on most UAVs currently in operation. The C.G. for the Metro-Scout is located at 8.3 feet from the nose tip of the aircraft. It was discovered that, to ensure adequate weight distribution between the nose gear and the mains, and to avoid placing the nose gear in the front portion of the Metro-Scout that included the camera canopy, that the distance between the nose gear and mains would have to be no more than 4.5 feet. Currently, the main landing gear takes 87 % of the weight of the aircraft during takeoff, landing and taxi, while the nose gear takes 13 % of the weight of the aircraft. This is a comfortable arrangement, as the nose gear doesn't take too little or too much of the aircraft weight. It is recommended that the nose gear take 8 – 15 % of the weight of the airplane. As a

result of this arrangement, the nose gear is located 3.9 ft from the C.G. and the mains are located 0.6 ft from the C.G. [3.1]

One of the requirements for the landing gear arrangement was to maintain 9" of propeller blade clearance from the ground during taxi. At the position that the mains were located in, the length of landing gear would have to be 3 ft to ensure adequate prop clearance. This gives the Metro-Scout a tip-back angle of 11.4^0.

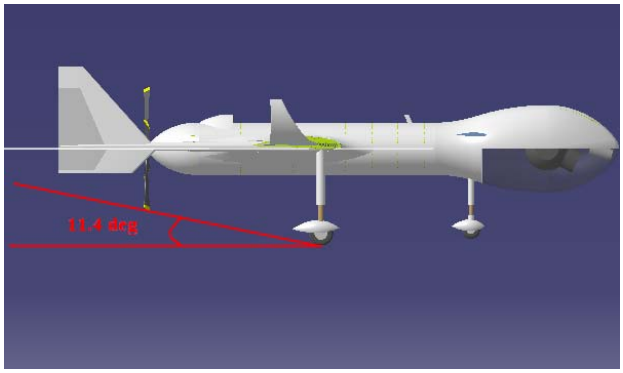

Figure 9.1: Tip-Back Angle for Landing gear

This is a manageable value, as anything over 25 degrees could present problems in getting the aircraft to lift the nose for take-off. Additionally, stability analysis conducted by the Team verified that this would be adequate to lift the nose for take-off. [3.1]

The next step in ensuring landing gear stability was to calculate the overturn angle, which is the measure of the aircraft's tendency to overturn when taxied about a sharp corner. This angle should be no greater than 63 degrees. Team 4 calculated the overturn angle, and found that it was 55.5^0 which is within the limit. [3.1]

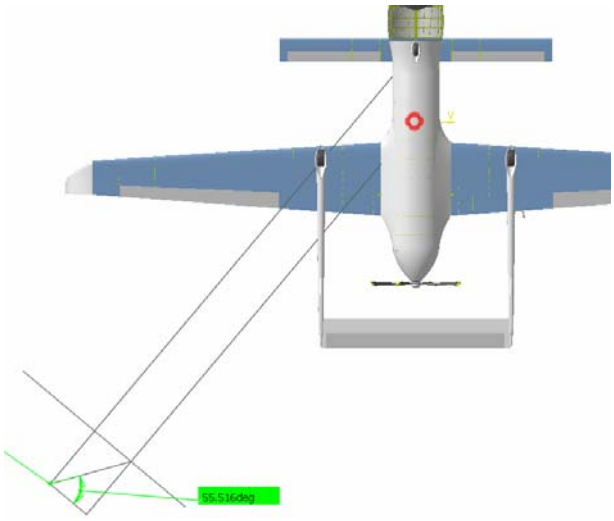

Figure 9.2: Overturn angle calculation method for the Metro-Scout

In order to determine the tire-size necessary to carry the weight of the airplane, table 11.1 in Raymer chapter 11 was used. The tire sizing is obtained from the equation diameter/width = $A*(W_w)^B$, where A and B are constants based on regression from a number of similar airplanes, and W_w is the weight carried by the tire. Using this equation, Team 4 found each of the two main tires would have a diameter of 8.96 inches, and a width of 3.5 inches. It is recommended that for initial sizing, the nose tire should be 60-100% of the size of the main tires. The nose tire for the Metro-Scout is 75% the size of the main tire, and has a diameter of 6.7" with a width of 2.6". Using equations 11.1 – 11.4 in Raymer, Chapter 11, Team 4 determined the static loads on the tires. The maximum static load on the main gear is found to be 176.17 lbs/tire with a load factor of 1g and 528.5 lbs/tire with a load factor of 3g's. [3.1]

As a next step, Team 4 elected to select oleo-pneumatic shock struts as the gear/shock arrangement for both the nose and main wheels. This is most common type of shock-absorbing device in use for landing gears on aircraft. Team 4 conducted a trade-study to choose between the oleo and solid-spring type shocks, and found that the oleo strut setup reduced tire wear, aircraft 'bounce' and vibrations on landing compared to solid-spring gear and levered-bungee gear. However, the downside is that oleo shocks do require an additional level of complexity in the airplane. Given that the payload being carried by the Metro-Scout is sensitive to vibrations and expensive to fix, the oleo type struts would be the best choice for the aircraft.

The stroke of the oleo strut was determined based on the maximum vertical loads placed on the landing gear. For the purposes of the Metro-Scout, it was assumed that the maximum vertical velocity during landing would be 10 ft/s. This is reasonable considering that 5 ft/s can cause enough of a jolt in a general aviation airplane to possibly injure passengers. Team 4 used a shock absorber efficiency of 0.80 for the oleo pneumatic strut and a gear load factor (N_{gear}) of 3. The gear stroke was determined using the equation 9.1.

$$S = \frac{V_{vertical}^2}{2g\eta N_{gear}} - \frac{\eta_T}{\eta} S_T \qquad 9.1$$

From equation 9.1 it was determined that the stroke, S, is 7.06 inches plus a safety factor of 1 inch totaling 8.06 inches.

The length of the oleo including the stroke distance and the fixed portion of the oleo is approximately $Length_{oleo}$ = 2.5 x Stroke = 17.65 inches = 1.47 feet.
The diameter, shown in equation 9.2, of the oleo strut is estimated using P is1800 psi, and L_{oleo} is maximum static load on the tire. The equation is:

$$D_{oleo} = 1.3\sqrt{\frac{4L_{oleo}}{P\pi}} \qquad 9.2$$

From this equation, the diameter is 0.79 inches (for a 3g gear load factor).

9.2 Materials

The team decided to use two different materials for the construction of our aircraft. Aluminum 2024 was used for all internal structures. The reason behind choosing this material was that it is a standard material for the aircraft industry. Since the aircraft would not be undergoing any extreme stresses and did not have any special weight constraints, aluminum 2024 would suite the weight and stress requirements at a standard price.

For the external skin, control surfaces and tail structure, a composite material was chosen. The reason this was possible was that the Metro-Scout cost estimate anticipated 50% composite material. Initially, aluminum 3003 was considered for the external structure due to its ability to be formed easily. This composite is also half the price of aluminum 2024, as well as lighter.

Still, the Aramid/epoxy composite is more beneficial for three reasons. First, Aramid/epoxy is a composite that is basically a Kevlar fiber in an epoxy matrix; this gives it excellent resistance to FOD. [9.1] Also, compared to several other composites it was more resistant to crack propagation. This would be especially beneficial to the tail structure, where even small cracks could grow quickly to catastrophic failure due to the extended configuration of the tail. Also, as an added benefit, it was slightly less dense than aluminum 3003. Though this was not a requirement, it was one more advantage of the composite.

10.0 Longitudinal Stability Analysis

10.1 Longitudinal Stability

The basic concept of stability is simply that a stable aircraft, when disturbed, tends to return, by itself, to its original state [3.1]. Stability is one of the important issues when building an aircraft. There are some terms associated with stability which are important to calculate and recalculate for optimization. These include center of gravity location (c.g), neutral point (n.p), and static margin (SM). Early estimations of what these values should be can help in determining the current stability of the aircraft. The methods of finding these variables are discussed here.

Before discussing such methods, some symbols and acronyms are noted:

M_{cg} - moment about c.g
M_w - wing aerodynamic pitching moment
M_c - canard aerodynamic pitching moment
M_h - horizontal stabilizer aerodynamic pitching moment
L_c - canard lift
L_w - wing lift
L_h - horizontal stabilizer lift
x_{ac_w} - aerodynamic center of the wing (with respect to wing L.E)
x_{ac_c} - aerodynamic center of the canard (with respect to wing L.E)
x_{ac_h} - aerodynamic center of the horizontal stabilizer (with respect to wing L.E.)
x_{cg} - center of gravity location
α - aircraft angle of attack
i_w - wing incidence angle
i_c - canard incidence angle
i_h - horizontal stabilizer incidence angle

ε_w - average downwash angle induced by canard on wing
ε_h - average downwash angle induced by wing on canard
c_w - wing mean chord
c_c - canard mean chord
c_h - horizontal stabilizer mean chord
q - dynamic pressure
S - wing area
S_c - canard area
S_h - horizontal stabilizer area
c - aircraft chord length (fuselage length)
W - aircraft total weight
V_p - aircraft forward velocity
V_w - air velocity over wing
V_h - air velocity over horizontal stabilizer

Figure 10.1 represents the free body diagram used as its base model. Taking into account all aspects of the force system, such as downwash and incidence angles, greatly complicates deriving an initial formula for neutral point. Thus, designers made several key assumptions for the initial analysis: drag, thrust, downwash, and fuselage effects are negligible, α is relatively small ($\cos(\alpha) \cong 1$), $q_c = q_w = q_h = q$, change in downwash angle with α is negligible ($\frac{\partial \varepsilon}{\partial \alpha} = 0$), and $\alpha_w = \alpha_c = \alpha_h = \alpha$.

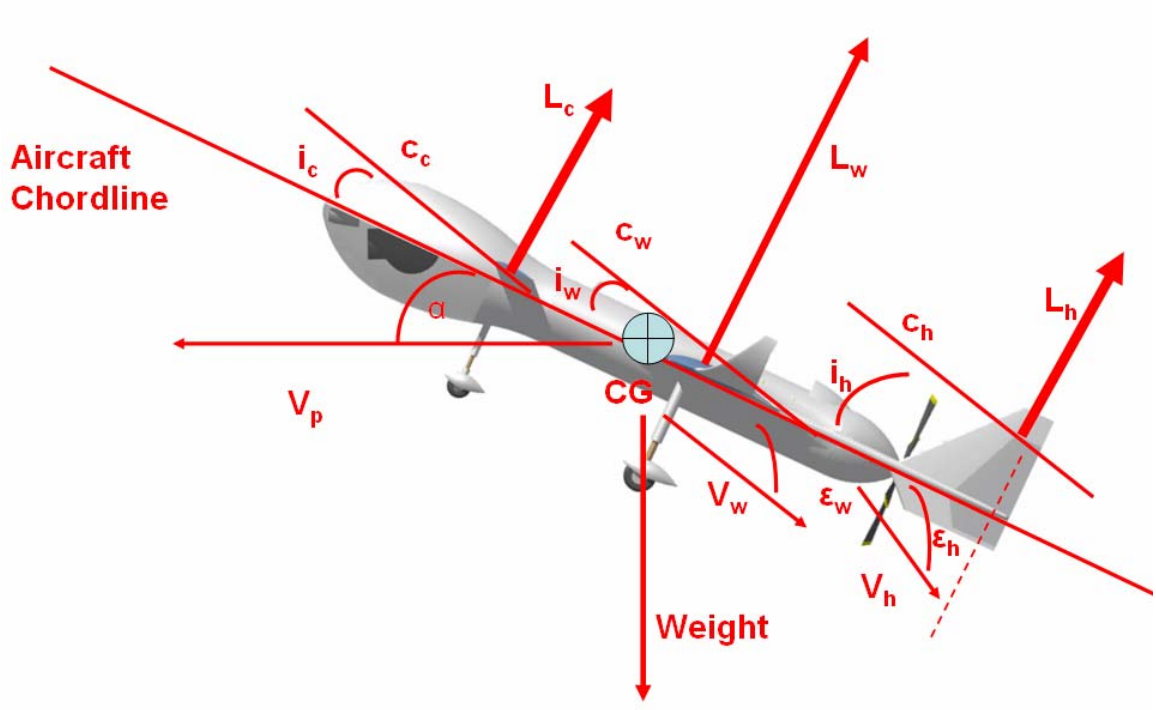

Figure 10.1Free Body Diagram [10.1]

10.2 Neutral Point Calculation

The team's first step in evaluating stability involved finding the location of the neutral point, or the point on the aircraft about which the net moment does not change with angle of attack [10.2]. This method essentially finds the point at which the aircraft center of gravity, c.g., rests in relation to the aircraft aerodynamic center. Figure 10.2 diagrams the forces on the aircraft and the locations of these forces with the designers' key assumptions in mind. The reference location for this analysis rests at the leading edge of the wing.

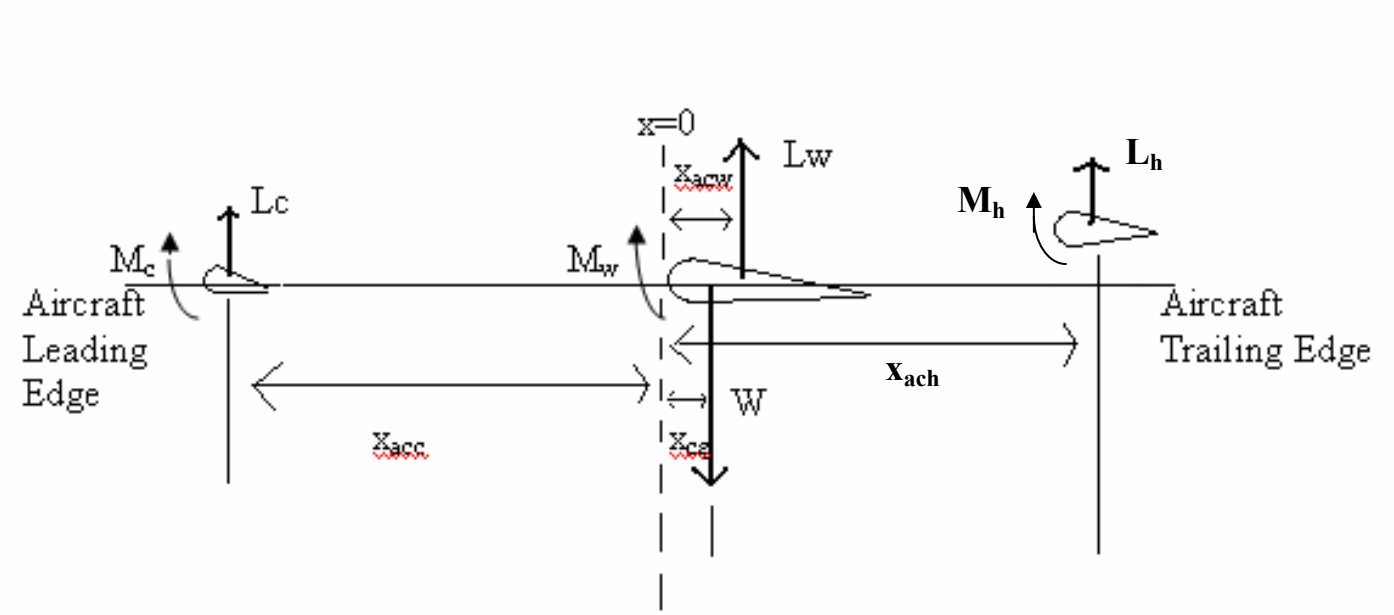

Figure 10.2: Forces and Reference Points for Neutral Point [10.1]

Based on figures 10.1 and 10.2, the team derived equation 10.1 for moment about the aircraft c.g. (or the point at which the weight force acts).

$$M_{cg} = M_w - (x_{ac_w} - x_{cg})L_w + M_c + (x_{cg} - x_{ac_c})L_c + M_h - (x_{ac_h} - x_{cg})L_h \qquad 10.1$$

Originally, the equation looked like equation 7.2.

$$M_{cg} = M_w - (x_{ac_w} - x_{cg})L_w \cos(\alpha + i_w - \varepsilon_w) + M_c + (x_{cg} - x_{ac_c})L_c \cos(\alpha + i_c) + M_h - (x_{ac_h} - x_{cg})L_h \cos(\alpha + i_h - \varepsilon_h) \qquad 10.2$$

In equation 10.2, the group assumed α, i_w and both ε values were small (≈ 0) and thus the cosine term equals one, leading to Equation 10.1.

Next, designers altered equation 10.1 to create equation 10.3 by dividing by aircraft mean chord, dynamic pressure, and wing area. This led to the non-dimensional coefficient form found in equation 10.4, where $c_m = M/qSc$ and $c_L = L/qSc$.

$$\frac{M_{cg}}{qSc}=\frac{M_w}{qSc}\frac{c_w}{c_w}-\frac{\left(x_{ac_w}-x_{cg}\right)}{c}\frac{L_w}{qS}+\frac{M_c}{qSc}\frac{c_c}{c_c}\frac{S_c}{S_c}+\frac{\left(x_{cg}-x_{ac_c}\right)}{c}\frac{L_c}{qS}\frac{S_c}{S_c}+\frac{M_h}{qS_hc_h}\frac{c_h}{c}\frac{S_h}{S}-\frac{(x_{ac_h}-x_{cg})}{c}\frac{L_h}{qS}\frac{S_h}{S_h}$$

7.3

$$c_{m,cg}=c_{m_w}\frac{c_w}{c}-\frac{\left(x_{ac_w}-x_{cg}\right)}{c}c_{L_w}+c_{m_c}\frac{c_c}{c}\frac{S_c}{S}+\frac{\left(x_{cg}-x_{ac_c}\right)}{c}c_{L_c}\frac{S_c}{S}+c_{m_h}\frac{c_h}{c}\frac{S_h}{S}-\frac{(x_{ac_h}-x_{cg})}{c}c_{L_h}\frac{S_h}{S}$$

10.4

Analysis required multiplying each moment term in Equation 10.3 by the respective chord length of its component (c_w/c_w for the wing and c_c/c_c for the canard) to obtain the proper moment coefficients for those components. Equation 10.5 represents equation 10.4 after taking the derivative of each term with respect to its corresponding component's angle of attack.

$$c_{m,cg_\alpha}\alpha=c_{m,w\alpha}\,\alpha_w\frac{c_w}{c}-\frac{\left(x_{ac_w}-x_{cg}\right)}{c}c_{L,w\alpha}\alpha_w+c_{m,c\alpha}\frac{Sc}{S}\frac{c_c}{c}\alpha_c+\frac{\left(x_{cg}-x_{ac_c}\right)}{c}c_{L,c\alpha}\frac{S_c}{S}\alpha_c+c_{m,h\alpha}\alpha_h\frac{c_h}{c}\frac{S_h}{S}-\frac{(x_{ac_h}-x_{cg})}{c}c_{L,h\alpha}\frac{S_h}{S}\alpha_h$$

10.5

Again, the following terminology applies:

α_w – wing angle of attack

α_c – canard angle of attack.

However, $\alpha_w=\alpha_c=\alpha$ is one of the assumptions. Taking a derivative and setting equation 10.5 to be equal to zero yields equation 10.6.

$$c_{m,cg,\alpha}=0=c_{m,w\alpha}\frac{c_w}{c}-\frac{\left(x_{ac_w}-x_{cg}\right)}{c}c_{L,w\alpha}+c_{m,c\alpha}\frac{S_c}{S}\frac{c_c}{c}+\frac{\left(x_{cg}-x_{ac_c}\right)}{c}c_{L,c\alpha}\frac{S_c}{S}+c_{m,h\alpha}\frac{c_h}{c}\frac{S_h}{S}-\frac{(x_{ac_h}-x_{cg})}{c}c_{L,h\alpha}\frac{S_h}{S}$$

10.6

The goal here is to find $\frac{x_{cg}}{c}$, hence rearranging equation 10.6 yields equation 10.7.

$$\frac{x_{cg}}{c}=\frac{\left(\frac{x_{ac_w}}{c}c_{L,w\alpha}-c_{m,w\alpha}\frac{c_w}{c}+\frac{x_{ac_c}}{c}c_{L,c\alpha}\frac{S_c}{S}-c_{m,c\alpha}\frac{c_c}{c}\frac{S_c}{S}+c_{m,h\alpha}\frac{c_h}{c}\frac{S_h}{S}-\frac{x_{ac_h}}{c}c_{L,h\alpha}\frac{S_h}{S}\right)}{\left(c_{L,w\alpha}+c_{L,c\alpha}\frac{S_c}{S}+c_{L,h\alpha}\frac{S_h}{S}\right)} \qquad 10.7$$

Finally, the team divided each term on the right hand side of equation 10.7 by $c_{L,w\alpha}$, and the ***final equation*** becomes equation 10.8.

$$\frac{x_{cg}}{c} = \frac{\left(\frac{x_{ac_w}}{c} - \frac{c_{m,w\alpha}}{c_{L,w\alpha}}\frac{c_w}{c} + \frac{x_{ac_c}}{c}\frac{c_{L,c\alpha}}{c_{L,w\alpha}}\frac{S_c}{S} - \frac{c_{m,c\alpha}}{c_{L,w\alpha}}\frac{c_c}{c}\frac{S_c}{S} - \frac{c_{m,h\alpha}}{c_{L,w\alpha}}\frac{c_h}{c} + \frac{x_{ac_h}}{c}\frac{c_{L,h\alpha}}{c_{L,w\alpha}}\frac{S_h}{S} \right)}{\left(1 + \frac{c_{L,c\alpha}}{c_{L,w\alpha}}\frac{S_c}{S} + \frac{c_{L,h\alpha}}{c_{L,w\alpha}}\frac{S_h}{S} \right)} \qquad 10.8$$

As mentioned before, this $\frac{x_{cg}}{c}$ is actually the aircraft neutral point ($\frac{x_{cg}}{c} = \bar{x}_{np}$) with respect to wing leading edge as the reference point. This implies the aircraft is neutrally stable when $\bar{x}_{cg} = \bar{x}_{np}$ (here, $\bar{x}_{cg}$ is the actual c.g. location). Theoretically, c.g. can be forward (ahead) or aft of the neutral point. To have a positive static margin and, therefore, stable aircraft, the c.g must be ahead (more toward the nose) of neutral point based on the static margin formula in equation 10.9.

$$SM = \bar{x}_{np} - \bar{x}_{cg} = \frac{x_{cg}}{c} - \bar{x}_{cg} = \frac{(x_{np} - x_{cg})}{c} x100 \qquad 10.9$$

The variable $\bar{x}_{cg}$ is the actual c.g. location. The team developed this location using the standard group weight method.

10.3 Group Weights and Aircraft Center of Gravity

The next step in determining the aircraft's stability involves determining the location of its center of gravity. The team used the statistical group weighted method summarized by equation 10.10 to accomplish this task.

$$\bar{x}_{cg} = \frac{\sum_{i=1}^{n} W_i \bar{x}_i}{\sum_{i=1}^{n} W_i} \qquad 10.10$$

Equation 10.10 sums the individual products of the weight of each main aircraft component (wings, canards, fuselage, etc.) at its respective center of mass and the component's distance from the leading edge of the aircraft. It then divides the result by the sum of the individual

weights of the components. Figure 10.3 presents a visual model of this method. In a dynamical analysis, this method essentially treats each component as a particle mass located some distance from a reference point, which in this case is the leading edge of the aircraft.

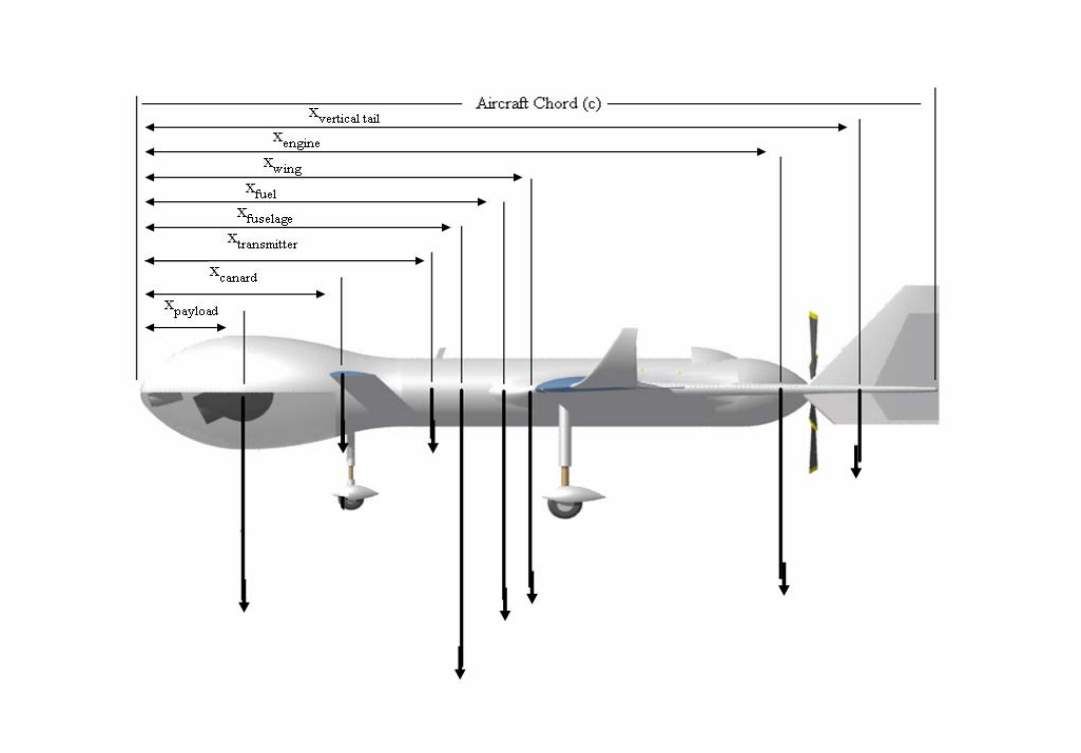

Figure 10.3: Geometry for Finding Aircraft Center of Gravity

Table 10.1 represents the group weight summary for the current Metro-Scout configuration. It displays the weight and location of each component, a summation of which by equation 10.10 locates the aircraft's center of gravity at 8.3 feet from the nose. Table 10.1 lists only a 67 pound payload because further stability analysis indicated some slight problems with a 64 pound payload; thus, three pounds of dead weight will be added to the 64 pound police payload. More detailed reasons for this decision will follow in the static margin analysis.

Group Weight Format			
Structures	**Weight, lb**	**Loc., ft**	**Moment, ft-lb**
Wing	60	9.5	570
Canard	12	4.5	54
Fuselage	29	7	203
Nose gear	15	3.9	59
Main gear	21	9.6	202
Boom Tail	18	16.8	302
Propulsion			
Engine installed (includes cooling devices)	57	13.5	770
Fuel system/tanks	9	8.2	74
Equipment			
Flight Controls	5	7	35
Avionics	10	7	70
Microwave transmitter	11	7.2	79
Total weight empty	**247**		
Useful load			
Fuel--usable	67	8.2	549
Fuel--trapped	1	8.2	11
Oil	1	13.5	15
Payload	67	2.2	147
Takeoff gross weight	**381**	**CG:8.3**	**3139**

Table 10.1: Group Weights

Center of gravity depends upon fixed weights, such as those for the structure and payload, along with variable weights, such as that of fuel. Therefore, as the plane uses fuel during the flight, the center of gravity will shift, thus changing the static margin. For this reason, the team placed the fuel tank as close to the center of gravity as possible to keep the center of gravity and, therefore, the static margin from moving out of tolerance ranges determined by the static margin during flight.

10.4 Static Margin Analysis

Once designers determined the respective locations of the neutral point and center of gravity, they could quantify the static margin. The team deemed a static margin of between 10 and 15 % appropriate for the Metro-Scout based on the static margins of other aircraft. The team decided this would give the aircraft enough stability to be easily flown while still

allowing tight maneuvering for following targets on the ground. After iterating through many configurations, designers settled on a configuration with a neutral point located at 10.2 feet from the nose. Based on the static margin requirements, this location led the group to position components such as the fuel tank and microwave transmitter such that the center of gravity fell between 8.4 feet (for 10% SM) and 7.5 feet (for 15% SM).

The center of gravity will shift based on the weight of the fuel at any point during the flight, all other component weights remaining constant. Thus, the team had to ensure that the burning of fuel would not shift the center of gravity past any bound. Figure 10.4 illustrates the center of gravity excursion diagram for the current Metro-Scout configuration. Table 10.2 is a summary of the center of gravity locations at different flight conditions.

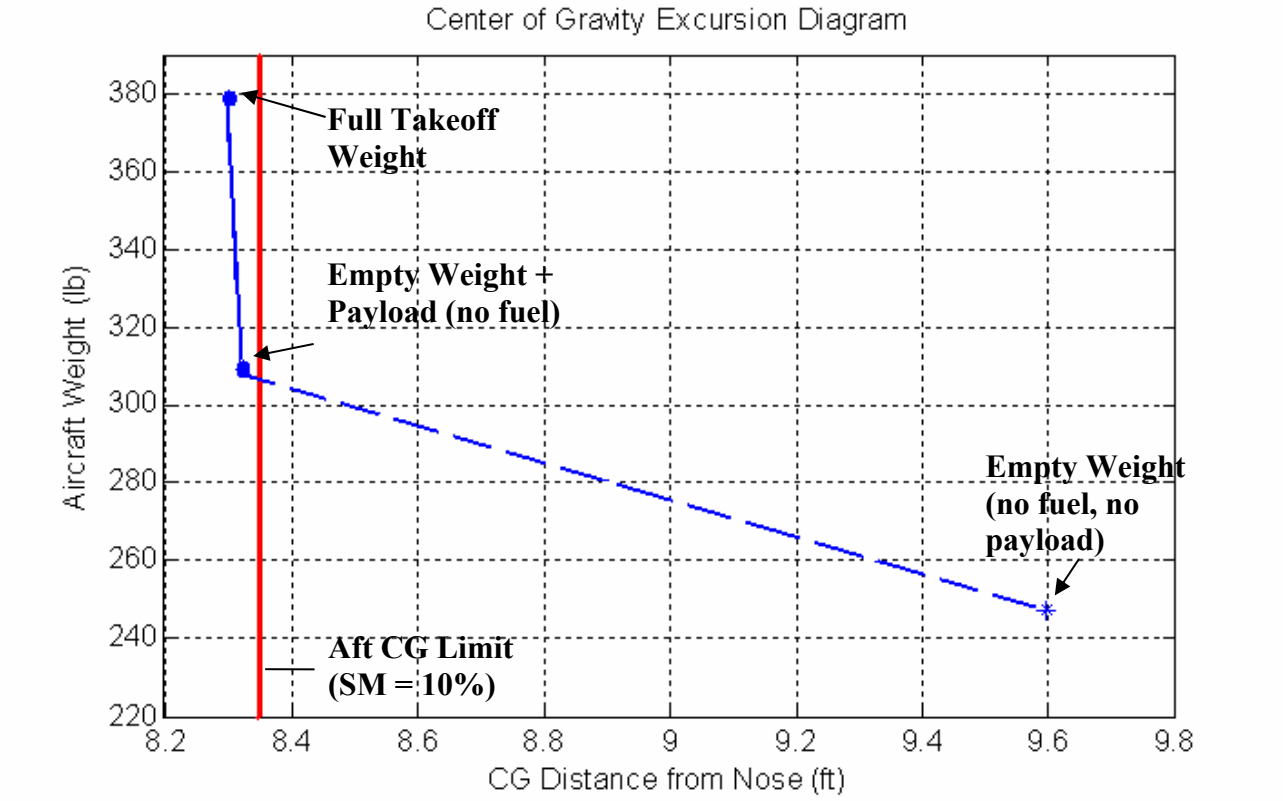

Figure 10.4: CG Excursion Diagram

Static Margin Shift	
At takeoff gross weight	10.3%
At empty weight + payload (no fuel)	10.2%
At empty weight (no payload, zero fuel)	0.94%

Table 10.2: Static Margin Shift

Both figure 10.4 and table 10.2 show that the aircraft remains stable (static margin above 0%) under each flight condition, but without the payload installed in the front of the aircraft, the static margin falls far below the acceptable 10%. For this reason, the team recommends the plane not be flown without the payload or an equivalent 67 pound counterweight installed in the payload position. This static margin analysis applies only to the payload weight of 67 pounds, as for the news payload. The police payload of 64 pounds causes the static margin to fall slightly below 10%, and for this reason the team recommends a weight of 3 pounds be added to the police payload to allow for better control qualities.

Further work and flight testing might indicate that the Metro-Scout needs a higher static margin for taking quality images or handling acceptably for a remote pilot. If this were the case, the team would use the same static margin analysis to try to increase this value. Aircraft configuration would change to alter center of gravity location, neutral point location, or both.

10.5 Canard and Horizontal Stabilizer Sizing

Along with providing some lift for the aircraft, the canard and horizontal stabilizer must be able to lift the nose of the aircraft to an appropriate angle of attack upon takeoff rotation. Elevators on both these surfaces deflect to create a moment that allows this process to occur. The rotation about the main gear (for tricycle gear aircraft) must proceed at an acceptable rate, which falls between 10 and 12 degrees/sec^2 for general aviation aircraft similar to the Metro-Scout [10.1]. Figure 10.5 displays the free body diagram for takeoff rotation.

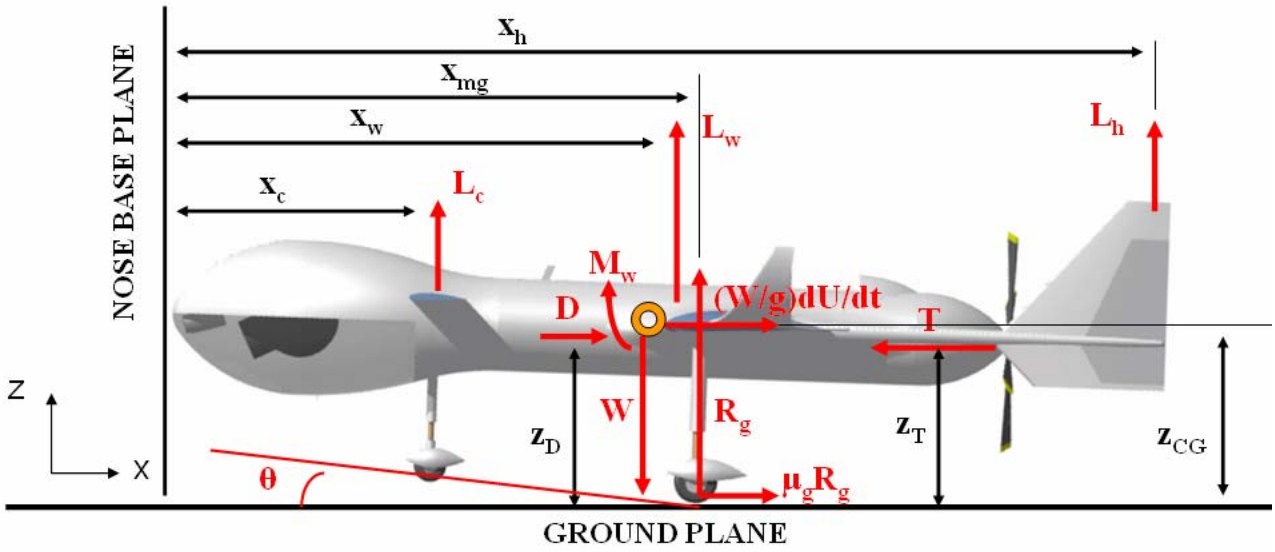

Figure 10.5 [10.1]

The aircraft rotates about the main gear, which the designers assumed to be in contact with the ground plane at rotation. Thus, there is a reaction force from the ground and rolling friction. This method of calculating rotation rate renders the ground plane the horizontal reference plane (z = 0) and the nose of the aircraft the vertical reference plane (x = 0). This is different from the neutral point analysis, which utilized the wing leading edge as the reference point. A summary of terms included in this analysis not previously defined follows:

z_D - vertical distance from ground to point at which drag acts
z_T - vertical distance from ground to point at which thrust acts
z_{CG} - vertical distance from ground to center of gravity
g - acceleration of gravity
U - horizontal (forward) aircraft velocity (becomes acceleration when differentiated with time)
D - aircraft drag
T - aircraft thrust
μ_g - runway friction coefficient
R_g - ground reaction force
x_h - horizontal distance from nose to horizontal stabilizer aerodynamic center

x_c - horizontal distance from nose to canard ac

x_w - horizontal distance from nose to wing ac

x_{mg} - horizontal distance from nose to main gear location

$\ddot{\theta}$ - angular acceleration rate about the main gear reference point

$I_{yy_{mg}}$ - aircraft rotational moment of inertia about the y-axis (rotation point about main gear)

The key assumptions made in this analysis are as follows:

a. Drag acts at the leading edge of the wing
b. Thrust is estimated at full power and acts at the propeller position
c. The main gear is on the ground at the time of rotation and the aircraft rotates about this point
d. $q_c = q_w = q_h = q$
e. Downwash effects and incidence angles are negligible
f. The aircraft is taking off on a paved runway where $\mu_g = 0.02$
g. Ground effects are negligible
h. Moment coefficients about both the canard and horizontal stabilizer are negligible

With these assumptions in mind, the free body diagram in figure 10.5 translates into the equations 10.11 through 10.13. Equation 10.11 is the sum of forces in the x-direction, equation 10.12 is the sum of forces in the z-direction, and equation 10.13 is the moment equation about the main gear with the nose at the reference point.

$$T - D_g - \mu_g R_g = \frac{W}{g}\dot{U} \qquad 10.11$$

$$L_w + L_h + R_g + L_c = W \qquad 10.12$$

$$-W(x_{mg} - x_{cg}) + D(z_D) - T(z_D) + L_w(x_{mg} - x_w) + M_w + L_c(x_{mg} - x_c) - L_h(x_h - x_{cg}) + \frac{W}{g}\dot{U}(z_{cg}) = I_{yy_{mg}}\ddot{\theta}_{mg} \qquad 10.13$$

The negative horizontal stabilizer lift term appears with the assumption that elevator deflection will produce a negative lift coefficient for the horizontal stabilizer upon rotation. Equation 10.13 also illustrates the need to know the aircraft moment of inertia about the y-axis. The team used equation 10.14, a standard dynamical method, to accomplish this task.

$$I_{yy_{mg}} = \sum \frac{W_{component}}{g}(x^2_{compoenent} + y^2_{component}) \qquad 10.14$$

Designers found a value of 1213 slug/ft^2 for the current Metro-Scout configuration using equation 10.14.

The next key in the rotation analysis involves the definition of lift coefficient found in equations 10.15. In this equation q is dynamic pressure, defined as $q = \frac{1}{2}\rho V_1^2$, where ρ is air density and V_1 is rotation airspeed.

$$C_L = \frac{L}{qS} \qquad 10.15$$

Using these definitions, one can choose to determine the appropriate area of either the canard or horizontal stabilizer based upon the given parameters. Designers chose to set a certain value for the horizontal stabilizer planform area (S_h) and determine the corresponding canard planform area (S_c).

To obtain canard area as a dependent variable, the team rearranged and substituted equations 10.11 and 10.12 into equation 10.13. They then substituted the equation for canard lift based on canard lift coefficient (equation 10.15) into the result to obtain equation 10.16.

$$[-W(x_{mg} - x_{cg} - \mu_g z_{cg}) + D(z_D - z_{cg}) - T(z_T) + L_w(x_{mg} - x_w + \mu_g z_{cg}) + M_w + L_h(x_{mg} - x_h + \mu_g z_{cg}) - I_{yy_{mg}}\ddot{\theta}]$$
$$= C_{l_c} qS_c(x_{mg} - x_c - \mu_g z_{cg}) \qquad 10.16$$

When rearranged to solve exclusively for canard area, equation 10.16 becomes equation 10.17.

$$S_c = \frac{[W(x_{cg} - xmg - \mu_g z_{cg}) + D(z_{cg} - z_D) + T(z_T) + L_w(x_{mg} - x_w + \mu_g z_{cg}) + M_w + L_h(x_{mg} - x_h + \mu_g z_{cg}) - I_{yy_{mg}}\ddot{\theta}]}{C_{l_c} q(x_c - x_{mg} - \mu_g z_{cg})} \qquad 10.17$$

To appropriately size the canard planform area, the team used the aerodynamic properties of the selected airfoils for the horizontal stabilizer, wing, and canard along with the wing and horizontal stabilizer areas with equation 10.17. They also set the locations of each of the surfaces, therefore producing a center of gravity location by equation 10.10. Designers then determined the resulting neutral point and static margin. If not within the set bound of 10-15%, the team altered a parameter such as horizontal stabilizer area or canard location and

repeated the process of determining the appropriate canard area and resulting static margin using a MATLAB code.

Table 10.3 summarizes the current location and areas of the wing, canard, and horizontal stabilizer, along with the resulting static margin and center of gravity.

Wing Area	69 ft^2	**Wing Location**	9.5 ft
Canard Area	11 ft^2	**Canard Location**	4.5 ft
Horizontal Tail Area	10.7 ft^2	**Horizontal Tail Location**	17.5 ft
Resulting Static Margin (at takeoff weight)	10.3%	**Resulting CG Location**	8.3 ft

Table 10.3: Location of Horizontal Surfaces

The configuration presented in table 10.3 would change if a greater or lesser static margin were required. In terms of takeoff performance, the team developed the current configuration to meet takeoff rotation rates at both standard and hot-day, high-altitude conditions. The team chose rotation speeds of 87 ft/s for a hot-day, high-altitude condition and 75.3 ft/s for the standard-day, sea-level rotation. This decision hinged on the need for lift from the wing, canard, and horizontal stabilizer at a limited angle of attack of around ten degrees due to the pusher propeller. These speeds are around 1.3 times the stall speed of the Metro-Scout.

10.6 Lateral Stability- Vertical Stabilizer Sizing

Tail Volume Coefficient

A vertical stabilizer (also referred to as vertical tail) with a rudder will control the aircraft yaw, or rotation about the vertical axis. For proper performance, the team had to size this surface correctly. The first process they used to accomplish this was the tail volume coefficient method presented in equation 10.18.

$$S_{VT} = c_{VT} b_W S_W / L_{VT} \qquad 10.18$$

Equation 10.18 specifies the vertical tail area by multiplying the tail volume coefficient (c_{VT}) by the wing area and wing span and dividing the result by the distance from the vertical tail to the aircraft center of gravity (L_{VT}).

Research showed an appropriate tail volume coefficient to be 0.065 for a canard aircraft such as the Metro-Scout (Howe). This resulted in a tail area of around 15 ft^2 when used in equation 10.18. Such a high number concerned designers, as detailed sizing predicted a tail height of nearly nine feet. Feeling that this number could be incorrect or a major tail design alteration would be necessary; the team looked into another sizing method.

Crosswind Landing Condition

To validate the tail volume coefficient used to initially size the vertical stabilizer, the team estimated the side force needed to successfully land the Metro-Scout in a crosswind. Figure 10.5 presents the free body diagram for this condition. In this representation, the y-axis corresponds to the runway heading and the desired path of the aircraft. The crosswind (V_c) acts parallel to the wingspan of the aircraft, while the aircraft thrust (T) produces a forward velocity (V_p) parallel to the aircraft chord. The resultant of the two winds is the total wind (V), assumed to act in the y-direction opposite the runway heading; the angle between this resultant and the forward velocity, V_p, is the sideslip angle, denoted as β.

This model makes several key assumptions, such as:

a) The only forces acting on the aircraft are drag from the resultant wind (D), thrust (T), and side force produced by the vertical tail (F_V)
b) Propeller moment (p-effect) and yawing moment are negligible
c) Drag acts at the aircraft center of gravity
d) Thrust (produced at the pusher prop) acts along the chord line
e) No net rolling moment exists
f) The wind is constant (not gusting).

These assumptions allow the designers to determine if the vertical tail can provide the sufficient side force to maintain the sideslip angle if it is the only surface on the aircraft that can create a moment about the center of gravity.

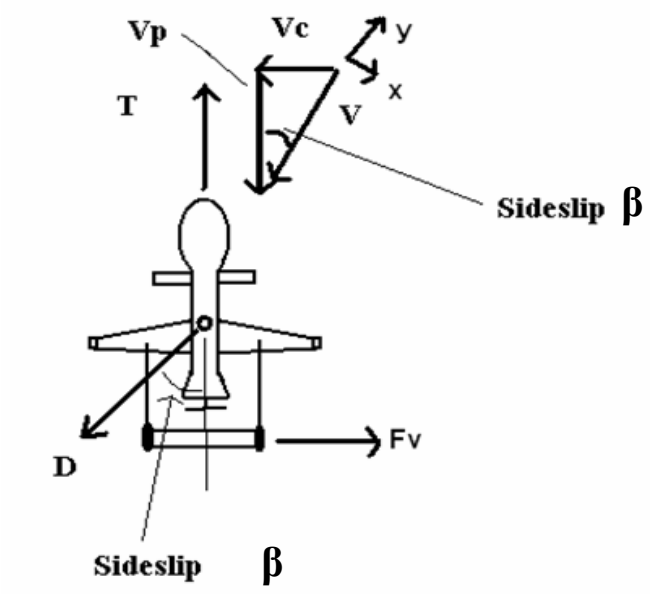

Figure 10.5 Free Body Diagram – Not to scale

Equation 10.19 represents the side force needed to keep the system in figure 10.5 in equilibrium. It equates this expression to the lift that should be produced by the vertical tail surface.

$$F_V = \frac{D}{\sin\beta} - \frac{T\cos\beta}{\sin\beta} = C_{Lv} q_v S_v \qquad 10.19$$

Equation 10.19 leads to an expression for side force F_V found in equation 10.20.

$$S_v = \frac{F_v}{C_{Lv} q_v} \qquad 10.20$$

The lift coefficient for the vertical tail corresponds to that of the NACA 0012 airfoil with twenty degrees of rudder deflection. The dynamic pressure (q_v) corresponds to approach velocity (73 ft/s). Designers estimated the drag by finding the wing lift coefficient and its corresponding drag coefficient on the aircraft drag polar. This information, along with the aircraft approach speed, determined the drag on the aircraft while landing.

The team determined a 15-kts crosswind would be an appropriate standard for the Metro-Scout. This wind is around 27% of the aircraft standard-day stall speed. Designers estimated a power of between 4 and 6.5 horsepower on landing condition. These numbers

along with equations 10.19 and 10.20 predict a necessary horizontal tail planform area of 15 ft^2. This matches the value of 15.5 ft^2 predicted by the tail volume coefficient method with c_{vt} of 0.065. Thus, the team concluded that a twin boom tail design would replace the previous single tail configuration, with each tail should having a planform area of 7.7 ft^2, leading to a total tail area of 15.4 ft^2.

10.7 Control Surface Sizing

The primary control surfaces are the ailerons (roll), elevators (pitch) and rudders (yaw). While the team did not perform detailed sizing analysis on these surfaces for conceptual design, they determined initial values for them based upon historical data. For ailerons and elevators sizing, the team used figure 6.3 and table 6.5 of Raymer, respectively to obtain the desired values. In summary, the ailerons occupy 50% of the wing span and its chord is one quarter of the wing chord. Each elevator's chord is 45% of the tail and canard chords and the elevators occupy 90% of the total span. [3.1]

For rudder sizing, the team decided to use the spin/stall recovery situation to determine the effective rudder areas that can recover from stall. With the aid of figures 16.31 and 16.32 of Raymer and a few equations, the team developed a code that can solve this problem. When the aircraft is entering spin/stall and needs to recover from the spin, two forces act on the aircraft which are the aerodynamic force and the inertial force. The aerodynamic force comes mostly from the rudder. Any stalled air over the rudder is very turbulent and the portion of the rudder that is blanketed in this air is ineffective in countering the spin. S_{R1} and S_{R2}, the area of the rudder above and below the turbulent wake, respectively, compose the only rudder area that is available to counter the spin. The inertial force opposing the spin comes mostly from the aft part of the fuselage and the part of the vertical tail under the horizontal tail, herein referred to as S_F. So S_F is all the area under the horizontal tail that is not part of the rudder. [3.1]

With this knowledge, the team moved forward for the analysis of the rudder sizing. Figure 16.32 of Raymer displays a plot of tail-damping power factor (TDPF) versus spin recovery

estimation with different aircraft relative density parameter (μ) values. TDPF is the minimum allowable tail-damping power factor and the spin recovery estimation has a formula of equation 10.23. This equation is a composition of equations 10.21 and 10.22.

$$I_x = \frac{b^2 W \overline{R}_x{}^2}{4g} \tag{10.21}$$

$$I_y = \frac{L^2 W \overline{R}_y{}^2}{4g} \tag{10.22}$$

$$\left[\frac{I_x - I_y}{b^2\left(W/g\right)}\right] \tag{10.23}$$

The values of $\overline{R}_x$ and $\overline{R}_y$ are 0.25 and 0.38, respectively. The Metro-Scout team obtained these values from table 16.1 of Raymer for the single-engine prop category. Also, the aircraft relative density parameter (μ) is defined as equation 10.24.

$$\mu = \frac{W/S}{\rho g b} \tag{10.24}$$

From the code that the team developed, spin recovery estimation and μ have values of 0.0114 and 2.7706, respectively. The team obtained a corresponding TDPF value of approximately 0.00011.

The team used three fundamental equations that can help determine the desired rudder areas. There are equations 10.25, 10.26 and 10.27 as follow:

$$TDPF = (TDR)(URVC) \tag{10.25}$$

$$TDR = \frac{S_F L^2}{S_w (b/2)^2} \tag{10.26}$$

$$URVC = \frac{S_{R1} L_1 + S_{R2} L_2}{S_w (b/2)} \tag{10.27}$$

The current Metro-Scout configuration has two rudders. Therefore, it gives $S_{R1} = S_{1,R1} + S_{2,R1}$ and $S_{R2} = S_{1,R2} + S_{2,R2}$ where subscript 1 and 2 denote rudder 1 and 2, respectively. Finally, the team determined the effective rudder areas from 10.28 and 10.29.

$$S_{1,R1} + S_{1,R2} + \text{(area of rudder 1 in turbulent wake)} \qquad 10.28$$

$$S_{2,R1} + S_{2,R2} + \text{(area of rudder 2 in turbulent wake)} \qquad 10.29$$

Equation 10.28 is the equation for rudder 1 and equation 10.29 is the equation for rudder 2. The team iterated on 10.26 and 10.27 to obtain a TDPF value 10.25 that is larger than the TDPF value of 0.00011. Both rudder 1 and 2 have the same values for planform area of 3.486 square ft area for each rudder. The coding for rudder sizing is available to view in the appendix section. Figure 10.6 displays a summary of the control surface sizing.

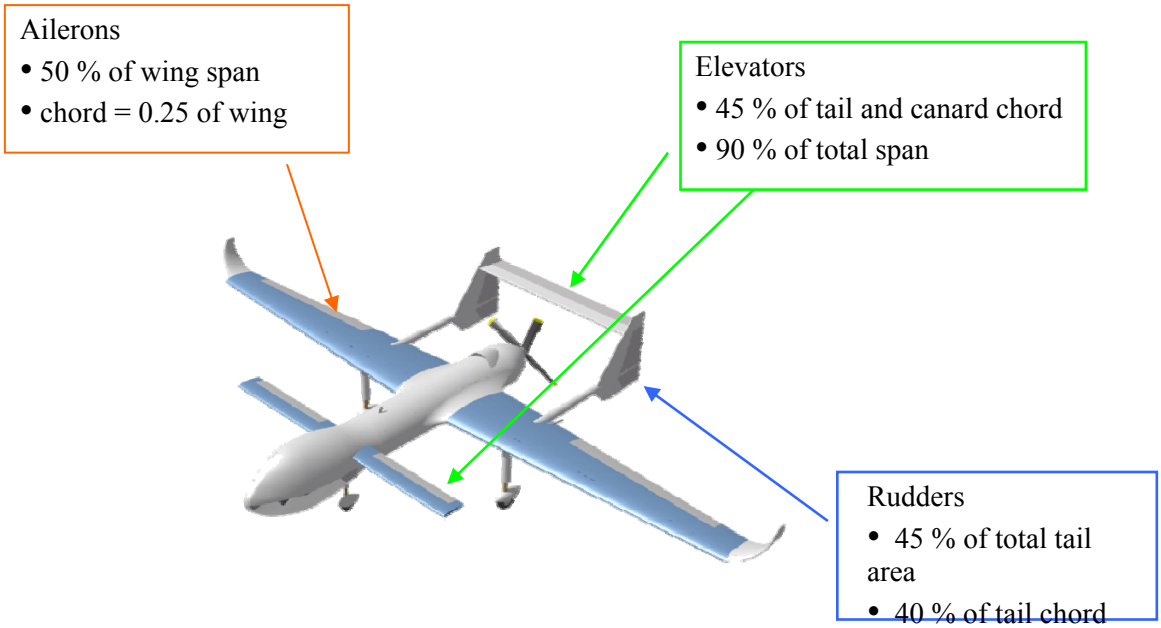

Figure 10.6: Summary of the Control Surface Sizing

Rudder Effectiveness in Crosswind Landing

The team's analysis of the crosswind landing condition for the vertical stabilizer assumed the rudder would be effective at twenty degrees deflection. To validate this assumption, the team developed a code that generates plots of rudder deflection, aileron deflection, and bank angle against crosswind velocity in knots. Figure 10.7 shows these three plots.

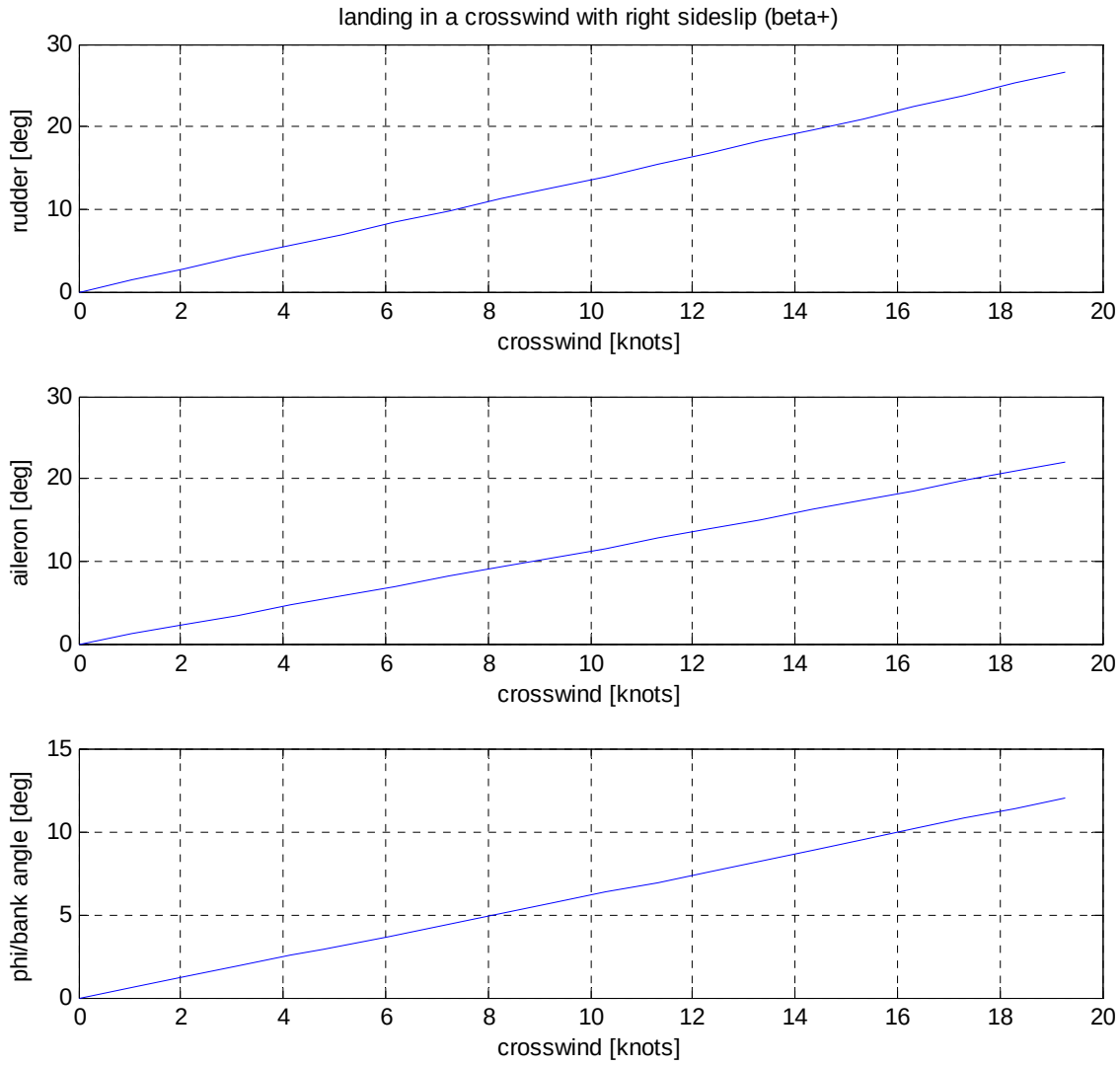

Figure 10.7: Crosswind Landing Condition

Figure 10.7 confirms that the rudder deflected at twenty degrees should allow for an effective landing in a twenty degree crosswind. At this condition, the ailerons will need to be deflected at around seventeen degrees, inducing a bank angle of about nine degrees.

11.0 Cost Analysis

The anticipated costs and monetary returns on the Metro-Scout UAV were determined using a modified version of the DAPCA IV model.

Production and development costs were estimated first. These expenses include:

(1) Program Development (RDT&E) costs: Includes Research, design, analysis, testing, tooling, engineering, and certification.

(2) Production costs: Includes Manufacturing, assembly, materials, quality control, labor, etc.

Given that there are very few readily available cost models for UAVs, it was decided to use the DAPCA IV model. However, given that the DAPCA IV model is usually applied to far larger military fighter and transport aircraft. Team 4 realized the importance of correlating the cost-model to other UAVs to find a correction factor that can be applied to the Metro-Scout. Team 4 decided to apply the DAPCA IV model to the Shadow 200 UAV since it was similar in weight and operating capabilities to the Metro-Scout, in order to find a correction factor. It was discovered that DAPCA IV over-predicted the per aircraft production costs for the Shadow 200 by 39.9 % (this was assuming that the Shadow 200 generated a 25% profit margin). DAPCA IV estimates $288,500 per aircraft compared to the $206,000 per aircraft production cost in reality. Since the per aircraft production costs include both the development and total manufacturing & systems integration costs of the airplane, the correction factor of -39.9% can be applied to all cost data predicted by the DAPCA IV model.

Team 4 applied this correction factor of -39.9% to the development and production costs predicted by the DAPCA IV model for the Metro-Scout UAV. Table 11.1 below shows the cost breakdown for expenses that go into the Metro-Scout program over the first five years of production (2010 – 2014 → with an anticipated 1st five year production run of 300 airframes). Note that the hourly wrap rates obtained from Raymer Ch. 18 have been adjusted for inflation from January 1999 to January 2007.

Program Cost Prediction				
Classification		**Hours**	**Wrap Rate ****	**Cost (2007 USD)**
RDT&E:				
	Engineering	85,859	105.95	$6,985,797
	Tooling	46,521	108.42	$3,949,448
	Development Support			$662,995
	Flight-Testing			$761,046
	Total RDT&E:			$12,359,286
Manufacturing:				
	Manufacturing	395,974	89.94	$29,473,401
	Quality Control	30,094	109.42	$3,780,347
	Mfg. Materials			$4,416,456
	Total Mfg. Cost:			$37,670,204
Flyaway Costs:	Payload Loadout			$60,000
	Avionics			$30,000
	Engine			$10,000
	Approx. Production cost per aircraft:			$203,200

Table 11. 1: Metro-Scout Cost Breakdown based on correlated DAPCA IV model

Team 4 estimates a production cost after payload, avionics and engine integration of approximately $203,200 per airframe. Team 4 estimates a market for approximately 950 airframes by 2021 before the Metro-Scout will be retired in favor of newer designs – which would generate sales figures of approximately $64.1 M. Factoring in the development cost of $12.36 M, Team 4 estimates a net return on the product of around $51.6 M spread over 11 years. (See table 11.2 below)

Net Sales figures	($ 256,180,000)
- Production Costs	($ 192,050,000)
-Development Costs	($ 12,360,000)
= Net Profit	($ 51,770,000)

Table 11. 3: Estimated Net Returns on the Metro-Scout Program

Team 4 estimates approximately 53 airframes to break even for both production and development costs. The following formula was used to arrive at this figure:

Development cost + (*n* x *production cost*) = *n* x Avg. *sale price*

(where, *n* = number of airframes to break even)

➔ *n* = *Development Cost* / (*Avg. Sale price – production cost*)

= $12,360,000 / ($285,00 - $203,200)

= 153

Equation 11.1: Developmental Cost

Based on this estimate, the project would break-even by the first quarter of 2013 (i.e, 3 ¼ years into production assuming sales go as anticipated).

However, if break-even costs were estimated off the development costs (initial investment) alone, then it would take just 43 airframes to break even for the initial investment of $12.36 Million.

Figure 11.1 below charts the yearly profit trend and marks out the break-even point for both production and development costs.

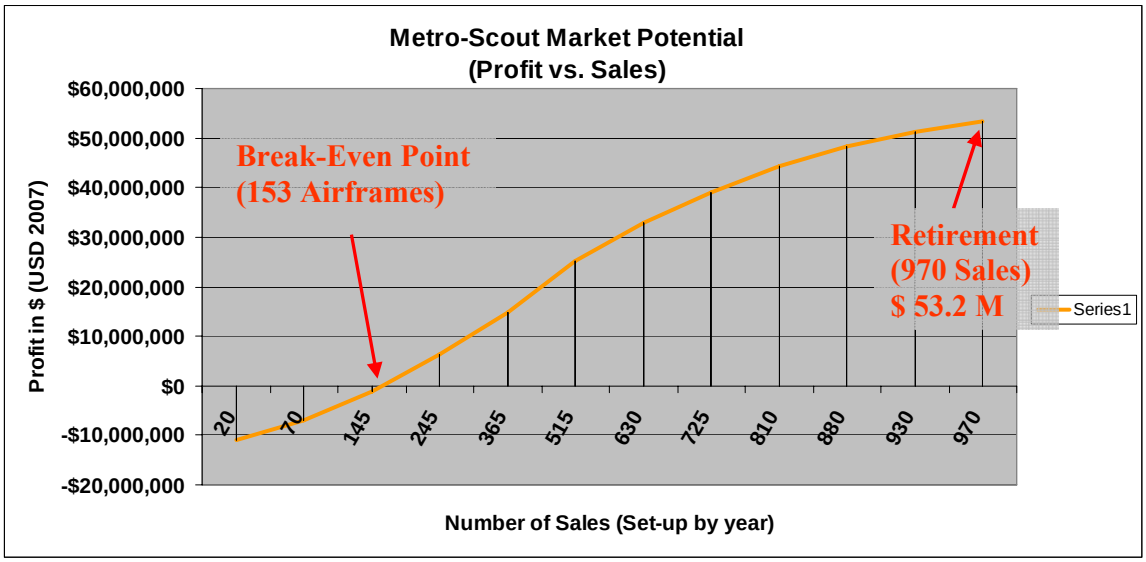

Figure 11.1: Profit trend vs. number of sales highlighting the break-even point for sales

The annual operating costs for the Metro-Scout were determined based on the cost equations from Raymer ch. 18. In order to perform the calculations, it was estimated that the Metro-Scout would be flown about 2000 hours a year. This would mean that the Metro-Scout would be flown on 7 hour endurance missions for 290 out of 365 days of the year. This is a reasonable estimate for the yearly flight hours expected out of the UAV for its type of operations. In April of 2007, the average nationwide cost of avgas (100LL) is $4.12/gal. This translates into $6.6/hr for a fuel-efficiency of $1.59 gal/hr, and a total annual fuel cost of $13,200/year. [3.1]

The maintenance costs of the Metro-Scout were estimated using a regression curve, since the Raymer equations were predicting negative and clearly wrong values for maintenance costs. The regression was based off of data obtained on five general aviation airplanes since reliable data for maintenance costs of UAVs could not be found – the Cessna 150, Cessna 172, Cessna 182, Piper Warrior III, and Piper Arrow. [11.1] Based on this regression data, Team 4 predicts that the Metro-Scout will have a maintenance cost of $3.5 per flight hour. Insurance was estimated at 3% of the yearly operating and maintenance costs since UAVs are a relatively new technology, and Raymer recommends 3% to be the high end for insurance costs. This is summarized in table 11.3 below:

Operating Costs		
	Estimated Flight Hours	2000
Variable Costs	AvGas cost (April 2007)	$4.12/gallon
	Fuel Use	1.59 gal/hr
	Fuel Cost per hour.	$6.6/hr
	Maintenance	$3.5/hr
	Crew Expenses	$106/hr
	Total (hourly)	**$117/hr**
	Total (Annual)	**$234,000/year**
Fixed Costs	Annual Insurance	$7020
	Tie-down & Hangar	$600
	Total Fixed + Variable	**$241,620/year**
	Total w/o crew expenses	**$27,600/year**

Table 11.3: Operating Costs Breakdown

A detailed comparison of the life-cycle costs incurred by the customer between the Metro-Scout and the Bell Jet-Ranger III (the current best-selling helicopter to the target customers) is shown in table 11.4 below. It is clear that the Metro-Scout is the more cost-effective option in every instance.

Comparison to Bell Jet-Ranger III		
Costs adjusted to 2007 USD	Metro-Scout	Bell Jet-Ranger
Acquisition Cost	$285,000	$1,200,000 + payload price
Hourly Oper. & Maint. Costs	$117	$795
2-Man Crew Cost (2k flt. Hrs)	$220,500/year (ground)	$375,720/year (air crew)
Fuel Usage	1.59 gal/hr = $6.6/hr	24 gal/hr = $99/hr
Yearly Fuel Costs (2k hrs)	$13,200	$197,760
Yearly Operating Expenses (w/o crew)	$27,600/year	$1,210,000/year

Table 11.4:Cost Comparisons with Bell Jet-Ranger III

In addition, the Metro-Scout cost estimates were compared to the Shadow 200 UAV as a sort of reality check to demonstrate that the calculated cost estimates were in-fact plausible. This is shown in table 11.5 below.

Comparison to Shadow 200 UAS		
2007 USD	Metro-Scout	Shadow 200
Acquisition Cost	$285,000	$275,000
Hourly Oper. & Maint. Costs*	$117	$110
Yearly Operating Expenses (w/o crew)	$27,600/year	$25,000/year

Table 11.5: Cost comparisons with Shadow 200 UAV

It is clear from the cost estimates shown here that the Metro-Scout UAS is clearly a more cost-effective alternative to helicopters for the target customers. Cost savings could be anywhere from the tens to hundreds of thousands of dollars a year depending on the number of flight hours that the customer decides to use the Metro-Scout for. Additionally, as demonstrated in table 11.5, the Metro-Scout is competitive with similar sized UAVs such as the Shadow 200.

12.0 Summary

Team 4 has decided to provide a primary customer base comprised of police and news organizations with the Metro-Scout, an unmanned aerial vehicle capable of performing those tasks for which those customers currently use conventional helicopters. This craft will perform both autonomously and with a remote pilot, depending on the mission such as safe operation at 1000-1500 ft above ground level, a coverage radius of 200mi, an endurance of at least five hours, and a payload weight of between sixty and seventy pounds. To perform such objectives, the team has determined key design attributes as outlined. The group aims to sell the Metro-Scout to target customers at a lower acquisition and operating cost than current helicopters to be competitive within the market.

After considering several possible designs for the aircraft, the team decided on

a canard configuration with a front mounted camera and pusher piston propeller that would best accomplish the necessary missions. Basic design decisions have been made including airfoil selections, wing, canard, and tail shapes, and the aircraft is designed to be inherently stable.

The next step forward in the design process involves several elements for the team. Many detailed design consideration should be addressed including detailed interior design, detailed drag analysis, detailed loading zones, detailed structural component built up, component material, and more accurate control surface sizing. An improved sizing analysis method for the aircraft and components, particularly the canard and tails, would also be beneficial. Continuing with the design would require more cost analysis, an engine out plan, and maintenance and manufacturing plans. Eventually the aircraft would need to be tested for flying qualities both autonomously and piloted, and for camera control.

While the basic idea and layout of the aircraft is now arranged and analyzed, increasingly accurate methods which require more in-depth analyses are required before the team would be able to move forward toward production. The aircraft has been found to accomplish the goal. It is expected to be able to meet all the customer requirements and perform the specified missions. The Metro-Scout will be able to powerfully compete with the competition and would be a profitable development.

R.0 References

[2.1] "Bell Helicopter Commercial." 2007. Bell Helicopter Textron Inc. 28 Jan. 2007 www.bellhelicopter.com.

[2.2] AOPA, "AOPA's 2006 Aviation Fact Card", download.aopa.org/epilot/2006/factcard.pdf [retrieved 18 February 2007].

[2.3] "The Helicopter Market Newsletter Piston", Helicopter International Association, published Nov. 28th, 2005, http://www.rotor.com/market_letter/Piston_ML_Oct2005.pdf [retrieved February 18th, 2007]

[2.4] "The Helicopter Market Newsletter Turbine", Helicopter International Association, published Oct. 25th, 2005, http://www.rotor.com/market_letter/turbine_ML_Sept05.pdf [retrieved February 18th, 2007]

[2.5] Clark, Larry K., "The Life of a Pilot Flying ENG (electronic news gathering)," justhelicopters.com (online), 2/21/2004, http://www.justhelicopters.com/Articles/detail.asp?iData=19&iCat=645&iChannel=2&nChannel=Articles , [retrieved February 15th, 2007]

[2.6] "2000 Aircraft Industry Studies", The Industrial College of Armed Forces, http://www.ndu.edu/icaf/industry/2000/aircraft/aircraft4.htm , [retrieved Feb. 15th, 2007]

[3.1] Raymer, Daniel. P., *Aircraft Design: A Conceptual Approach* (4th Ed.), Blacksburg, VA: AIAA Inc, (2006).

[3.2] Kroo, Ilan., Shevell, Richard., Chapter 13.1, Aircraft Design: Synthesis and Analysis , Retrieved April 1st, 2006, from http://adg.stanford.edu/aa241/noise/noise.html, © Desktop Aeronautics Inc., (2006).

[3.3] Lennon, Andy., *Canard: A Revolution in Flight (1st Ed.)*, Hummelstown, PA: Aviation Publishers, (1984).

[4.1]Clausing, Don. Total Quality Development. New York: ASME P, 1994. 150-164.

[4.2] "Mobile police radar gun" simicon specifications page http://www.simicon.com/eng/product/gun/radis.html [Retrieved 10-Feb-07].

[4.3] "Pixel 275 III" polytech specifications page http://www.polytech.us/pixel275III_specs.htm [Retrieved 10-Feb-07].

[4.4] ThermaCAM® SC3000 Flir Systems therma cam specification page http://www.flirthermography.com/media/SC3000%20datasheet.pdf [Retrieved 10-Feb-07].

[4.5] Hal, "Sony Dvcam DSR-PD150 DV Specifications" product wiki database http://www.productwiki.com/sony_dvcam_dsr_pd150_dv/article/sony_dvcam_dsr_pd150_dv_specifications.html [Retrieved 10-Feb-07].

[4.6] "3400 Full featured UAV autopilot" 3400 Auto pilot specifications http://www.u-nav.com/3400autopilot.html [Retrieved 10-Feb-07].

[4.7] "Specification PowerShot S3 IS" S3 IS specifications http://www.usa.canon.com/consumer/controller?act=ModelTechSpecsAct&fcategoryid=144&modelid=13077 [Retrieved 10-Feb-07].

[4.8] "Specifications EF 55-200mm f/4.5-5.6 II USM" EF f/4.5-5.6 II USM specifications http://www.usa.canon.com/consumer/controller?act=ModelTechSpecsAct&fcategoryid=150&modelid=9435 [Retrieved 10-Feb-07].

[4.9] "C I N E F L E X V 1 4 M A G N U M - M U LT I S E N S O R" Cineflex 14 M Specifications http://www.helinetaviation.com/downloads/pdf/Cineflex_Magnum_V14-MS.pdf [Retrieved 10-Feb-07].

[7.1]Husa, B "Airfoil Selection" http://www.oriontechnologies.net/Documents/Airfoil.htm [Retrieved April 2nd 2007]

[7.2] "NACA Airfoil Series" http://www.aerospaceweb.org/question/airfoils/q0041.shtml [Retrieved April 2nd 2007]

[7.3]Heperlle, M "Location of Camber and Moment Coefficient"http://www.mh-aerotools.de/airfoils/nf_5.htm [Retrieved April 2nd 2007]

[7.4]Abbott, I.H., and von Doenhoff A. E., " Theory of Wing Sections: Including a Summary of Airfoil Data", Dover, pp 288.

[7.5]Lyrintzis, A.S., "AAE 514 Intermediate Aerodynamics Spring 2006", Copymat, West Lafayette, 2006,pp 59-62.

[7.6]"Induced drag", http://en.wikipedia.org/wiki/Induced_drag [Retrieved April 2nd 2007]

[6.1] "AR801 - 50bhp." UAV Engines Ltd. 2004. UAV Engines Ltd. 27 Feb. 2007 http://www.uavenginesltd.co.uk/index.php?id=402

[6.2] "Shadow-200." Unmanned Aerial System. 2005. AAI Corp. 25 Mar. 2007 http://www.aaicorp.com/New/UAS/html/shadowr_200.html

[6.3] "Rotax® 503UL DCDI." 1999. Kodiak Research Ltd. 6 Mar. 2007 http://www.kodiakbs.com/engines/503.htm

[6.4] Bent, Ralph D., and James L. McKinley. *Aircraft Powerplants*. 5th ed. NY, NY: McGraw-Hill Book Co., 1985. 375-383.

[9.1] Baker, Alan, Stuart Dutton, and Donald Kelly. Composite Materials for Aircraft. 2nd ed. AIAA. 20 Apr. 2007 http://www.knovel.com/knovel2/Toc.jsp?BookID=1598&VerticalID=0

[10.1] Roskam, Jan. Airplane Flight Dynamics and Automatic Flight Controls. 4th ed. Lawrence, KS: DARcorporation, 2003.

[10.2] Steve, Brandt. Introduction to Aeronautics: a Design Perspective. Reston, VA: American Institute of Aeronautics, 2004.

[11.1] "Aircraft for Sale." PlaneQuest. 1999. AOPA. 18 Apr. 2007 http://www.planequest.com/

A.0 APPENDIX

A.1 Project Timeline Description

Team 4 elected to develop a project timeline to establish a baseline measure of progress through the course of the semester. Team 4 has specifically targeting a number of phases in the design for overlap to allow the team greater freedom to make design changes and foster greater customer participation in formulating design requirements. For instance, the project timeline shows that Customer Attribute Identification phase goes hand in hand with the Initial Conceptual Design phase until the date of the Systems Requirements Review whereat all the customer attributes need to be finalized. The same is true for certain aspects of the Initial Conceptual Design and the Design Analysis and Tweaking phases. The premise behind the layout of the timeline is to establish constraints and deadlines that keep Team 4 moving forward in the design process while giving it the freedom to make changes as deemed necessary to keep the project competitive. The five main stages in Team 4's timeline and their ultimate progress were –

(1.)	Establish Customer and Product:	Phase Complete
(2.)	Customer Attribute Identification:	Phase Complete
(3.)	Initial Conceptual Design	Phase Complete
(4.)	Design Analysis/Tweaking	Phase Complete
(5.)	Design Finalization	Phase Complete

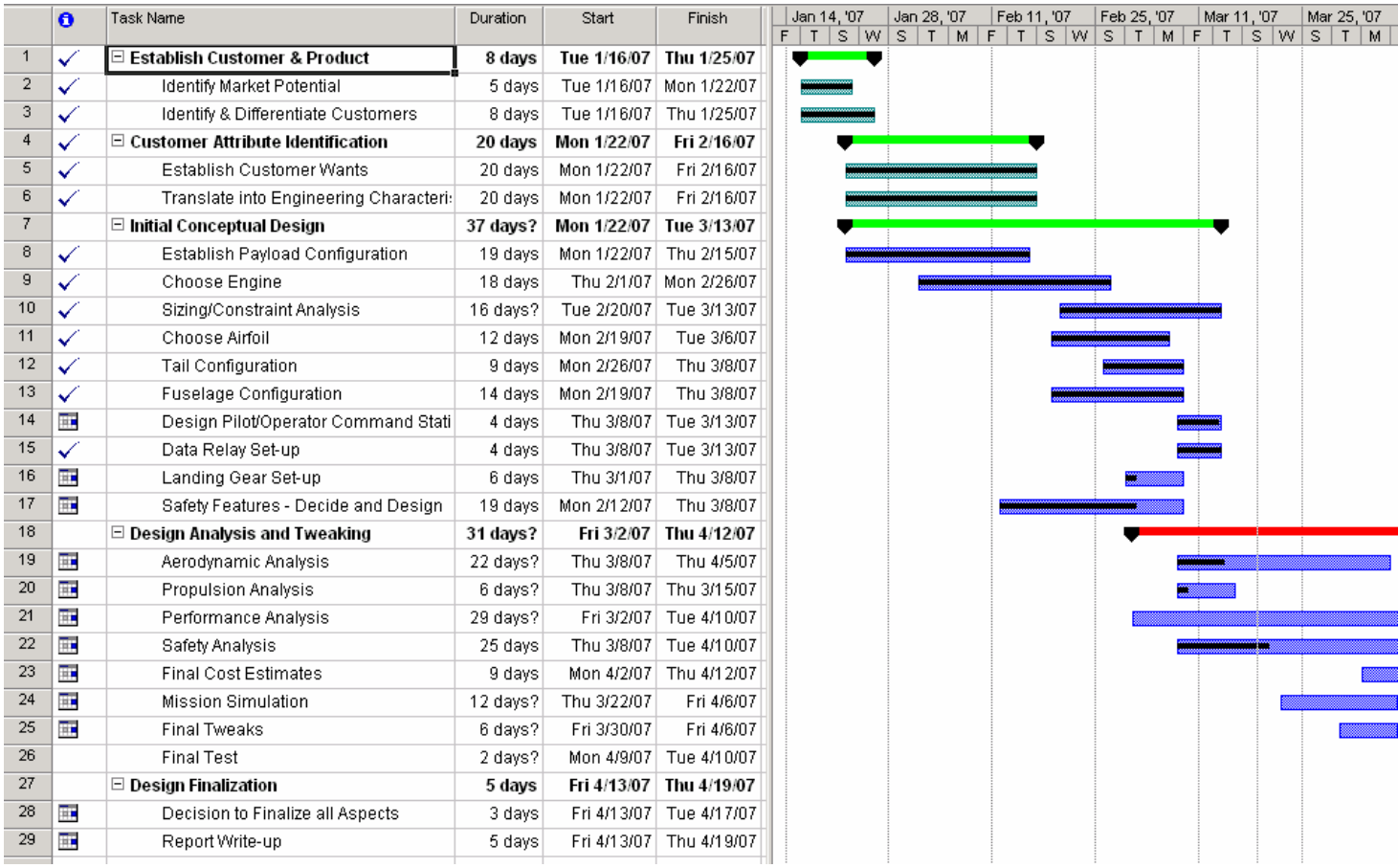

	Task Name	Duration	Start	Finish
1	**Establish Customer & Product**	**8 days**	**Tue 1/16/07**	**Thu 1/25/07**
2	Identify Market Potential	5 days	Tue 1/16/07	Mon 1/22/07
3	Identify & Differentiate Customers	8 days	Tue 1/16/07	Thu 1/25/07
4	**Customer Attribute Identification**	**20 days**	**Mon 1/22/07**	**Fri 2/16/07**
5	Establish Customer Wants	20 days	Mon 1/22/07	Fri 2/16/07
6	Translate into Engineering Characteri	20 days	Mon 1/22/07	Fri 2/16/07
7	**Initial Conceptual Design**	**37 days?**	**Mon 1/22/07**	**Tue 3/13/07**
8	Establish Payload Configuration	19 days	Mon 1/22/07	Thu 2/15/07
9	Choose Engine	18 days	Thu 2/1/07	Mon 2/26/07
10	Sizing/Constraint Analysis	16 days?	Tue 2/20/07	Tue 3/13/07
11	Choose Airfoil	12 days	Mon 2/19/07	Tue 3/6/07
12	Tail Configuration	9 days	Mon 2/26/07	Thu 3/8/07
13	Fuselage Configuration	14 days	Mon 2/19/07	Thu 3/8/07
14	Design Pilot/Operator Command Stati	4 days	Thu 3/8/07	Tue 3/13/07
15	Data Relay Set-up	4 days	Thu 3/8/07	Tue 3/13/07
16	Landing Gear Set-up	6 days	Thu 3/1/07	Thu 3/8/07
17	Safety Features - Decide and Design	19 days	Mon 2/12/07	Thu 3/8/07
18	**Design Analysis and Tweaking**	**31 days?**	**Fri 3/2/07**	**Thu 4/12/07**
19	Aerodynamic Analysis	22 days?	Thu 3/8/07	Thu 4/5/07
20	Propulsion Analysis	6 days?	Thu 3/8/07	Thu 3/15/07
21	Performance Analysis	29 days?	Fri 3/2/07	Tue 4/10/07
22	Safety Analysis	25 days	Thu 3/8/07	Tue 4/10/07
23	Final Cost Estimates	9 days	Mon 4/2/07	Thu 4/12/07
24	Mission Simulation	12 days?	Thu 3/22/07	Fri 4/6/07
25	Final Tweaks	6 days?	Fri 3/30/07	Fri 4/6/07
26	Final Test	2 days?	Mon 4/9/07	Tue 4/10/07
27	**Design Finalization**	**5 days**	**Fri 4/13/07**	**Thu 4/19/07**
28	Decision to Finalize all Aspects	3 days	Fri 4/13/07	Tue 4/17/07
29	Report Write-up	5 days	Fri 4/13/07	Thu 4/19/07

Figure A.1: Gantt chart – Team 4's Project Timeline

A.2 UAV Database

Database sources:

www.shephard.co.uk/UVonline

www.fas.org/irp/program/collect/uav_roadmap

www.milnet.com/pentagon/uavs

http://csat.au.af.mil/2025/vol3ch13.pdf

http://uav.noaa.gov

www.navy.mil

UAV	Length (ft)	Wing Span (ft)	GW (lbs)	Payload (lbs)	Fuel Capacity (lbs)	Wf_W0	We_W0	Endurance(hr)	Power(hp)	Propulsion	Vmax (kts)	Vloiter (kts)	Ceiling (ft)
Predator	26.7	48.7	2250	450	665	0.295555556	0.504444444	24	115	piston prop	118	70	25000
Predator B	36	66	10500	750	4000	0.380952381	0.547619048	30	900 (shp)	piston prop	225		50000
Pioneer	14	17	452	75	76	0.168141593	0.665929204	5	26	piston prop	110	65	15000
Global Hawk A	44.4	116.2	26750	1950	14700	0.54953271	0.377570093	32	7600 (lbs)	turbofan	350	340	65000
Global Hawk B	47.6	130.9	32250	3000	16320	0.506046512	0.400930233	28	7600 (lbs)	turbofan	340	310	60000
Hunter A	22.6	29.2	1620	200	421	0.259876543	0.616666667	11.6	57 (x2)	piston prop	106	89	15000
Hunter B	23	34.25	1800	200	421	0.233888889	0.655	18	56 (x2)	piston prop	106	89	18000
Shadow A	11.2	12.8	327	60	51	0.155963303	0.660550459	5	38	piston prop	110	70	14000
Shadow B	11.2	14	375	60	73	0.194666667	0.645333333	7	38	piston prop	105	60	15000
X-45	39	49	36500	4500	14000	0.383561644	0.493150685	7		turbojet?	460		40000
X-47	38	62	46000	4500	17000	0.369565217	0.532608696	9		turbojet?	460		40000
I-GNAT	27	49	2300	450	625	0.27173913	0.532608696	30	115	piston prop	120	70	25000
Neptune	6	7	80	20	18	0.225	0.525	4	15	piston prop	84	60	8000
Prowler II	14	24	546	96			0.824175824	18		piston prop	125		20000
Altus	22	55	1200	330			0.725	24	100	turbo charged piston	125		18000
D'Humbug	6.5	6.5	180	25			0.555555556	4	36	piston prop	215		18000
Eagle Eye TR911B	18	13	2250	500			0.555555556	8		rotor	220		20000
Horus-SD	26.7	48.7	1042	450			0.655	40	105	piston prop	100		25000
KillerBee 4		10	172	66			0.561395349	16	450 V	electric	125	55	16000
Seascan II	4.6	9.5	45.6	19			0.592105263	80	82	piston prop	68	57	20000

A.3 Pugh's method for vertical tail selection

		CONCEPTS						
	DATUM HILIGHTED IN RED	Single Vertical Tail	Single Vert. + winglets	Winglets, unswept	Swept wing w/ winglets	Twin-extended	Twin-extended + Wingtips
	CRITERIA						
1	Lower Parasite Drag	-	-	-	s	s	\
2	Lower Induced Drag (endplate effect)	-	s	s	s	-	\
3	Lower Weight Required (structure)	s	s	-	-	s	\
4	Added Load on Wing Structure	+	s	-	-	s	\
5	-ve impact on stall characteristics	s	s	s	-	s	\
6	-ve impact on c.g. position	s	s	+	-	s	\
7	-ve impact on propeller efficiency	-	-	s	s	s	\
	Total Positives (+)	1	0	1	0	0	
	Total Negatives (-)	3	2	3	4	1	
	Net	-2	-2	-2	-4	-1	DATUM BEST CONFIG.
	Influencing Criteria for above char.						
	Smaller Tail Area	-		-	s	s	\
	Smaller Tail Height	-		-	s	-	\
	Longer Tail Moment Arm	-		-	+	s	\
	Tail Area	20.2 ft^2	> 20.2 ft^2 <	34.6 ft^2	15.13 ft^2	15.13 ft^3	slightly > 15.13 ft^2
	Tail Height (each tail)	10.7 ft	reduced, distributed	15.4 ft	8.073 ft	4.034 ft	slightly < 4 ft, distributed
	Moment Arm (From c.g.)	6 ft	>5 , <6	3.5 ft	8	8	8
	Weight (per item of itself, structure n.a)	14.43 lbs		11.38 lbs	5.6 lbs	5.6 lbs	
					8.073 - 0.25 tr		winglet size = 1.6 ft x 0.85 ft
					6.72 - 0.5 tr	3.36 - 0.5 tr	twin-tail size = 3 ft x 4.1ft
							(taper ratio = 0.25)
							(size shown in root chord x he
							Per Winglet Area = 0.854 ft^2
							Per Tail Area = 7.686 ft^2
							Total Area = 17.08 ft^2

A.4 Constraint Analysis Matlab Code

```
%%%%%%%%%%%%%%%%%%%%%%%%%%%%%%%%%%%%%%%%%%%%%%%%%%%%%%%%%%%%%%%%%%%%%%%%%%%%%%%
% Constrain_Analysis.m
%  by Team 4 -- Kevin Kwan
% This program requires following m-file: stdatm2.m;
%                                         size_aircraft_451_prop.m
%                                         Vn.m
% Developed for:
%       -AAE 451 UAV Sizing
% Last Revision: 04/15/2007
%%%%%%%%%%%%%%%%%%%%%%%%%%%%%%%%%%%%%%%%%%%%%%%%%%%%%%%%%%%%%%%%%%%%%%%%%%%%%%%

function Constraint_Analysis
clear all
clc
%% Input Section
AR = 11; % Aspect Ratio
h = 1500; % Cruise altitude [ft]
V = 73; %Cruise velocity [ft/s] (73.33 ft/s = 50mph)
V_max = 176; % Max speed [ft/s] (176ft/s = 120mph)
dvdt = 6; %Accleration [ft/s^2]
n = 2; %load factor of the aircraft
n_at_max_speed = 1.5;
sto = 500; %takeoff distance constraint (in ft)
sland = 250; %landing distance constraint (in ft)
CDo_to = 0.0239; % take off drag coefficient
CDo = 0.0239; % minimum drag coefficient
e = 0.75; %Oswald's efficiency factor
np = 0.75; %propeller efficiency
CLmax_to = 1.5; %maximum take-off coefficient of lift
CLmax = 1.5; %maximum coefficient of lift

Wpay = 67.1;    % payload weight of the aircraft [lbs](73 lb for Shadow 200 RQ-
7B)
R = 200;        % Cuurse Range (one way) [nmi]
E = 7;          % Loiter Endurence [hr] (7 hr for Shadow 200 RQ-7B)

%% Main
x = stdatm2(h,1);
density = x(3)/32.2;

q = 0.5*(density)*(V^2);
takeoffmiu = 0.03;     % friction for takeoff   %Assumption taken from 251
textbook page 250
landingmiu = 0.5;      % Friction for landing   %Assumption taken from 251
textbook page 251
g= 32.2;
x0= stdatm2(0,1);
density0 = x0(3)/32.2;
alpha = density/density0;
beta = 0.8;  %Weight fraction for specific constrain %Assumption that the weight
fraction for the aircraft during the turn is 0.8

% Turn Constraints
wingloading = linspace(0.1,20);
```

```
turnconstraint =
q*CDo./(alpha.*beta.*wingloading)+beta.*wingloading.*(n^2/(q*pi*AR*e));
pwlturnconstraint = V.*turnconstraint./(550*np);

q_max=0.5*density*V_max^2;
h_turn =
q_max*CDo./(alpha.*wingloading)+wingloading.*(n_at_max_speed^2/(q_max*pi*AR*e));
plt_h_turn= V_max*h_turn./(550*np);

%Take off Constraint
V_stall=(wingloading.*2./(density0*CLmax_to)).^0.5;  %page 96
V_to=1.2.*V_stall;
beta0=1;
alpha0=1.1;
q_to=0.5.*density0.*(0.7.*V_to).^2;
takeoff =
(((1.44*beta0^2)/(alpha0*density0*CLmax*g*sto))*wingloading)+((CDo_to*0.7)/(beta
0*CLmax))+takeoffmiu; %page 252 of 251 text
pwltakeoff = takeoff.*0.7.*V_to./(550*np);

%Steady level Flight Constraint p.516
K=1/(pi*AR*e);
ss_flight_TW=q.*CDo./(wingloading)+wingloading.*(K./q);
plt_ss_flight= V*ss_flight_TW./(550*np);

%Max Speed Steady level Flight Constraint p.516
K=1/(pi*AR*e);
ss_flight_TW=q_max.*CDo./(wingloading)+wingloading.*(K./q_max);
plt_ss_flight_max= V_max*ss_flight_TW./(550*np);

% Landing Constrant
beta_land = 0.8;
landing = (sland*density0*CLmax_to*g*landingmiu)/(1.69*beta_land);
wingloading_land = [landing landing];

% Acceleration Constraint

acc =
(beta/alpha)*((q/beta)*(CDo./wingloading+K*(beta/q)^2*(wingloading))+dvdt/g);
plt_acc=V*acc./(550*np);

figure (1)
plot(wingloading,pwlturnconstraint,...wingloading,plt_h_turn,
    wingloading,pwltakeoff, ...wingloading,plt_ss_flight,...wingloading,
plt_ss_flight_max,
    wingloading,plt_acc, wingloading_land,[0 1])
%plot([wingloading(1) wingloading(1000)],[pwl_Vmax pwl_Vmax],'m')

xlabel('Wing Loading [lb/ft^2]');
ylabel('Power Loading [hp/lb]');
title('Power Loading Constraint Analysis')
%legend (['Loiter Turn Constraint with Load Factor =',num2str(n)],['Max Speed
Turn Constraint with Load Factor =',num2str(n_at_max_speed)],['Takeoff
constraint for takeoff distance=',num2str(sto),'ft'],['Max Speed Powerloading
```

```
Requirement for Vmax=',num2str(V_max),'ft/s'])
legend (['Loiter Turn Constraint with Load Factor =',num2str(n)],...['Max Speed
Turn Constraint with Load Factor =',num2str(n_at_max_speed)],
    ['Takeoff constraint for takeoff distance=',num2str(sto),'ft'],...['Loiter
Steady Flight Constraint for ',num2str(V),' ft/s'],...['Max Speed Steady Flight
Constraint for ',num2str(V_max),' ft/s'],...
    ['Acceleration Constraint for ',num2str(dvdt),' ft/s^2'], ['Landing
Constraint for Landing distance = ',num2str(sland),' ft'])
tolerance = 0.0005;
for n=1:100
    x1=abs(pwlturnconstraint(n)-plt_h_turn(n))/2;
    x2=abs(plt_h_turn(n)-pwltakeoff(n))/2;
    x3=abs(pwltakeoff(n)-pwlturnconstraint(n))/2;
    if x1<=tolerance
        Powerloading(1) = (pwlturnconstraint(n)+pwlturnconstraint(n+1))/2;
        y(1)=n;
    elseif x2<=tolerance
        Powerloading(2) = (plt_h_turn(n)+plt_h_turn(n+1))/2;
        y(2)=n;
    elseif x3<=tolerance
        Powerloading(3) = (pwltakeoff(n)+pwltakeoff(n+1))/2;
        y(3)=n;
    end
end

if Powerloading(1)>=Powerloading(2)% && Powerloading(1)>=Powerloading(3)
    Wingloading = wingloading(y(1))
    Powerloading = Powerloading(1)
elseif Powerloading(2)>=Powerloading(1)% && Powerloading(2)>=Powerloading(3)
    Wingloading = wingloading(y(2))
    Powerloading = Powerloading(2)
%elseif Powerloading(3)>=Powerloading(1) && Powerloading(3)>=Powerloading(2)
%    Wingloading = wingloading(y(3))
%    Powerloading = Powerloading(3)
else
    disp 'ERROR in finding design point (intersection) in figure 1'
end
Wingloading=5.98
Powerloading=0.0525
[W0]=size_aircraft_451_prop (Wpay, R, E, AR, Powerloading, Wingloading,1);
Vn([-0.6 CLmax], [-1.5 2], V_max, 69, W0);

%% Carpet Plots

AR= [AR-1 AR AR+1 AR+2];
c=2;

step=11;

Powerloading_range = Powerloading-0.02:0.004:Powerloading+0.02;
Wingloading_range = Wingloading-2:0.4:Wingloading+2;

W0=[];
figure (4)
title 'Carpet plot with constrants'
```

```
for m=1:11
    for n=1:11
        W0n(n)=size_aircraft_451_prop (Wpay, R, E, AR(c), Powerloading_range(m),
Wingloading_range(n),0);
    end
    plot (Wingloading_range,W0n,'y')
    hold on
%    legend (m,['P/W = ',num2str(Powerloading_range(m))])
    W0(:,m)=W0n';
end
xlabel 'Wing Loading [lb/ft^2]'
ylabel 'Take-off Weight [lb]'
figure (2)
mesh(Powerloading_range, Wingloading_range, W0)
title 'Carpet Plot'
xlabel 'Powerloading [hp/lb]'
ylabel 'Wingloading [lb/ft^2]'
zlabel 'Take-off Weight [lb]'



%% Take-off Distance
figure (3)
title 'Take-off Distance'
for k=1:11
    for l=1:11
        V_stall(l)=(Wingloading_range(l)*2/(density0*CLmax))^0.5;
        V_to(l)=1.2.*V_stall(l);
        q_to(l)=0.5.*density0.*(0.7.*V_to(l)).^2;

Sto(l)=(Wingloading_range(l)*1.44*beta0^2/(alpha0*density0*CLmax*g))*(Powerloadi
ng_range(k)*(550*np/(0.7*V_to(l)))-(CDo*0.7/(beta0*CLmax))-takeoffmiu)^-1;
    end
    subplot(11,1,k), plot(Wingloading_range, Sto, [Wingloading_range(1)
Wingloading_range(11)],[sto sto])
    title ([' Powerloading = ',num2str(Powerloading_range(k))])
    tolerance = 30;
    for n=1:11
        x1=abs(Sto(n)-sto);
        if x1<=tolerance
            if n~=11
                Sto_n = (Sto(n)+Sto(n+1))/2;
                break
            else
                Sto_n = Sto(n);
                break
            end
        end
    end
    Wingloading_sto(k)=Wingloading_range(n);

    if n==11
        Sto_n=Sto(11);
    end
    sto_range(k)=Sto_n;
```

```
    W0_sto(k)=size_aircraft_451_prop (Wpay, R, E, AR(c), Powerloading_range(k),
Wingloading_sto(k),0);

end
xlabel 'Wingloading [lb/ft^2]'
ylabel 'Take-off Distance [ft]'

figure (4)
dum = polyfit (Wingloading_sto, W0_sto, 2);
W0_sto_fit = polyval(dum, Wingloading_sto);
plot (Wingloading_sto, W0_sto_fit, 'r')

%% Accelerate
dhdt=0; % rate of climb when accelerating
n_dvdt=1; %load factor when accelerating
beta=0.6; % fuel weight fraction when acclerating
figure (5)
title 'Specific Excess power'
for k=1:10
    for l=1:11
        q=0.5*density*((V_max+V)/2)^2;
        % !!
        Dvdt(l)=g*(Powerloading_range(k)*(550*np/((V_max+V)/2))*(alpha/beta)...
            -(dhdt/((V_max+V)/2))-
(((q/beta)*(CDo)/(Wingloading_range(l)))+(((1/(pi*AR(c)*e*alpha))*((n_dvdt*beta)
^2)/q)*(Wingloading_range(l)))));
    end
    subplot(11,1,k), plot(Wingloading_range, Dvdt, [Wingloading_range(1)
Wingloading_range(11)],[dvdt dvdt])
    title ([' Powerloading = ',num2str(Powerloading_range(k))])
    tolerance = 5.5;
    for n=1:11
        x1=abs(Dvdt(n)-dvdt);
        if x1<=tolerance
            if n~=11
                Dvdt_n = (Dvdt(n)+Dvdt(n+1))/2;
                break
            else
                Dvdt_n = Dvdt(n);
            break
            end
        end
    end
    Wingloading_dvdt(k)=Wingloading_range(n);
    if n==11
        Dvdt_n = Dvdt(1);
    end
    dvdt_range(k)=Dvdt_n;
    W0_dvdt(k)=size_aircraft_451_prop (Wpay, R, E, AR(c), Powerloading_range(k),
Wingloading_dvdt(k),0);

end
xlabel 'Wingloading [lb/ft^2]'
ylabel 'dvdt [ft/s^s)'
```

```
figure (4)
dum = polyfit (Wingloading_dvdt, W0_dvdt, 2);
W0_dvdt_fit = polyval(dum, Wingloading_dvdt);
plot (Wingloading_dvdt, W0_dvdt_fit, 'c')
```

A.5 Sizing Matlab Code

```
% Last Revision: 04/15/2007
%%%%%%%%%%%%%%%%%%%%%%%%%%%%%%%%%%%%%%%%%%%%%%%%%%%%%%%%%%%%%%%%%%%%%%%%%%%%
% size_aircraft_451_prop.m
%  by Team 4 -- Kevin Kwan
% This program requires following m-file: stdatm2.m
% Developed for:
%       -AAE 451 UAV Sizing
%%%%%%%%%%%%%%%%%%%%%%%%%%%%%%%%%%%%%%%%%%%%%%%%%%%%%%%%%%%%%%%%%%%%%%%%%%%%

function [W0] = size_aircraft_451_prop (Wpay, R, E, AR, Powerloading,
Wingloading, display)
%% Input Section

if nargin~=7 && nargin~=6
clc
    Wpay = 67.1;    % payload weight of the aircraft [lbs](73 lb for Shadow 200
RQ-7B)
    R = 200;         % Cuurse Range (one way) [nmi]
    E = 7;              % Loiter Endurence [hr] (7 hr for Shadow 200 RQ-7B)
    AR = 11;
    Powerloading = 0.0525; % from constraint analysis [btu/lb.s]
    Wingloading = 5.98; % from constraint analysis [lb/ft^s]
    display=1;
end

Vmax = 176;    % Speed Chase speed [ft/s] (104.2kts=120mph)
h = 1500; % Cruise altitude [ft]
V_loiter = 73;    % Loiter Speed [ft/s]  (21.7kts = 25mph)
E_SC = 1.5;        % Average Speed Chase endurence [hr]
W0_guess = 700.0001;     % Take off Wright guess [lb]
c_cruise = 0.6;     % SFC for cruise [lb/hp.hr]
c_loiter = 0.52;     % SFC for loiter [lb/hp.hr]
np = 0.75;          % Propellent Efficiency
CDo = 0.0239; % minimum drag coefficient
n = 3; %load factor of the aircraft
n_at_max_speed = 1.5;
e = 0.75; %Oswald's efficiency factor
tapper=0.5;

%% Main

%approxmation of (L/D)max as a function of AR
L_per_D=(11/8)*AR^0.8+6; % =16.0 for current configuration
L_per_D_maxspeed=0.866*L_per_D;

ftpers_to_knot=0.59248; % convert ft/s to knot factor
x = stdatm2(h,1);
%!!
density = x(3)/32.2;  % slag/ft^3
q = 0.5*density*(V_loiter)^2;  % V has to be in ft/s

nmi_to_mi=(871.5888/757.39);  % convert nmi to mi factor
Vmax=Vmax*ftpers_to_knot; %convert to knot
V_loiter=V_loiter*ftpers_to_knot; %convert to knot
```

```
beta = 0.6;
q_maxspeed = 0.5*density*(176)^2;
beta = 0.6;
%L_per_D_maxspeed =
1/((q_maxspeed*CDo/(n_at_max_speed*beta*Wingloading))+(n_at_max_speed*beta*Wingl
oading/(q_maxspeed*pi*AR*e)))

%first cruise
Wf2_per_Wf1=exp((-R*c_cruise)/(325*np*(0.8*L_per_D)));    % Range equation for
Prop
%loiter
Wf3_per_Wf2=exp(-E*c_loiter*V_loiter/(325*np*(L_per_D)));     % Endurance
Equation for Prop
%Max speed Chase
Wf4_per_Wf3=(exp(-E_SC*c_loiter*Vmax/(325*np*(0.8*L_per_D_maxspeed))));  % Speed
Chase at MAx Speed
%Second cruise
Wf5_per_Wf4=exp((-R*c_cruise)/(325*np*(0.8*L_per_D)));    % Range equation for
Prop


tolerance=5;
error=100;
if display
    disp ('W0, guess      We/W0     We          W0,calculated     error')
    disp ('-------------------------------------------------------------')
end
n=1;
while (abs(error)>tolerance && n<50)
    Wf_per_W0 =1.06*(1-Wf2_per_Wf1*Wf3_per_Wf2*Wf4_per_Wf3*Wf5_per_Wf4);
    We_per_W0=-0.1+0.71*W0_guess^-0.13*AR^0.085*Powerloading^0.08*Wingloading^-
0.05*Vmax^0.21;
    W0 = Wpay/(1-(We_per_W0)-(Wf_per_W0));
    We = We_per_W0*W0;
    error = (W0-W0_guess);
    if display
        disp ([num2str(W0_guess),'     ',num2str(We_per_W0),'
',num2str(We),'      ',num2str(W0),'       ',num2str(error)])
    end
    if W0>W0_guess
        W0_guess = W0_guess+abs((W0-W0_guess)/2);
    elseif W0<W0_guess
        W0_guess = W0_guess-abs((W0-W0_guess)/2);
    end
    n=n+1;
    if W0 < 0
        disp (' ')
        disp ('ERROR!!: bad initial guesses')
        disp (' ')
        break
    end
end

if display
```

```
Wf = Wf_per_W0 * W0;
Power = Powerloading*W0;
S_actural=69;

safe_factor=0.7;

best_R=safe_factor*(325*np/c_cruise)*(L_per_D)*0.78*log(W0/(W0-Wf))*nmi_to_mi;
best_E=safe_factor*(325*np/c_loiter)*(L_per_D)*log(W0/(W0-Wf))*(1/V_loiter);
best_E_Vmax=safe_factor*(325*np/c_cruise)*(L_per_D)*0.78*log(W0/(W0-
Wf))*(1/Vmax);

best_E_range=linspace(0,best_E);
logweightfraction=(1/safe_factor)*best_E_range./((325*np/c_loiter)*(L_per_D)*(1/
V_loiter));
best_R_range=safe_factor*((325*np/c_cruise)*(L_per_D)*0.78).*(log(W0/(W0-Wf))-
logweightfraction);
figure (12)
plot(best_E_range,best_R_range)
ylabel 'Range [mi]'
xlabel 'Endurance [hr]'
title 'Range and Endurance Frontier'

s = W0/Wingloading; % Wing Area
disp (' ')
disp ('Aircraft Data')
disp (' ')
disp (['Total Aircraft Takeoff Weight = ', num2str(W0),' lbs'])
disp (['Fuel Weight = ',num2str(Wf),' lbs'])
disp (['Payload Weight= ',num2str(Wpay),' lbs'])
disp (['Aircraft Inert Weight = ',num2str(We),' lb'])
disp (['Engine Power = ',num2str(Power),' hp'])
disp (['Wing Area = ',num2str(s),' ft^2'])
disp (' ')
disp (['Best Range = ',num2str(best_R),' mi'])
disp (['Best Endurance = ',num2str(best_E), 'hr'])
disp (['Best Endurance on max speed = ',num2str(best_E_Vmax), ' hr'])

%AR plot
figure(10)
title 'Take-off weight vs. Aspect Ratio'
plot (AR, W0,'o')
xlabel 'Aspect Ratio'
ylabel 'Take-off Weight [lbs]'
hold on
end
```

A.6 Trade-off Analysis Matlab Code

```
%%%%%%%%%%%%%%%%%%%%%%%%%%%%%%%%%%%%%%%%%%%%%%%%%%%%%%%%%%%%%%%%%%%%%%%%%%%%%%%
% Trade_offs.m
%  by Team 4 -- Kevin Kwan
% This program requires following m-file: size_aircraft_451_prop.m;
%                                         stdatm2.m
% Developed for:
%       -AAE 451 Sizing UAV / Trade off
% Last Revision: 03/25/2007
%%%%%%%%%%%%%%%%%%%%%%%%%%%%%%%%%%%%%%%%%%%%%%%%%%%%%%%%%%%%%%%%%%%%%%%%%%%%%%%
function Trade_offs

%% Main
Value = [63 43.4 5];
Wpay = linspace (48, 100);
R = linspace (400, 600)./2;
E = linspace (1, 11);
W0_Wpay=[];
W0_R=[];
W0_E=[];

Payload = [63.19 67.19];
Range = 200;
Endurance = [3 5 7];
    AR = 11;
    Powerloading = 0.0525; % from constraint analysis [btu/lb.s]
    Wingloading = 5.98; % from constraint analysis [lb/ft^s]
    display=0;
for m=1:5
    if m==1
        Value = [Payload(1) Range Endurance(2)];
    elseif m==2
        Value = [Payload(2) Range Endurance(2)];
    elseif m==3
        Value = [Payload(1) Range Endurance(1)];
    elseif m==4
        Value = [Payload(1) Range Endurance(3)];
    elseif m==5
        Value = [Payload(2) Range Endurance(3)];
    end
    for n=1:100
        W0_Wpay(n)=size_aircraft_451_prop
(Wpay(n),Value(2),Value(3),AR,Powerloading,Wingloading,display);
        W0_R(n)=size_aircraft_451_prop
(Value(1),R(n),Value(3),AR,Powerloading,Wingloading,display);
        W0_E(n)=size_aircraft_451_prop
(Value(1),Value(2),E(n),AR,Powerloading,Wingloading,display);
    end
    figure (7)
    hold on
    if m==1
        plot (Wpay,W0_Wpay)
    elseif m==3
        plot (Wpay,W0_Wpay,'g')
    elseif m==4
        plot (Wpay,W0_Wpay,'c')
```

```
    end
    grid on
    legend (['Coverage Radius=',num2str(Range),'[mi] and
Endurance=',num2str(Endurance(2)),'[hr]'],['Coverage
Radius=',num2str(Range),'[mi] and
Endurance=',num2str(Endurance(1)),'[hr]'],['Coverage
Radius=',num2str(Range),'[mi] and Endurance=',num2str(Endurance(3)),'[hr]'])
    title (['Take-off Weight vs. Payload Weight for different Endurance'])
    xlabel 'Payload Weight [lb]'
    ylabel 'Take-off Weight [lb]'

    figure (8)
    hold on
    if m==1
        plot (R, W0_R)
    elseif m==2
        plot (R, W0_R,'r')
    elseif m==4
        plot (R, W0_R,'g')
    elseif m==5
        plot (R, W0_R,'c')
    end
    grid on
    legend (['Payload=',num2str(Payload(1)),'[lb] and
Endurance=',num2str(Endurance(2)),'[hr]'],['Payload=',num2str(Payload(2)),'[lb]
and
Endurance=',num2str(Endurance(2)),'[hr]'],['Payload=',num2str(Payload(1)),'[lb]
and
Endurance=',num2str(Endurance(3)),'[hr]'],['Payload=',num2str(Payload(2)),'[lb]
and Endurance=',num2str(Endurance(3)),'[hr]']);
    title (['Take-off Weight vs. Range for for Payload'])
    xlabel 'Coverage Radius [mi]'
    ylabel 'Take-off Weight [lb]'


    figure (9)
    hold on
    if m==1
        plot (E, W0_E)
    elseif m==2
        plot (E, W0_E, 'r')
    end
    grid on
    title (['Take-off Weight vs. Endurance for different Payload'])
    legend (['Coverage Radius=',num2str(Range),'[mi],
Payload=',num2str(Payload(1)),'[lb]'],['Coverage Radius=',num2str(Range),'[mi],
Payload=',num2str(Payload(2)),'[lb]'])
    xlabel 'Endurance [hr]'
    ylabel 'Take-off Weight [lb]'
end
```

A.7 V-n Diagram Matlab Code

```
%%%%%%%%%%%%%%%%%%%%%%%%%%%%%%%%%%%%%%%%%%%%%%%%%%%%%%%%%%%%%%%%%%%%%%%%%%%%%%%
% VN.m     by Team4 -- Kevin Kwan
% This program requires following m-file: stdatm2.m
% Developed for:
%       -AAE 451 UAV Sizing
% Last Revision: 04/10/2007
%%%%%%%%%%%%%%%%%%%%%%%%%%%%%%%%%%%%%%%%%%%%%%%%%%%%%%%%%%%%%%%%%%%%%%%%%%%%%%%
function [ans]= nV(CLmax, n_max, V_max, S, W0)
%% input section
if nargin~=5
CLmax = [-0.6,1.5];
n_max=[-1.5,2];
V_max=233;
S=70;
W0=378;
V_loiter=73;
V_cruise=176;
end
alt=1500;

%% Main
figure(11)
x=stdatm2(alt,1);
density=x(3)/32.2;
V=linspace (1,180);
W=0.7*W0;
n_pos=density.*V.^2*S*CLmax(2)./(2*W);
n_neg=density.*V.^2*S*CLmax(1)./(2*W);
plot (V,n_pos,'-.',V,n_neg,'-.')
hold on
tolerance=0.1;
for k=1:100
    x1=abs(n_pos(k)-n_max(2));
    if x1<=tolerance
        if k~=100
            n_pos_k = (n_pos(k)+n_pos(k+1))/2;
            break
        else
            n_pos_k = n_pos(k);
            break
        end
    end
end
V_rerange=linspace(1,V(k));
n_pos_rerange=density.*V_rerange.^2*S*CLmax(2)./(2*W);

plot (V_rerange,n_pos_rerange,'r')


plot ([V(k) V_max],[n_max(2) n_max(2)],'r')
plot ([V_max V_max], n_max, 'r')
plot ([V_loiter V_loiter], n_max,[V_cruise V_cruise], n_max)

for k=1:100
```

```
    x1=abs(n_neg(k)-n_max(1));
    if x1<=tolerance
        if k~=100
            n_neg_k = (n_neg(k)+n_neg(k+1))/2;
            break
        else
            n_neg_k = n_neg(k);
            break
        end
    end
end
V_rerange=linspace(1,V(k));
plot ([V(k) V_max],[n_max(1) n_max(1)],'r')
n_neg_rerange=density.*V_rerange.^2*S*CLmax(1)./(2*W);
plot (V_rerange,n_neg_rerange,'r')
%grid on
title 'V-n diagram'
ylabel 'n -- load factor'
xlabel 'velocity [ft/s]'
ans=1;
```

A.8 Center of Gravity

```
%Sean R. Woock
% AAE 451  Metro-Scout Design Project
% Longitudinal Stability/Control Section
% Finding Center of Gravity for Aircraft
%%%%%%%%%%%%%%%%%%%%%%%%%%%%%%%%%%%%%%%%%%%%%%%%%%%%
% This code uses the standard statistical group weight method
% to estimate aircraft center of gravity.
%
%% INPUT %%
% Enter aircraft chord length.
c_ac = 18; % ft
% Enter location of wing leading edge from aircraft leading edge
x_w_le = x_wing; %ft
% Enter weights of each component.
% Canard
W_c = 14;   % lb
% Payload
W_pay = 0; % lb
% Fuselage
W_fus = 47.8+40; % lb
% Fuel is assumed to be place in multiple tanks.  If fuel is placed in
% less than 5 tanks, enter "0" for the weight of each unused tank.
% NOTE: THESE FUEL WEIGHTS ARE AT TAKEOFF!
W_f1 = 0; %lb
W_f2 = 0; %lb
W_f3 = 0; %lb
W_f4 = 0; %lb
W_f5 = 0; %lb
% Wings (weight of both wings added together)
W_w = 60; %lb
% Vertical Tail
W_vt = 18; %lb
% Engine
W_eng = 57; %lb
```

```
% Propeller
W_prop = 0;
% Main gear
W_mg = 0; % lb
% Nose Gear
W_ng = 0; %lb
% Transmitter
W_t = 11; %lb
% Enter location of each component c.g. wrt leading edge.
% Canard
x_c = x_c_wing + x_w_le; % ft
% Payload
x_pay = 2.19; % ft
% Fuselage
x_fus = 7; %ft
% Fuel
x_f1 = 8.2; % ft
x_f2 = 0; %ft
x_f3 = 0; %ft
x_f4 = 0; %ft
x_f5 = 0; %ft
% Wing
x_w = x_w_le + 1.23; %ft
% Vertical tail
x_vt = 16.8; %ft
% Engine
x_eng = 13.5; %ft
% Propeller
x_prop = 14; %ft
% Main gear
x_mg = 0; %ft
% Nose gear
x_ng = 0; %ft
% Transmitter
x_t = 7.2; %ft
%% Summation and CG Calculation%%
S_wx = W_c.*x_c + W_pay.*x_pay + W_fus.*x_fus + W_f1.*x_f1 + W_f2.*x_f2 + ...
    W_f3.*x_f3 + W_f4.*x_f4 + W_f5.*x_f5 + W_w.*x_w + W_vt.*x_vt + W_eng.*x_eng
+...
    W_prop.*x_prop + W_mg.*x_mg + W_ng.*x_ng + W_t.*x_t;
S_w = W_c + W_pay + W_fus + W_f1 + W_f2 + W_f3 + W_f4 + W_f5 + W_w + W_vt + ...
    W_eng + W_prop + W_mg + W_ng + W_t;
% x_cg from leading edge of AIRCRAFT
x_cg_le = S_wx./S_w;
% In terms of a/c chord
x_bar_cg_le = x_cg_le./c_ac;
% x_cg from leading edge of WING
x_cg = x_cg_le - x_w_le;
x_bar_cg = x_cg./c_ac;
return
```

A.9 Center of Gravity Function

```
function[x_bar_cg,x_bar_cg_le]=CG_loc2(x_c_wing,x_wing,We_fuel,We_pay)
% Sean R. Woock
% AAE 451  Metro-Scout Design Project
```

```
% Longitudinal Stability/Control Section
% Finding Center of Gravity for Aircraft
%%%%%%%%%%%%%%%%%%%%%%%%%%%%%%%%%%%%%%%%%%%%%%%%%%%%
% This code uses the standard statistical group weight method
% to estimate aircraft center of gravity.
%
%% INPUT %%
% Enter aircraft chord length.
c_ac = 18; % ft
% Enter location of wing leading edge from aircraft leading edge
x_w_le = x_wing; %ft
% Enter weights of each component.
% Canard
W_c = 14;   % lb
% Payload
W_pay = We_pay; % lb
% Fuselage
W_fus = 47.8+40; % lb
% Fuel is assumed to be place in multiple tanks.  If fuel is placed in
% less than 5 tanks, enter "0" for the weight of each unused tank.
% NOTE: THESE FUEL WEIGHTS ARE AT TAKEOFF!
W_f1 = We_fuel; %lb
W_f2 = 0; %lb
W_f3 = 0; %lb
W_f4 = 0; %lb
W_f5 = 0; %lb
% Wings (weight of both wings added together)
W_w = 60; %lb
% Vertical Tail
W_vt = 18; %lb
% Engine
W_eng = 57; %lb
% Propeller
W_prop = 0;
% Main gear
W_mg = 0; % lb
% Nose Gear
W_ng = 0; %lb
% Transmitter
W_t = 11; %lb
% Enter location of each component c.g. wrt leading edge.
% Canard
x_c = x_c_wing + x_w_le; % ft
% Payload
x_pay = 2.19; % ft
% Fuselage
x_fus = 7; %ft
% Fuel
x_f1 = 8.2; % ft
x_f2 = 0; %ft
x_f3 = 0; %ft
x_f4 = 0; %ft
x_f5 = 0; %ft
% Wing
x_w = x_w_le + 1.23; %ft
% Vertical tail
```

```
x_vt = 16.8; %ft
% Engine
x_eng = 13.5; %ft
% Propeller
x_prop = 14; %ft
% Main gear
x_mg = 0; %ft
% Nose gear
x_ng = 0; %ft
% Transmitter
x_t = 7.2; %ft
%% Summation and CG Calculation%%
S_wx = W_c.*x_c + W_pay.*x_pay + W_fus.*x_fus + W_f1.*x_f1 + W_f2.*x_f2 + ...
    W_f3.*x_f3 + W_f4.*x_f4 + W_f5.*x_f5 + W_w.*x_w + W_vt.*x_vt + W_eng.*x_eng
+...
    W_prop.*x_prop + W_mg.*x_mg + W_ng.*x_ng + W_t.*x_t;
S_w = W_c + W_pay + W_fus + W_f1 + W_f2 + W_f3 + W_f4 + W_f5 + W_w + W_vt + ...
    W_eng + W_prop + W_mg + W_ng + W_t;
% x_cg from leading edge of AIRCRAFT
x_cg_le = S_wx./S_w;
% In terms of a/c chord
x_bar_cg_le = x_cg_le./c_ac;
% x_cg from leading edge of WING
x_cg = x_cg_le - x_w_le;
x_bar_cg = x_cg./c_ac;
%% Output %%
%disp(['Aircraft CG location from leading edge of aircraft: ', x_cg_le,' ft'])
%disp(['Normalized by aircraft chord: ', x_bar_cg_le ])
%disp(['Aircraft CG location from leading edge of wing: ', x_cg,' ft'])
%disp(['Normalized by aircraft chord: ', x_bar_cg])
return
```

A.10 CG Migration

```
% Team 4 - MetroScout
% CG Migration during flight
% NOTE: This code uses the function "CG_loc2" instead of "CG_loc"
%% Fuel Weight As Input %%
W_fuel = 67:-0.01:0; %lb
% Payload Weight
W_pay = 67; %lb
x_c_wing = -5; %lb
x_wing = 9.5; %ft
% Aircraft Weight
W = 381; %lb
%% Function Call
% News
[x_bar_cg,x_bar_cg_le]=CG_loc2(x_c_wing,x_wing,W_fuel,W_pay);
plot(x_bar_cg_le.*18,W_fuel+311)
grid
title('Center of Gravity Excursion Diagram')
xlabel('CG Distance from Nose (ft)')
ylabel('Aircraft Weight (lb)')
hold on
% Police
W_pay = 63; %lb
W_fuel = 71:-0.01:0; %lb
```

```
[x_bar_cg,x_bar_cg_le]=CG_loc2(x_c_wing,x_wing,W_fuel,W_pay);
%plot(x_bar_cg_le.*18,W_fuel+307,'--')
% No Payload
W_pay = 0; %lb
W_fuel = 67; %lb
[x_bar_cg,x_bar_cg_le]=CG_loc2(x_c_wing,x_wing,W_fuel,W_pay);
W_pay = 67; %lb
plot(x_bar_cg_le.*18,W-W_fuel-W_pay,'*')
% SM 10% Limit
x_np = 10.15; %ft
x_cg_low = x_np-0.1*18; %ft
x_cg_high = x_np-0.15*18; %ft
W_ac = 220:0.1:400; %ft
x_cg_low_r = linspace(x_cg_low,x_cg_low,1801);
x_cg_high_r = linspace(x_cg_high,x_cg_high,1801);
plot(x_cg_low_r,W_ac,'r')
plot(x_cg_high_r,W_ac,'r')
%legend('Flying w/ Payload','Flying w/out Payload')
```

A.11 Drag Polar

```
% Team 4
% MetroScout Design Project
% from Brandt, page 130
% Drag Polar
%%%%%%%%%%%%%%%%%%%%%%%%%%
% This code computes the aircraft drag polar.
Cd0 = 0.0239;
AR = 11;
k = 1/(pi.*AR.*0.8);
Cl = linspace(-0.5,1.5,1000);
Cd = Cd0+k.*Cl.^2;
plot(Cl,Cd)
title('Metro-Scout Aircraft Drag Polar (C_D_0=0.0239)')
xlabel('C_L')
ylabel('C_D')
grid
```

A.12 Moment of Inertia

```
function[MIyy]=Iyy(Weight,x,y)
% Team 4- Metro-Scout Design
% Moment of Interia (quick-calc function)
g=32.2; %ft/s^2
MIyy = Weight./g.*(x.^2+y.^2);
```

A.13 Moment of Inertia

```
% Team 4 - Metro-Scout Design
% Moment of Inertia
%%%%%%%%%%%%%%%%%%%%%%%%%%%%%
% This code computes the aircraft moment of inertia about the y-axis using
% the Iyy function.
% Enter aircraft chord length.
c_ac = 14; % ft
x_c_wing = -7; %ft
% Enter location of wing leading edge from aircraft leading edge
```

```
x_w_le = 9; %ft
% Enter weights of each component.
% Canard
W_c = 17.5;   % lb
% Payload
W_pay = 67; % lb
% Fuselage
W_fus = 150.9; % lb
% Fuel is assumed to be place in multiple tanks.  If fuel is placed in
% less than 5 tanks, enter "0" for the weight of each unused tank.
% NOTE: THESE FUEL WEIGHTS ARE AT TAKEOFF!
W_f1 = 67; %lb
W_f2 = 0; %lb
W_f3 = 0; %lb
W_f4 = 0; %lb
W_f5 = 0; %lb
% Main wing
W_w = 60; %lb
% Vertical Tail
W_vt = 11.2; %lb
% Engine
W_eng = 45; %lb
% Propeller
W_prop = 12; %lb
% Main gear
W_mg = 23.4; % lb
% Nose Gear
W_ng = 17.6; %lb
% Enter location of each component c.g. wrt leading edge.
% Canard
x_c = x_c_wing + x_w_le; % ft
% Payload
x_pay = 2.19; % ft
% Fuselage
x_fus = 7; %ft
% Fuel
x_f1 = 8; % ft
x_f2 = 0; %ft
x_f3 = 0; %ft
x_f4 = 0; %ft
x_f5 = 0; %ft
% Wing
x_w = x_w_le + 1.23; %ft
% Vertical tail
x_vt = 14; %ft
% Engine
x_eng = 13; %ft
% Propeller
x_prop = 14; %ft
% Main gear
x_mg = 8.58; %ft
% Nose gear
x_ng = 4.08; %ft
z=4; %ft
%         Payload               Canard          Fuselage         Wing
```

```
I_yy =
Iyy(W_pay,x_pay,z)+Iyy(W_c,x_c,z)+Iyy(W_fus,x_fus,z)+Iyy(W_w,x_w,z)+Iyy(W_f1,x_f
1,z)+Iyy(W_eng,x_eng,z)+Iyy(W_vt,x_vt,z)+Iyy(W_mg,x_mg,0)...
    +Iyy(W_ng,x_ng,0)+Iyy(W_prop,x_prop,z)
```

A.13 Neutral Point

```
% Team 4 - Metro-Scout Design
% Calculation of Neutral Point
%%%%%%%%%%%%%%%%%%%%%%%%%%%%%%%%%%
% This code uses aircraft characteristics to determine the neutral point.
c= 18;%fuselage chord length
c_w= 2.468;%wing chord
c_c= 0.25*c_w;%canard chord
c_h = 0.14*c_w; % horizontal stabilizer tail
xac_w= 0.25.*c_w;%aerodynamic center of wing wrt wing LE
xac_c= -5;%aerodynamic center of canard wrt wing LE ( Idon't think this is
termed as aerodynamic center (more like a distance to wing LE)
Sc_S= 0.16;%ratio of canard area/wing area
% ADD IN HORIZONTAL STABILIZER
Sh_S = 0.155;
xac_h =8;
cl_calpha= 5.37;%cl_alpha of canard
cm_calpha= .318;%cm_alpha of canard
cm_walpha= .318;%cm_alpha of wing
cl_walpha= 5.37;%cl_alpha of wing
cl_halpha = 5.37; %cl_alpha of hs
cm_halpha = 0.318; %cm_alpha of hs

x_np = ((xac_w./c)-
(cm_walpha./cl_walpha).*(c_w./c)+(xac_c./c).*Sc_S.*(cl_calpha./cl_walpha)-
(cm_calpha./cl_walpha).*Sc_S.*(c_c/c)+(xac_h./c).*(cl_halpha./cl_walpha).*Sh_S-
(cm_halpha./cm_walpha).*c_h./c.*Sh_S)./...
    (1+(cl_calpha./cl_walpha).*Sc_S+(cl_halpha./cl_walpha).*Sh_S);

plot(xac_c,x_np,'k')
legend('Sc/S=0.45','Sc/S=0.50','Sc/S=0.55','Sc/S=0.60')
hold off

%Determine Static Margin
% Find CG location.
x_wing_le = 9.5; %ft
[x_bar_cg, x_bar_cg_le]= CG_loc(xac_c,x_wing_le);
SM = (x_np-x_bar_cg)*100;
plot(xac_c,SM)
grid
title('Static Margin w/ Varying Canard Location (x_w_i_n_g = 8 ft)')
xlabel('Canard Location from Wing Leading Edge (ft)')
ylabel('Static Margin (%)')
hold on
```

A.14 Rotation Calculation

```
% Team 4 - Metro-Scout Design
% Takeoff rotation
%%%%%%%%%%%%%%%%%%%%%%%%%%%%%%
```

```
%This code calculates the canard surface area (Sc) value that is adequate to
achieve
%takeoff rotation.

clear all
clc

%all locations are wrt nose (x-axis) or ground (y-axis)
Wing_load = 5.48;
% Wing Chord
c_w = 2.468; % (ft) wing chord
% Distance Wing LE from nose
x_w = 9.5; %ft
% Distance from wing LE to Canard AC
x_w_cac = 5; %ft
% Distand from wing LE to HS AC
x_w_hac = 8; %ft
% Wing Area
S = 69; %ft^2 (wing)
% Horizontal Tail
Sh_S= 0.155;
Sh = S.*Sh_S; %ft^2
xcg=8.3; %center of gravity location wrt nose
xmg=8.8; %main-gear location
zcg=3; %center of gravity location wrt ground
zdg=2.7; %location of where drag acts at wrt ground (basically at wing)
ztg=2.7; %location of where thrust is driven wrt ground (center of the engine)
xac_w=x_w+0.25.*c_w; %aerodynamic center of the wing location wrt nose
xac_c=x_w-x_w_cac; %aerodynamic center of the canard location wrt nose
xac_h=x_w+x_w_hac; %aerodynamic cneter of the canard location wrt nose
% Engine Power
P = 50; %bhp
% Air desity
rho = 0.001756; %hot day, high altitude (lb/ft^3)
% Coefficients AT ROTATION, but ignoring ground effects!
Cd = 0.033;
Cl_w = 1.4;
Cm = -0.05;
eta_p = 0.78; %prop efficiency at rotation
% WE MIGHT HAVE TO INCREASE ROTATION SPEED!!
V1 = 1.3.*sqrt(2.*Wing_load./(rho.*Cl_w)); %ft/s
q_rot = 1/2.*rho.*V1.^2; %dynamic pressure at rotation
W=378; %gross-weight
D=Cd.*q_rot.*S; %drag
T= 550.*P.*eta_p./V1; %thrust
Lw= Cl_w.*q_rot.*S; %wing lift
Mac_w= Cm.*S.*q_rot.*c_w; %aerodynamic moment of the wing
Iyy=1213;%moment of inertia about y-axis (slug*ft^2)
theta_doubledot= 10*pi/180; %angular acceleration (for light airplanes = 10-12
deg/sec^2)
ug=0.02; %wheel ground friction coefficient (0.02 for asphalt/macadam)
Clmax_c = 1.3; %Clmax of the canard
Clmax_h = -1.3; %Clmax of horizontal (this should be NEGATIVE!)
%qbar_rotate=; %dynamic pressure at rotation (need to know what altitude the a/c
takes off)
```

```
%calculate canard surface area
Sc = (W.*(xcg-xmg-ug.*zcg) + D.*(zdg-zcg) + T.*(zcg-ztg) + Lw.*(xmg-
xac_w+ug.*zcg) + Clmax_h.*q_rot.*Sh.*(xmg-xac_h+ug.*zcg) + Mac_w -
Iyy.*theta_doubledot)./...
    ((Clmax_c.*q_rot).*(xac_c-xmg-ug.*zcg));
Sc_S = Sc./S;
%plot(x_w_cac,Sc_S)
```